UNIVERSITÉ DE STRASBOURG

Université de Strasbourg

msii ÉCOLE DOCTORALE

ÉCOLE DOCTORALE ED 269 Mathématiques, Sciences de l'Information et de l'Ingénieur

[*ICube – UMR 7357*]

THÈSE présentée par :

Nariaki OKAMOTO

Soutenue le : 06/03/2023

pour obtenir le grade de : **Docteur de l'université de Strasbourg**

Discipline/ Spécialité : Sciences médicales

The application of intraoperative optical imaging to optimize colorectal oncological surgery and prevent complications.

THÈSE dirigée par :

M DIANA Michele   HDR, Directeur Médico-Scientifique IRCAD, Université de Strasbourg

M MONTGOMERY Paul   HDR, Directeur de recherche CNRS, Laboratoire ICube,
                                   Université de Strasbourg

RAPPORTEURS:

M SPINOGLIO Giuseppe   PU-PH, Director Robotic Surgery and Educational IEO
                                   (European Institute of Oncology) IRCCS

M MORALES-CONDE Salvador   PU-PH, Hospital Universitario Virgen del Rocio, Universidad de Sevilla

AUTRES MEMBERS DU JURY:

M LECLER Sylvain   HDR, PU, INSA Strasbourg

M CAHILL Ronan   PU-PH, Mater Misericordiae University Hospital, University College Dublin

M VAHRMEIJER Alexander L.   PU-PH, Leiden University Medical Center, Universiteit Leiden

Mme Elisa Cassinotti   Chercheur, DISCCO (Dipartimento di Scienze Cliniche e di Comunità)
                                   Université de Milan

INVITE:

M GIOUX Sylvain   HDR, PU, Laboratoire ICube, University of Strasbourg

INDEX

ABSTRACT

Colorectal cancer is the third leading cause of cancer and the second leading cause of cancer-related mortality worldwide. Over the last decades, the surgical approach to colorectal cancer has significantly changed, including the introduction of innovative surgical techniques such as total mesorectal excision (TME) and complete mesocolic excision (CME), advances in minimally invasive procedures, and near-infrared fluorescence (NIRF) image-guided surgery.

In colorectal cancer surgery, 'en bloc' tumor resection, including nourishing vessels and lymph nodes which have shown to have a clear impact on recurrence is still one of the primary mainstays of treatment. CME with central vascular ligation (CVL) for colon cancer and TME for rectal cancer have been proposed as surgical approaches that require a thorough understanding of the anatomical dissection planes to prevent any recurrences. During such surgery, it is essential to distinguish the tumor's nourishing vessels from the main lymphatic drainage.

A second key mainstay of treatment consists of creating an intestinal anastomosis to maintain hindgut continuity. Complications such as leaks and strictures may arise, hence representing a major surgical concern; they are closely correlated with insufficient perfusion. The conventional assessment via the surgeon's eye perception of the anatomical embryological planes and the intestinal viability has been used for several decades. However, the naked eye is insufficient to detect small variabilities with potential clinical repercussions. As a result, intraoperative optical imaging has been particularly helpful in providing a precise and quantitative method to recognize the correct dissection layers and bowel perfusion with the ultimate objective of reducing recurrences and complications. The overgrowing significant progress of intraoperative image-guided surgery accounts for its seminal place in the surgical field, along with new symposia and sessions being regularly organized during international surgical conferences.

The present research has focused on implementing novel approaches in colorectal surgery using intraoperative optical imaging to promote better clinical outcomes and prevent recurrences and complications.

This research aims to implement a new approach using intraoperative optical imaging, with the following three specific main research objectives; (1) to develop new imaging strategies to assess the complete resection of colorectal cancer, (2) to evaluate new imaging technologies enabling the accurate evaluation of perfusion to prevent complications such as leaks, and (3) to evaluate new fluorescent imaging techniques to improve the accuracy of intraoperative lymph node detection. These three objectives are correlated with colorectal cancer recurrence, leading to better clinical outcomes.

We studied "Computer-Assisted Differentiation between Colon-Mesocolon and Retroperitoneum Using Hyperspectral Imaging (HSI) Technology" (1) in order to obtain "Quantification of bowel ischaemia using real-time multispectral Single Snapshot Imaging of Optical Properties (SSOP)" (2) "Simultaneous, multi-channel, near-infrared fluorescence visualization of mesenteric lymph nodes using indocyanine green and methylene blue: a demonstration in a porcine model" (3).

RESUME EN FRANÇAIS

Positionnement de la recherche

Le cancer colorectal est la troisième cause de cancer et la deuxième cause de mortalité liée au cancer dans le monde [1]. Au cours des dernières décennies, l'approche chirurgicale du cancer colorectal a considérablement évolué, notamment grâce à l'introduction de techniques chirurgicales innovantes comme l'excision totale du mésorectum et l'excision complète du mésocôlon, grâce aux progrès des procédures mini-invasives et au recours à la chirurgie guidée par imagerie par fluorescence dans le proche infrarouge.

Dans la chirurgie du cancer colorectal, la résection "en bloc" de la tumeur, y compris des vaisseaux nourriciers et des ganglions lymphatiques demeure l'un des principaux piliers thérapeutiques, dont l'impact sur les récidives est évident. L'excision complète du mésocôlon avec ligature vasculaire centrale pour traiter le cancer du côlon et l'excision totale du mésorectum pour traiter le cancer du rectum ont été proposées comme des approches chirurgicales qui permettent de réduire tout risque de récidives et nécessitent une compréhension approfondie des plans anatomiques de dissection [2, 3]. Au cours de ces opérations, il est crucial de discerner les vaisseaux nourriciers de la tumeur du drainage lymphatique principal.

Un deuxième élément clé consiste à créer une anastomose intestinale pour maintenir la continuité de l'intestin grêle postérieur. Des complications telles que les fistules et les sténoses peuvent survenir, représentant une préoccupation chirurgicale majeure ; elles sont étroitement corrélées à une perfusion insuffisante. L'évaluation classique via la perception oculaire du chirurgien des plans anatomiques embryologiques et de la viabilité intestinale s'effectue depuis plusieurs décennies. Toutefois, une vision à l'œil nu est insuffisante pour détecter de petites variations susceptibles d'entraîner une répercussion clinique potentielle. Par conséquent, l'imagerie optique peropératoire

s'est avérée particulièrement utile en apportant une stratégie précise et quantitative permettant de reconnaître les couches de dissection adéquates et la perfusion intestinale afin de réduire toutes récidives et complications.

Les progrès significatifs et croissants de la chirurgie guidée par l'image peropératoire s'incarnent à travers son rôle déterminant dans le domaine chirurgical, comme en témoignent les nombreux symposiums régulièrement organisés lors de congrès de chirurgie dans le monde [4].

La présente recherche s'est polarisée sur la mise en œuvre de nouvelles approches en chirurgie colorectale utilisant l'imagerie optique peropératoire afin de promouvoir de meilleurs résultats cliniques et prévenir toutes récidives et complications.

Objectifs de la recherche

Cette recherche vise à développer une nouvelle approche utilisant l'imagerie optique peropératoire, avec les trois principaux objectifs de recherche spécifiques suivants : (1) créer de nouvelles stratégies d'imagerie pour évaluer la résection complète du cancer colorectal, (2) évaluer de nouvelles technologies d'imagerie permettant une évaluation précise de la perfusion pour prévenir les complications comme les fistules et (3) évaluer de nouvelles techniques d'imagerie par fluorescence afin d'améliorer la précision de la détection peropératoire des ganglions lymphatiques qui sont corrélés avec la récidive du cancer colorectal, ouvrant la voie à de meilleurs résultats cliniques. Nous avons étudié (1) la « Différenciation assistée par ordinateur entre le côlon-mésocôlon et le rétropéritoine à l'aide de la technologie d'imagerie hyperspectrale.» pour (2) obtenir une « Quantification de l'ischémie intestinale à l'aide de l'imagerie multispectrale en temps réel des propriétés optiques par instantané unique » et pour (3) obtenir une « Visualisation simultanée, multicanaux et par fluorescence dans le proche infrarouge des ganglions lymphatiques mésentériques à l'aide du vert d'indocyanine et du bleu de méthylène : une démonstration sur modèle porcin » dans le programme du cours de doctorat.

Etapes expérimentales

1) Différenciation assistée par ordinateur entre le côlon-mésocôlon et le rétropéritoine à l'aide de la technologie d'imagerie hyperspectrale

L'excision complète du mésocôlon qui implique la résection adéquate du segment colique porteur de la tumeur avec ablation "en bloc" de son mésocôlon le long des plans fasciaux embryologiques, est associée à des résultats oncologiques supérieurs. Toutefois, cette excision complète du mésocôlon (CME) présente un taux de complication plus élevé que les résections non CME en raison d'un risque plus élevé de lésion vasculaire. L'imagerie hyperspectrale (HSI) est une technologie d'imagerie optique sans contraste, qui facilite l'imagerie quantitative des paramètres physiologiques des tissus et la visualisation des structures anatomiques. Cette étude évalue la précision cette technologie associée au deep learning ou apprentissage profond afin de différencier le côlon et son tissu mésentérique du tissu rétropéritonéal. *Matériels et méthodes :* Dans une étude animale incluant 20 modèles porcins, des images hyperspectrales peropératoires du côlon sigmoïde, du mésentère sigmoïde et du rétropéritoine ont été enregistrées. Un réseau neuronal convolutif (CNN) a été entraîné à distinguer les deux classes de tissus à l'aide des données de la technologie HSI, validées par un processus de validation croisée d'un contre tous ("leave-one-out"). *Résultats :* La sensibilité globale de reconnaissance des tissus à préserver (rétropéritoine) et des tissus à réséquer (côlon et mésentère) était respectivement de 79,0 ± 21,0 % et 86,0 ± 16,0 %. *Conclusion :* La classification automatique s'appuyant sur les technologies HSI et CNN est un outil prometteur qui permet de différencier automatiquement le côlon et son mésentère du tissu rétropéritonéal, de manière non invasive et objective.

2) Quantification de l'ischémie intestinale à l'aide du multispectrale en temps réel des propriétés optiques par instantané unique

L'imagerie instantanée des propriétés optiques (SSOP) est une technologie relativement nouvelle d'imagerie optique non invasive, en temps réel et sans contraste, qui permet l'évaluation quantitative en temps réel des propriétés physiologiques, dont notamment l'oxygénation des tissus (StO2). Cette étude évalue la précision de la SSOP multispectrale pour quantifier l'ischémie intestinale dans un modèle expérimental préclinique. *Méthodes :* Dans 6 modèles porcins, un segment d'intestin ischémique a été créé en divisant les branches de l'arcade vasculaire. Cinq régions d'intérêt (ROIs) ont été identifiées sur la boucle intestinale, comme suit : ROI 1 : ischémique centrale ; ROI 2 : marginale gauche ; ROI 3 : vascularisée gauche ; ROI 4 : marginale droite ; et ROI 5 : vascularisée droite. Le système d'imagerie Trident, spécialement conçu pour l'imagerie de l'oxygénation du tissu en temps réel à l'aide de l'imagerie SSOP, a été utilisé pour obtenir des images avant (T0) et après l'induction de l'ischémie. Les lactates capillaires et systémiques ont été mesurés à chaque point temporel (T0, T15, T30, T45, T60), ainsi que les valeurs de StO2 acquises au moyen de l'imagerie SSOP (SSOP-StO2). *Résultats :* La valeur moyenne de StO2 acquise au moyen de l'imagerie SSOP dans la ROI 1 était de $30{,}08 \pm 6{,}963$ et était significativement plus faible par rapport aux ROIs marginales (ROI 2 + ROI 4 : $45{,}67 \pm 10{,}02$ $p = {<}0{,}0001$) et aux ROIs vascularisées (ROI 3 + ROI 5 : $48{,}08 \pm 7{,}083$ $p = {<}0{,}0001$). La valeur moyenne de StO2 acquise au moyen de l'imagerie SSOP était significativement corrélée aux lactates normalisés $r = -0.5892$ ($p {<} 0.0001$) et à l'histologie $r = -0.6251$ ($p = 0.0002$). *Conclusion :* L'imagerie SSOP multispectrale permet une évaluation précise et sans contraste de la perfusion de l'intestin grêle en identifiant l'oxygénation physiologique des tissus, confirmée par les biomarqueurs de perfusion.

3) Visualisation simultanée, multicanaux et par fluorescence dans le proche infrarouge des ganglions lymphatiques mésentériques à l'aide du vert d'indocyanine et du bleu de méthylène : une démonstration sur modèle porcin

La chirurgie guidée par imagerie en fluorescence proche infrarouge (NIRF) est un outil utile qui peut contribuer à réduire les complications péri-opératoires et à améliorer la reconnaissance des tissus. Bien que le colorant vert d'indocyanine (ICG) soit le plus couramment utilisé dans les études cliniques, il est de plus en plus évident que le bleu de méthylène (MB), un autre colorant fluorescent disponible en milieu clinique, peut également être utile pour l'identification guidée par fluorescence des uretères, des glandes thyroïdes et parathyroïdes, des tumeurs neuroendocrines pancréatiques et des ganglions lymphatiques sentinelles dans le cancer du sein, entre autres. L'objectif de cette étude était d'évaluer la faisabilité de la détection peropératoire par fluorescence des ganglions lymphatiques en utilisant du bleu de méthylène administré par voie intraveineuse (IV) et de le comparer au vert d'indocyanine. *Méthodes :* Trois modèles porcins ont été utilisés dans cette étude. Le vert d'indocyanine (0,2 mg/kg) a été administré via un cathéter veineux périphérique, suivi par l'administration immédiate de bleu de méthylène (0,25 mg/kg). Les images en fluorescence proche infrarouge ont été acquises sous forme d'enregistrements vidéo à différents moments (toutes les 10 minutes) pendant une heure à l'aide du système d'imagerie QUEST SPECTRUM® 3 (Quest Medical Imaging, Middenmeer, Pays-Bas), qui possède deux canaux en proche infrarouge dédiés au guidage peropératoire simultané par fluorescence. Le canal de 800 nm a été utilisé pour capturer la fluorescence par vert d'indocyanine et le canal de 700 nm a été utilisé pour le bleu de méthylène. La cible (ganglions lymphatiques et intestin grêle) et le fond (champ avasculaire du mésentère) ont été mis en évidence en tant que région d'intérêt (ROI) et les intensités de fluorescence (IF) correspondantes à ces ROI ont été mesurées. L'intensité de fluorescence a été

mesurée à l'aide du logiciel Quest Artemis (Quest Medical Imaging, Middenmeer, Pays-Bas) (TBR tool v1.0.). Le rapport cible/arrière-plan (TBR) a ensuite été calculé comme étant l'IF moyen de la cible moins l'IF moyen de l'arrière-plan divisé par l'IF moyen de l'arrière-plan. *Résultats :* Chez tous les animaux inclus, une identification claire des ganglions lymphatiques a été obtenue à tous les points temporels. Le TBR moyen du vert d'indocyanine dans les ganglions lymphatiques et l'intestin grêle était de 4,57 ± 1,00 et 4,37 ± 1,70 respectivement, pour l'ensemble du temps expérimental. En ce qui concerne le bleu de méthylène, le TBR moyen dans les ganglions lymphatiques et l'intestin grêle était de 4,60 ± 0,92 et 3,27 ± 0,62 respectivement. Le test U de Mann-Whitney du TBR des ganglions lymphatiques divisé par le TBR de l'intestin grêle a montré que le rapport TBR du bleu de méthylène était statistiquement plus élevé que celui du vert d'indocyanine. *Conclusion :* La technologie d'imagerie optique par fluorescence utilisée permet une évaluation à plusieurs longueurs d'onde. Cette étude de faisabilité prouve que les ganglions lymphatiques peuvent être détectés en utilisant deux fluorophores différents (bleu de méthylène et vert d'indocyanine) avec des longueurs d'onde différentes. La performance du bleu de méthylène peut représenter un moyen plus précis permettant de détecter les tissus lymphatiques pendant une chirurgie guidée par l'image. D'autres essais précliniques de confirmation sont nécessaires avant toute application clinique.

INTRODUCTION GENERALE

(Partie en anglais)

1. Colorectal cancer surgery

Colorectal cancer (CRC) is the third leading cause of cancer and the second leading cause of cancer-related mortality worldwide [1]. In France, CRC was diagnosed in 43,000 persons and was accountable for 17,000 deaths in 2018. It is estimated that there were approximately 1 million cases of CRC and 88,000 deaths worldwide in 2018 [5]. Typical symptoms of CRC include rectal bleeding, bloody stools, altered bowel habits, and chronic abdominal pain [6]. The number of cases of CRC under the age of 50 is still small (approximately 10% [7]), but increases each year. Morbid obesity, diets high in processed food, and a sedentary lifestyle may contribute [8, 9].

The surgical approach to CRC has changed significantly over the last few decades, including the introduction of innovative surgical techniques such as total mesorectal excision (TME) and complete mesocolic excision (CME), advances in minimally invasive procedures, and near-infrared fluorescence (NIRF) image-guided surgery.

In oncological surgery, accurate lymph node assessment enables pathological staging and prognosis and guiding postoperative therapies. Indeed, an adequate lymphadenectomy has shown to improve overall survival [10]. In CRC, the main objective of oncologic resection consists of resecting the primary tumor along with its blood supply and lymph node drainage [3, 11–15]. While the primary objective is the complete removal of cancerous tissue, the prevention of postoperative complications and recurrence remains one of the most significant issues.

1.1. Total mesorectal excision (TME)

In the surgical treatment of rectal cancer, ways of preventing local recurrence remain a major concern. Since rectal cancer has a higher postoperative local recurrence rate than colon cancer, various efforts have been made to reduce the local recurrence rate and improve postoperative oncological outcomes. Total mesorectal excision (TME) represents one of the most significant pivotal advances in the history of CRC treatment over the past 50 years.

Histological assessment provided by Cuthbert Dukes allowed to conclude that the majority of lymph nodes were running either parallel or proximal to the level of the primary tumor [16]. As a result, in the 1980s, there was a growing interest in studying circumferential margins. In 1982, Heald et al. proposed TME as a surgical technique which accomplished lower local recurrences. Heald's TME was based on a thorough understanding of rectal embryology, which included the mesorectum [2].

Distal tumor spread was also considered a major recurrence factor by Scott *et al*. Authors performed a histopathological analysis of 20 rectal cancer TME specimens. After slicing TME specimens every 1 cm, the authors observed cancer invasion both macroscopically and microscopically with mesorectal invasion on the anal side of the tumor in 4 cases, which was 1 cm to 3 cm on the distal side of the tumor [17].

The rectum and mesorectum constitute a single package surrounded by the visceral pelvic fascia, and TME is an 'en bloc' intact resection of the rectum and its mesorectum, which includes the majority of regional lymph nodes, lymph vessels, and surrounding adipose tissue, without damaging this package [18]. In 1986, this essential understanding on anatomical planes led Quirke *et al*. to report the importance of the circumferential resection margin (CRM) [19]. Afterwards,

Adam et al. showed that the local recurrence rate was significantly higher in circumferential margin-positive cases than in negative ones [20].

Completion of TME and CRM have significantly contributed to reducing the local recurrence rate after rectal cancer surgery, decreasing the incidence of permanent stomas, improving the curative resection rate, and improving survival and tumor-free survival rates. TME has become the "gold standard" treatment for rectal cancer worldwide [21, 22].
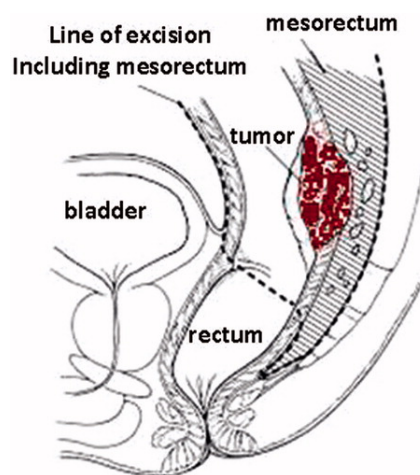
Figure 1. Drawing showing the principles and extent of TME (from Lirici MM *et* Hüscher CG. Techniques and technology evolution of rectal cancer surgery: a history of more than a hundred years. Minim Invasive Ther Allied Technol. 2016 Oct;25(5):226-33).

1.2. Complete mesocolic excision (CME)

Over the past few decades, the management of CRC has improved significantly due to better screening policies and to the introduction of extended radical 'en bloc' surgical resection based on TME principles such as complete mesocolic excision (CME) [23]. Hohenberger proposed CME for colon cancer treatment in 2009 [3]. CME consists of the substantial resection of tumor-bearing bowel segments with 'en bloc' removal of the mesocolon along embryological fascial planes

(Figure 2). Although CME has been associated with adverse outcomes such as a greater intraoperative blood loss and a higher incidence of postoperative surgical complications [24], several studies have shown that CME has superior oncological outcomes [25–28]. As previously emphasized, the number of lymph nodes harvested in oncological resection is an independent prognostic factor for survival [29–31], and CME specimens provide a better quality with a higher number of lymph nodes as compared to non-CME resections, which may account for the lower risk of local recurrence [32]. In a systematic review including 18,989 patients comparing CME with conventional colorectal resection for CRC, CME was associated with improved 3- and 5-year overall survival, improved 3-year disease-free survival, and decreased local and distant recurrences. Additionally, the study reported that CME did not increase the risk of postoperative mortality or anastomotic leakage [33, 34]. However, CME was associated with an increased risk of postoperative complications such as splenic and superior mesenteric vein injuries. Additionally, structures behind the peritoneum are called 'retroperitoneal', and the ureter and gonadal vessels stand for primary retroperitoneal organs [35].

The figure under copyright,
unauthorized distribution
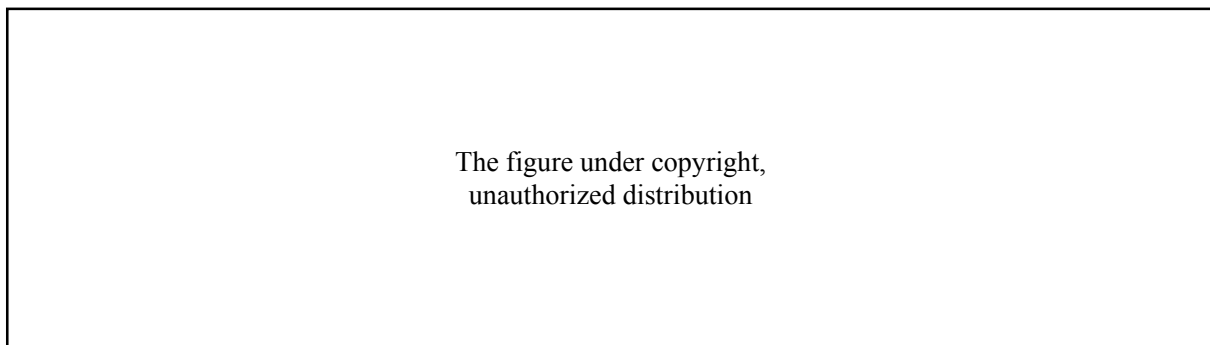
Figure 2. (a) Overview of standard arterial anatomy of the colon. (b) In right-sided colon cancer, the mesentery should be resected to the extent indicated in blue. (c) In left-sided colon cancer, the mesentery should be resected to the extent indicated in purple (from Bates DDB *et al.* Complete mesocolic excision and central vascular ligation for right colon cancer: an introduction for abdominal radiologists. Abdom Radiol (NY). 2019 Nov;44(11):3518-3526).

1.3. Minimally invasive colorectal surgery

Since the 1990s, the biggest innovation in digestive and colorectal surgery has been the introduction of laparoscopic surgery. Initially, laparoscopic surgery was used for purely diagnostic purposes. Semm introduced laparoscopic appendicectomy in 1983 [36], and developments in surgical techniques led to its use for more advanced therapeutic procedures. Subsequently, laparoscopic surgery gained prominence after Muhe in Germany and Mouret in France performed laparoscopic cholecystectomy in 1985 and 1987, respectively [37, 38].

In 1991, Jacobs *et al.* successfully performed the first laparoscopic sigmoid resection for cancer [39]. However, laparoscopic colon resection for cancer was not readily accepted because of early reports of port-site metastases, which questioned its safety.

Since the year 2000, randomized controlled trials of laparoscopic versus open colectomy such as the Barcelona, COST, and CLASSIC trials demonstrated that laparoscopic colectomy for cancer was oncologically safe [40–42]. In respect to rectal cancer, in 2015, a randomized controlled trial (COLORII Tri-al) of laparoscopy versus open surgery showed that laparoscopic surgery had a similar survival rate compared to open surgery [43].

Minimally invasive surgical techniques have reduced the physical burden on the patient and provided benefits such as fast postoperative recovery, less pain, and early return to daily activities even though they maintained the same oncologic outcomes as open surgery. In addition, intraoperative real-time sharing of surgical knowledge with trainees and the magnification effect on structures that are conventionally difficult to see represent another major benefit of laparoscopic surgery. Surgical techniques have been effectively demonstrated, contributing to surgical education and enabling precise procedures following anatomical dissection planes.

However, smaller incision sites have led to limitations in the size and view of the surgical field, which has greatly impacted the difficulties and limitations related to the surgical techniques. In rectal cancer, the positive CRM rate in the ALaCaRT Trial from Australia was 3% for open surgery, whereas it was as high as 7% for laparoscopic surgery, and similarly [44], in the ACOSOG trial, 8% for open surgery and 12% for laparoscopic surgery [45], pinpointing certain concerns about laparoscopic surgery. Laparoscopic outcomes tend to depend on the surgeon's level of skills. In our recent published study, we surveyed 440 surgeons who performed right hemicolectomy from 78 countries all over the world. It shows that over half of the respondents perform < 25% of right hemicolectomies laparoscopically [46]. We also conducted a survey of rectal surgical strategy including 535 surgeons who performed rectal cancer surgery in 89 countries and found similar results. Survey results highlight the real worldwide use of laparoscopic surgery for CRC treatment, stressing the need for training and, resource allocation, thereby improving intraoperative guidance [47].

In light of this situation, the focus of attention has been on "the augmented hand", i.e. the improvement of surgical instruments including robotic technology, and "the augmented eye", i.e. the development of image-guided surgery concepts, with the aim of solving problems in terms of surgical techniques and treatment strategies [48]. Laparoscopic CRC surgery still needs to be improved and the introduction of various surgical technologies may lead to better clinical outcomes in the future.

1.4 Major complications

1.4.1. Recurrence

Thirty to 40% of advanced CRC can be resected, and patients experience a recurrence within five years after the surgical resection [49, 50]. Rectal cancer has a higher recurrence rate compared to colon cancer. About 80% of recurrences are distant metastases [51], and the liver is the most common metastatic site, followed by the lungs and pelvic region. Local recurrence is about 20% [52], and perhaps due to the difficulty of surgical techniques, local recurrence is more common in the rectum [50]. Lymph node recurrence is also relatively common, particularly in rectal cancer [52, 53].

There are multiple risk factors correlated with recurrence [53]. Demographic factors include older age and male gender [54]. Factors related to tumor morphology and histopathology include higher T or N stage at diagnosis and the presence of extramural vascular invasion, signet cells, and tumor budding [51, 55–57]. Treatment-related factors include a positive CRM, anastomotic leakage, suboptimal preoperative (neoadjuvant) or postoperative (adjuvant) therapy, and a suboptimal number of lymph nodes in the resected specimen [49, 52, 58–60]. Other factors include high preoperative carcinoembryonic antigen (CEA) levels [61].

1.4.2. Anastomotic leak

Anastomotic leak (AL) is a major complication in digestive surgery. It is accountable for considerable morbidity and mortality [62, 63]. The AL incidence is particularly high following oesophageal (20–35%) and colorectal resections (4–19%) [64], and in cases which require extraperitoneal anastomosis [65]. The pathophysiology of AL is multifactorial and includes patient non-modifiable factors such as associated medical conditions, nutritional score, and oncological

status including neoadjuvant treatment. On the other hand, there are surgical modifiable factors, which influence the incidence of AL such as the transection level ensuring optimal perfusion. Adequate perfusion is a key component of the anastomotic healing process. However, an intraoperative evaluation of perfusion is mostly based on often unreliable clinical criteria, namely serosal discoloration, blood flow from the marginal artery, and pulsatile bleeding at the cut edge of the bowel [66]. As a result, there is a compelling clinical need to develop intraoperative technologies which enhance the surgeon's ability to quantify and identify transection and anastomotic sites.

1.4.2. Ureteral injury

Ureteral injury is a serious complication during intrapelvic surgery, and the majority of iatrogenic ureteral injuries may lead to severe morbidity and even mortality [67, 68].

The incidence of ureteral injury in colorectal surgery is not that high (0.25-1.1%). However, several studies showed that only 15 to 30% of intraoperative ureteral injuries are recognized [69–73]. Ureteral injury most frequently occurs during proctectomy and sigmoidectomy [74, 75]. Andersen *et al*. reviewed 18,474 colorectal resections based on the Danish National Colorectal Cancer database and reported that laparoscopic procedures were correlated with the risk of iatrogenic ureteral injury [76]. Surgeons should be familiar with the anatomy of the ureter and risk factors for injury [77], and research should be focused on finding accurate optical imaging modalities in order to prevent ureteral injury.
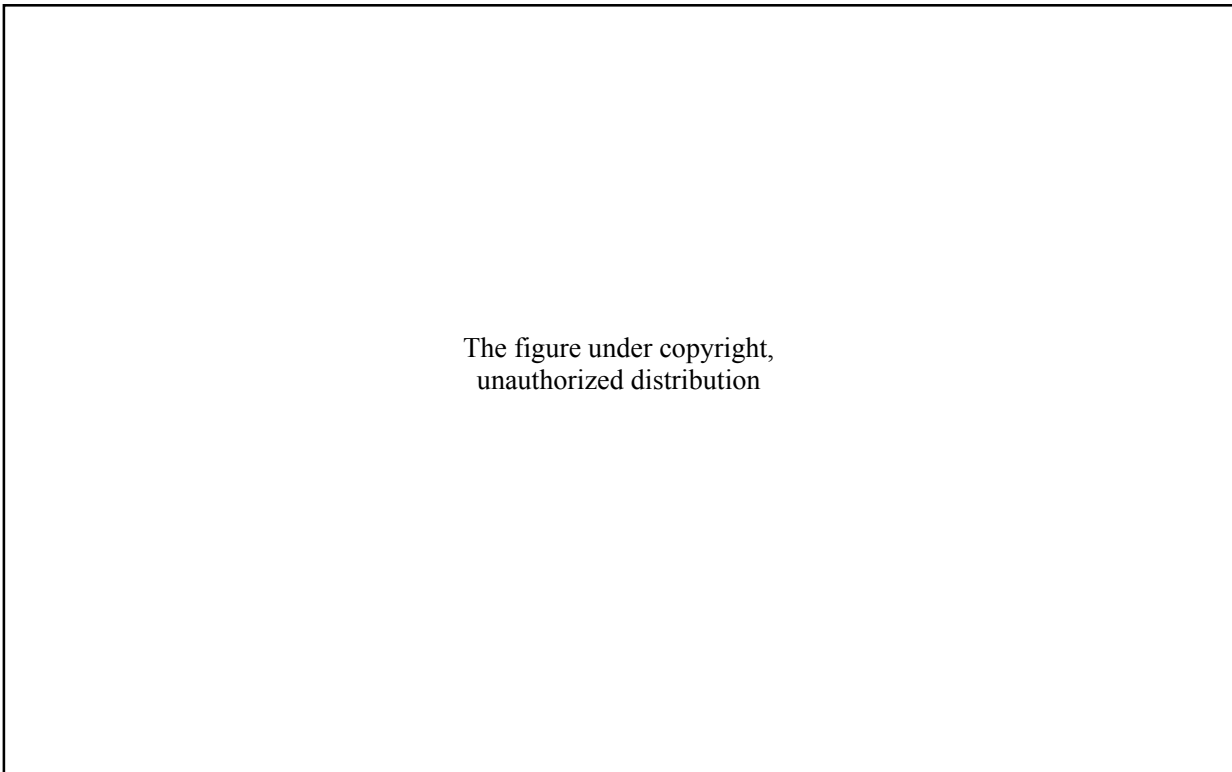
2. Image-guided surgery

One of the most important factors in performing a precise and safe surgery is the visibility of the anatomical structures of interest. The acquisition of high-quality information on tissues/structures in the body that cannot be seen with the naked eye without an incision in the body, or noninvasive imaging diagnostic technologies, began with the discovery of X-rays by Röntgen [78], and the development of ultrasound, X-ray computed tomography (CT) [79], as well as nuclear magnetic resonance imaging (MRI) [80] have made it possible to obtain multiple, high-quality in vivo images.

As mentioned earlier, minimally invasive surgery contributes to a reduced physical burden on the patient, such as early postoperative recovery, less pain, and shorter hospital stays, without compromising the outcomes of cancer treatment. However, there are some problems such as decreased visibility of lesions in the operating field and diminished tactile feedback. In conventional open surgery, the range of structures visible to the naked eye is wide, and the surgeon can directly touch and recognize key structures such as tumor-bearing organs and blood vessels which are not visible to the naked eye. In minimally invasive surgery, it is more difficult to confirm the anatomical structures of interest. It is crucial to assess the anatomical information obtained through diagnostic imaging modalities in the therapeutic strategy.

One of the solutions to this problem is to perform intraoperative diagnostic imaging to visualize the anatomy of the patient and the placement of surgical instruments. However, the use of X-rays and MRI during surgery mandates for hybrid operative rooms and adds complexity to the surgery. These intraoperative imaging technologies and equipment occupy a large surface area at the OR, and can only be introduced in very few facilities [81].

The second solution for surgical guidance is image-assisted navigation surgery, which aligns the patient with preoperative images taken by means of CT or MRI and presents the positional relationship between the lesion or surrounding tissues to the surgeon during the operation in real time. It has been used to provide surgeons with objective, quantitative, and accurate information on the location of tissues that cannot be seen during minimally invasive surgery and that have until now been assessed by the physician's experience and spatial cognitive abilities in the body. This system has the potential to contribute to the improvement of surgical accuracy and procedural safety. Many studies have been published showing the usefulness of this system in medical practice in orthopedics [82, 83] and neurosurgery [84] for rigid bones or stable organs surrounded by bones, urology for retroperitoneal organs [85], and thyroid surgery [86] surrounded by muscles. Surgical image-assisted navigation technology has made remarkable progress over the last decade.

The figure under copyright,
unauthorized distribution

Figure 3. A) Segmentation of a magnetic resonance, showing the fat around the rectum (=mesorectum) in orange, the rectum in brown, a tumour in green and the urinary bladder in yellow. B) 3D Virtual Reality model of the anatomy viewed on VR headset (HoloLens, Microsoft); the arrow displays the urethra (yellow circle); C) Intraoperative alignment of the virtual model to patient anatomy (Augmented Reality) using surface anatomy marking. D) Surgeon aligning the 3D virtual model.

However, preoperative images cannot accommodate intraoperative changes in the surgical field. In abdominal surgery, the intraoperative anatomy of soft organs, which are not rigid, is very different from that of preoperative imaging because soft organs are easily deformed and moved by respiratory and pulsatile motion and gravity, not to mention direct interference by the surgeon during surgery and this system is not easy to implement.

2.1. Near-infrared fluorescence (NIRF) image-guided surgery

NIRF image-guided surgery is a real-time medical imaging technique designed to intraoperatively guide the surgeon using an optical phenomenon [87].

Fluorescence is characterized by the emission of light via molecules (i.e. the fluorophores) excited by absorbing the energy of photons. In other words, the fluorophore (fluorescent contrast agent) absorbs (excites) light energy and becomes electronically excited. The fluorophore then emits photons and returns to its initial state. This post-excitation emission can be as small or as large as the same wavelength as the excitation wavelength. The magnitude of the displacement of the emission signal in the spectrum correlates with the detectability of the fluorescence. In Figure 4, we refer to fluorescence in the near-infrared (NIR) visible spectrum, although this phenomenon concerns the entire electromagnetic spectrum.
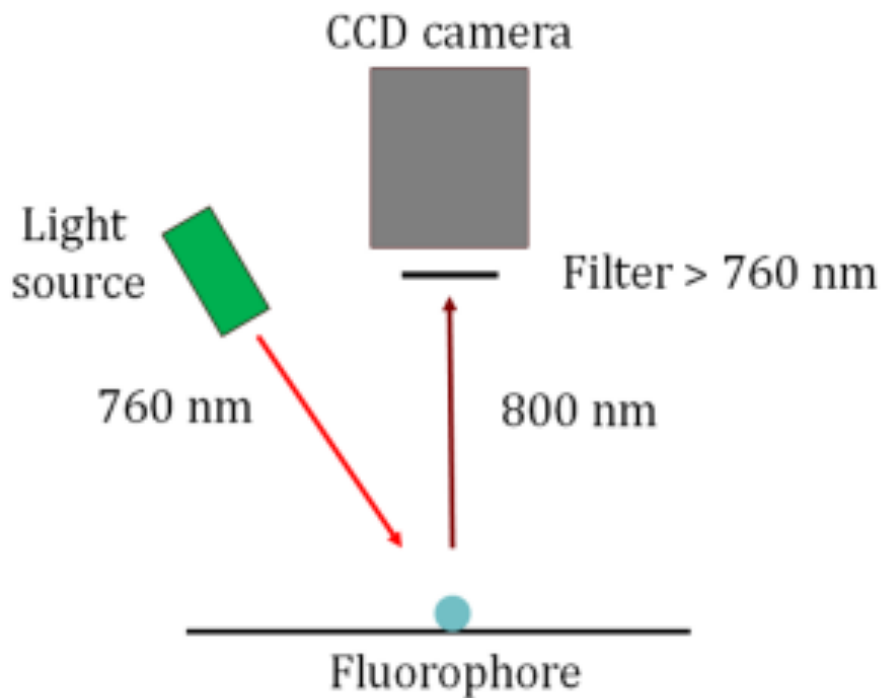
Figure 4. Basic schematic of the fluorescence-guided surgery principle.

Intraoperative fluorescence imaging is performed by administering an agent (fluorophore) locally or intravenously and irradiating a NIR light source with a wavelength of 700-900 nm into the surgical field. The NIR light source excites the fluorophore by changing its energy state, causing it to emit a fluorescent signal. Both the fluorescence excitation and fluorescence wavelengths are outside the absorption wavelength range of hemoglobin (<600 nm) and water (>900 nm), which exist in large amounts in the blood, and outside of the wavelength range of autofluorescence of living tissue (450 to 700 nm). NIR light has the advantages of a deeper tissue penetration depth and less autofluorescence than visible light, allowing visualization of not only the surface of the structure/tissue but also the inside of the structure/tissue.

NIRF imaging enhances intraoperative visualization of anatomical structures that should be respected during surgery. It can thereby influence surgical outcomes, such as the prevention of complications, diagnosis, staging, and improved radical resection of cancer.
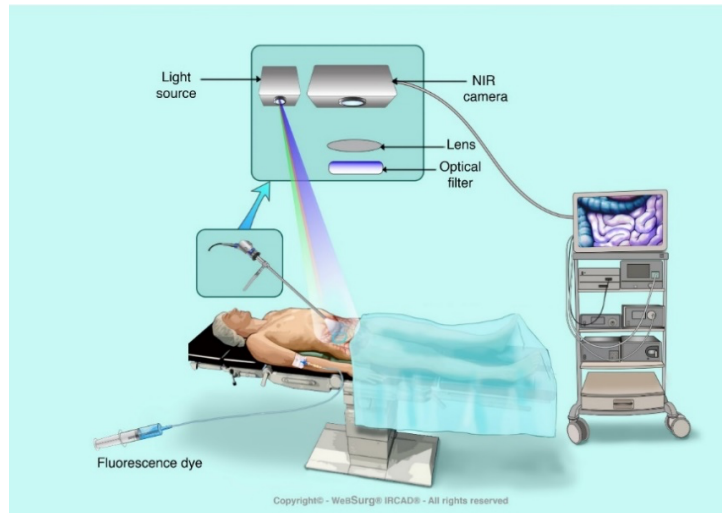
Figure 5. Schematic image showing the basic components required for NIRF imaging. The figure shows intravenous administration and visualization of a fluorescent contrast agent during laparoscopic surgery using a NIRF imaging system that includes a light source, optical filters, camera, image processing software, and hardware (©WebSurg® IRCAD®).

The figure under copyright, unauthorized distribution
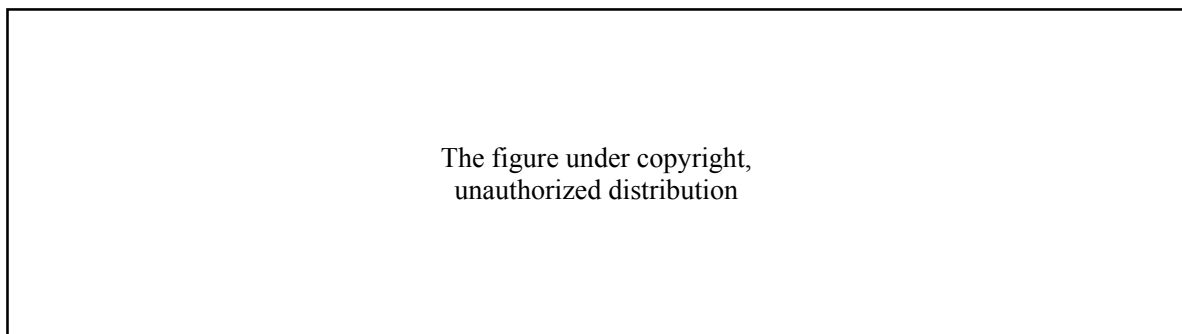
Figure 6. Image of NIRF currently used in rectal surgery to evaluate blood flow. (A) Red, Green, Blue(RGB) image. The white arrow is at the level of planned transection. (B) NIR camera image. The anastomosis was performed with the planned transection line (white arrow) (from Watanabe *et al.* Indocyanine green fluorescence imaging to reduce the risk of anastomotic leakage in laparoscopic low anterior resection for rectal cancer: a propensity score-matched cohort study. Surg Endosc 2020 Jan;34(1):202-208).

2.1.1. Selection of the dye

Various fluorophores, which can be characterized by their excitation and emission spectra, are available or under development. They can be classified into targeted and non-targeted fluorescent agents [88]. Non-targeted fluorescent agents are more common than targeted dyes, and more clinical trials are being performed.

It is essential to select the appropriate agent dependent on the targeted organ to obtain the correct image because each agent has different pharmacodynamic profiles including renal or hepatic clearance. In addition, the selection of a fluorescent dye requires consideration of 1) dosage, 2) time from administration to visualization, 3) pharmacological effects, and 4) route of administration (systemic or local).

2.1.1.1. Non-targeted agents

Indocyanine green

Indocyanine green (ICG) is currently the most widely used cyanine-based non-targeted fluorescent dye. Since ICG was approved by Food and Drug Administration (FDA) in 1959, it has been used primarily for the evaluation of blood vessels in contrast studies. In 1960, it was reported that it was used in transvenous administration in the evaluation of blood vessels in the ocular retina [89], and since then, other uses have expanded to include the assessment of cardiac output, assessment of liver function, measurement of blood flow in the liver, and ophthalmic angiography. Indocyanine green is a powder with a molecular weight of 775 and when it is bound to $\alpha 1$ lipoprotein in the body, it absorbs light at 790 to 805 nm and has a peak emission at 835 nm [90]. ICG has a half-life of 150 to 180 seconds and is removed from circulation rapidly and exclusively by the liver to bile juice. ICG is a non-toxic dye and the probability of allergy is very low (1:40,000

- 1:60,000) [91–94]. Intravenous administration of ICG has been used in, among others, intraoperative tumor demarcation [95], perfusion assessment at the level of the anastomosis [95–99], and extrahepatic bile duct differentiation [11, 101].

Methylene blue

Methylene blue (MB) has an excitation peak of about 700 nm, an excitation wavelength of 668 nm, and an emission of 688 nm [102–104]. It has also been approved by the FDA. However, it has lower fluorescence properties than ICG, displaying an excitation coefficient and quantum yield below the one of ICG. It has been used to identify sentinel lymph nodes in breast surgery [105]. In abdominal surgery, MB, which is partially cleared by the kidneys, is used to visualize the ureter [101, 102, 106]. However, Al-Taher *et al.* stated that its additional value for ureteral delineation in clinical practice is limited [107].

Sodium fluorescein

Sodium fluorescein (SF) is FDA-approved for ophthalmic applications (retinal and iris vasculature). It has a peak emission wavelength of 520 nm and it is used as a fluorescent contrast agent in multiple applications off-label or for research purposes [108]. SF is an essential fluorophore for confocal laser endoscopy imaging.

5-aminolevulinic acid

5-aminolevulinic acid (5-ALA), which has an emission peak at 635 nm, is a bioactive fluorophore and it has been used in a broad spectrum of surgical techniques such as guided ablation of malignant gliomas in neurosurgery [109] and detection of bladder cancer [110]. In recent years, it

has been successfully used to detect CRC [111]. The mechanism by which it selectively accumulates in tumors is unknown.

2.1.1.2. Targeted agents

Targeted agents are designed to bind to specific sites (ligands) and allow for the clear visualization of target tissues/structures where the ligand is highly expressed. Visualization of cancer cells by means of targeted agents is expected to allow very early-stage cancer detection and precise tumor demarcation and resection.

Anti-CA19-9 [112], anti-CEA [113], anti-EPCAM [114], anti-PSMA [115], and anti-EGFR [116] are some of the available target-specific fluorescent probes. However, there are significant regulatory barriers to this type of approach, as it takes a very long time to obtain approval for the clinical translation of these dyes [117].

2.1.2. Current situation

Over the past few decades, surgeons have made use of optical imaging technologies to enhance their vision in digestive surgery. The advantages of NIRF-guided surgery include high sensitivity, rapid feedback, no radiation, safety, user-friendliness, and this surgery does not require large devices that would take up the entire operating room space, and that do not interfere with the surgical workflow [118]. It is increasingly adopted, or at least for research, in the surgical field [48].

In colorectal surgery, there are a large number of studies on intraoperative NIRF surgery, which have been used to characterize tumors [95] and to evaluate perfusion at the level of anastomoses [90–93]. It is also known that ICG has a tendency to migrate to lymphoid tissues as well. It has also been used to identify sentinel lymph nodes [119], and to visualize real-time lymphatic flow intraoperatively [10, 120].

However, due to the limitation of the fluorescence intensity and the scattering effect of light by the tissue, the maximum wavelength is a few millimeters to 1cm from the tissue surface even with a relatively high-sensitivity camera [121]. Its limitation makes it challenging to visualize deeper anatomical structures. In addition, the narrow range of optimal concentrations makes it difficult to improve administration protocols (concentration, dose, and timing). For example, NIRF-guided surgery using ICG lymphadenectomy in CME requires endoscopic submucosal injection into the proximity of the tumor for at least 12 hours prior to the operation for precise intraoperative mapping [122]. Subserosal dye injection has also been studied to intraoperatively demonstrate lymphatic drainage [123]. However, one of the drawbacks of ICG is its water-soluble nature; as it diffuses over time, the ability to accurately locate affected areas is reduced.

2.2. Non-invasive contrast-free real-time optical imaging technologies

In NIRF imaging, the slow consistent diffusion of the fluorophore from perfused to non-perfused areas, as well as the lack of quantification of the fluorescence signal may lead to errors in the identification of marginal zones. Additionally, the estimation of perfusion using fluorescence angiography is limited to perfusion-only metrics (as opposed to the functional tissue status) and necessitates the injection of an exogenous agent [66].

In parallel to exogenous fluorescence, non-invasive contrast-free (i.e. endogenous) real-time optical imaging technologies have been developed. They are promising tools since they allow for an adequate surgical workflow without the constraints of administering external chemical compounds to the human body. Consequently, the clinical translation of endogenous optical imaging devices is strongly accelerating and disseminated.

In order to obtain physiological local information, most devices used are based on NIR spectroscopy, such as hyperspectral and multispectral imaging technologies [124–126]. Spectroscopic imaging allows for the non-contact reading of StO2 with high spatial resolution and with a large field of view (>15 by 15 cm^2), thereby improving intraoperative decision-making by adding quantitative information.

2.2.1. Hyperspectral imaging

Hyperspectral imaging (HSI) is a contrast-free optical imaging technology, which combines a photo camera and a spectroscope. It originated from remote sensing and was developed by NASA. It has been explored for various applications such as aerospace, vegetation analysis, and crime scene detection [127].

Most conventional optical imaging methods can only capture gray or Red, Green, Blue (RGB) color images. On the other hand, HSI, extending information beyond the boundaries of visible light to ultraviolet (UV) and NIR, can acquire two-dimensional images over a wide range of electromagnetic radiation (Figure 7).

The figure under copyright,
unauthorized distribution
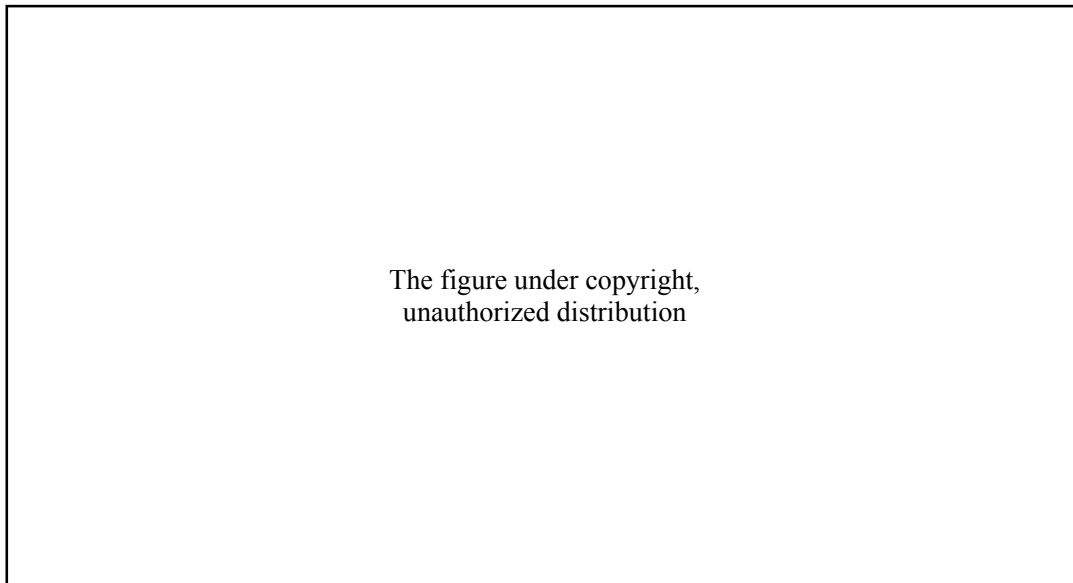
Figure 7. Schematic diagram of the electromagnetic spectrum; HSI can acquire images of a wide range of the electromagnetic spectrum beyond visible light (© 2016 SUNTORY GLOBAL INNOVATION CENTER LTD).

HSI acquires a three-dimensional dataset called a hypercube with two spatial dimensions (x, y) and one spectral dimension (λ). This spatial information allows the source of each spectrum on the sample to be identified [127] (Figure 8). As a result, it can be used to detect changes in the chemical composition of an object that cannot be identified via conventional imaging or spectroscopy alone.
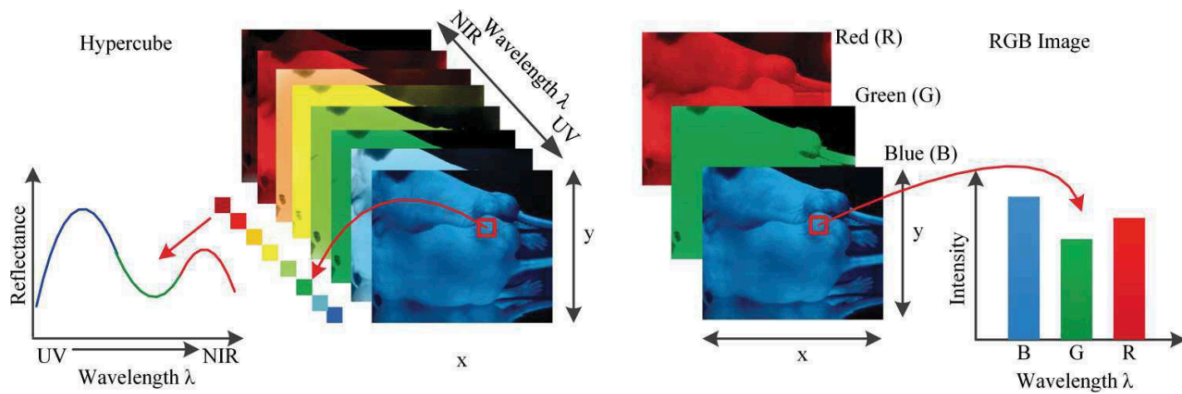
Figure 8. Comparison between hypercube and RGB image. Hypercube is a three-dimensional dataset of a two-dimensional image on each wavelength. The lower left is the reflectance curve (spectral signature) of a pixel in the image. The RGB color image only has three image bands on red, green, and blue wavelengths respectively. The lower right is the intensity curve of a pixel in the RGB image (from Lu G *et* Fei B. Medical hyperspectral imaging: a review. J Biomed Opt. 2014 Jan;19(1):10901).

HSI has the potential to be a useful tool in the medical field because it can expand the field of vision at molecular, cellular, and tissue levels. It is widely recognized that monochrome and RGB color imaging methods have limitations in detecting tissue abnormalities [128]. HSI can identify various abnormal conditions from the spectral features of each pixel in the image.

In surgery, HSI provides intraoperative and contactless quantitative imaging of intrinsic physiological properties [129], including tissue oxygenation, tumor identification [130, 131], and organ perfusion assessment [132, 133] (Figure 9).
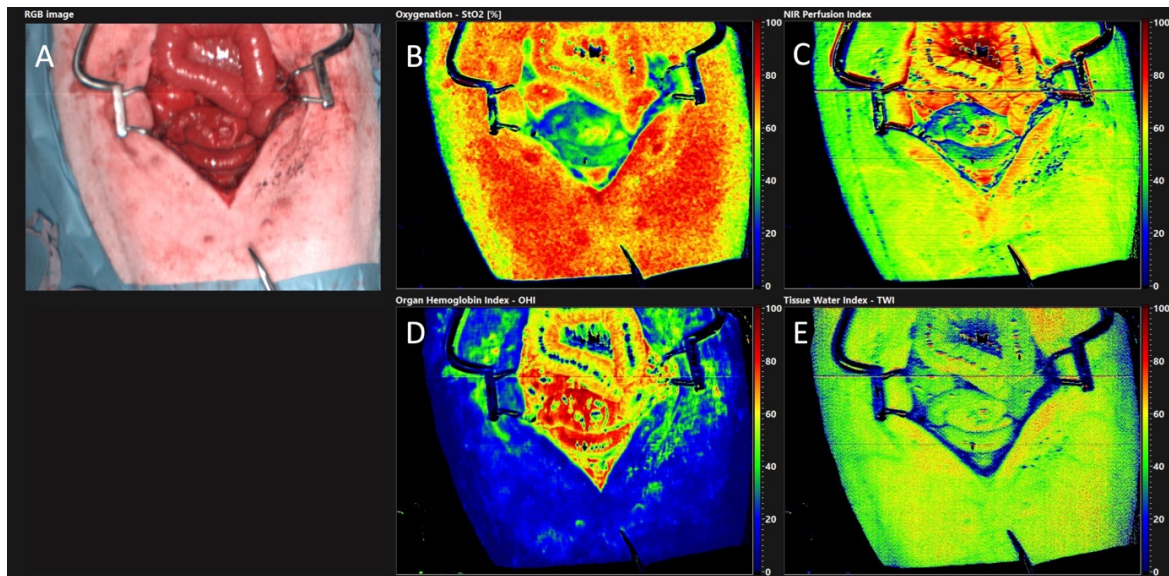
Figure 9. Hyperspectral imaging acquisition. The following images and biological parameters are acquired in a single shot; (A) RGB image, (B) Tissue oxygen saturation (StO2 [%]), (C) NIR Perfusion Index (NIR [index value]), (D) Organ Hemoglobin Index (OHI [index value]), (E) Tissue Water Index (TWI [index value]) (TIVITA Tissue, i) age reproduced (from Diaspective Vision GmbH, Germany, all rights reserved).

The research units at the Research Institute against Digestive Cancer (IRCAD) and The Institute of Image-Guided Surgery (IHU) of Strasbourg have developed a method of computer-assisted overlay of hyperspectral images to real images, defined as HYPER (HYPerspectral-based Enhanced Reality), and published their studies on intraoperative real-time bowel perfusion assessment [64] and the application for hepatic resection [134] as an image-guided surgical tool. The extracted hyperspectral data are also used to feed a machine learning system which enables automatic tissue recognition of tissues, and several studies have been published by their respective research units on the automatic recognition of nerves, blood vessels, and other key anatomical structures that are critical during surgery [135, 136], although research is still in its experimental stage.

2.2.2. Multispectral (MSI) imaging

An imaging technique using spectroscopy to measure light in multiple spectral bands is called multispectral imaging (MSI). Multispectral means multiple spectral bands. Whereas conventional RGB imaging uses three spectral bands (red, blue, and green), MSI acquires images by measuring multiple spectral bands (typically 4 to 15 bands) [137]. It was originally developed for military target identification and reconnaissance. MSI has been mounted on a small satellite to map the Earth's details regarding coastal boundaries, vegetation, and topography [138]. This image processing has also been used to analyze documents and works of art [137, 139].

The main differences between RGB imaging, spectroscopy, multispectral and hyperspectral imaging are listed in Table 1.
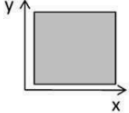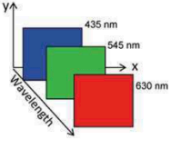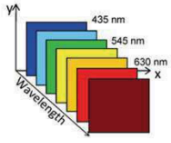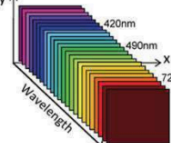
Feature	Monochrome	RGB	Spectroscopy	Multispectral	Hyperspectral
Spatial information	Yes	Yes	No	Yes	Yes
Band numbers	1	3	From several dozens to hundreds	3 to 10	From several dozens to hundreds
Spectral information	No	No	Yes	Limited	Yes
Multiconstituent information	No	Limited	Yes	Limited	Yes
Sensitivity to minor components	No	No	No	Limited	Yes

Table 1. Main differences between monochrome, RGB, spectroscopy, MSI, and HSI (from Li Q *et al.* Review of spectral imaging technology in biomedical engineering: achievements and challenges. J Biomed Opt. 2013 Oct;18(10):100901).

HSI has more spectral bands (up to several hundreds) and a higher spectral resolution than MSI. However, it takes longer to acquire and measure images. On the other hand, MSI can measure wavelength-dependent changes in the amount of light reflected by tissue and uses it to infer fundamental real-time physical properties such as oxygen saturation [140]. This technique has been demonstrated, albeit in its experimental stage, to be available in several organs, including the kidney [141], liver [142], brain [143], breast [144], as well as head and neck [145, 146]. In the field of digestive surgery, it has been demonstrated as a surgical application for the assessment of intestinal perfusion.

3. Current issues

Unfortunately, the recurrence rate remains high with a large worldwide variation. Almost 55% of CRC cases occur in more developed regions of the world, mortality is higher in underdeveloped countries [147]. Partially, this can be attributed to insufficient screening and to the difficulty related to rectal cancer surgery.

As previously referred to, results from our right colectomy survey including 440 surgeons from 78 countries and from our rectal surgery survey including 535 surgeons from 89 countries provided a general overview of the current situation. Over half of the respondents performed <25% of laparoscopic surgeries, stressing the low rate of laparoscopic surgery particularly in Africa and the Middle East. These surveys yielded a variety of valuable results [46, 47].

First, from an anatomical standpoint, a large heterogeneity was found in the respondents' definition of the rectosigmoid junction. Accurately defining the upper limit of the rectum is essential since preoperative staging, (neo)adjuvant radiotherapy/chemotherapy, surgical approaches, and adjuvant treatment differ significantly between sigmoid and rectal cancers. As a result, the accurate localization of a tumor originating from the sigmoid colon or rectum can have a significant impact on therapeutic decisions. However, accurately defining the upper limit of the rectum remains challenging to clinicians, and this is perhaps best illustrated by the variety of definitions described in clinical practice guidelines [148–150]. The most commonly chosen definition of the upper limit of the rectum was a fixed distance from the anal verge (23.4%). This definition is in line with the most recently published guideline on rectal cancer by the American Society of Colorectal Surgeons (ASCRS) [148]. The ASCRS classifies tumors with a distal extension to ≤15cm from the anal margin as rectal and more proximal tumors as colonic. However, this definition might not be a stable landmark as the length of the rectum may vary, depending on habitus and gender [148]. The

European Society for Medical Oncology (ESMO) defines tumors above the peritoneal reflection as colonic [150]. Nineteen percent of respondents used the sigmoid takeoff as the definition of the upper limit of the rectum. The sigmoid takeoff is defined as the transition of the sigmoid mesocolon to the mesorectum. In an international Delphi consensus survey, the most agreed consensus definition was the sigmoid takeoff (56% of respondents agreed upon this definition [151]) among 132 experts in CRC. Several retrospective studies and a surgical specimen validation study found that the sigmoid takeoff was a stable and consistent radiographic landmark which was less affected by the tumor's extent [152–154]. In our survey, only 19% of respondents used this landmark as the definition of the upper limit of the rectum. Inter-observer variability remains an issue [153].

Secondly, regarding surgical techniques, there is a large variation in anastomotic methods among institutions. In the laparoscopic right hemicolectomy, the majority of respondents (68.6%) stated that they perform an extracorporeal anastomosis. There are several studies comparing extracorporeal anastomosis with intracorporeal anastomosis [155–159]. A recently published meta-analysis including 4,450 patients showed that intracorporeal anastomoses are associated with smaller extraction site incisions, earlier bowel recovery, fewer complications, and lower rates of conversion, surgical site infections, anastomotic leakage, and incisional hernia as compared to extracorporeal anastomosis [160]. However, many of the included studies have a short-term follow-up and remain unclear with regards to both groups for oncological outcomes.

In rectal surgery, more than half of the respondents routinely used a high-tie technique as opposed to a low-tie technique during TME. A 'low-tie' is performed by ligating the inferior mesenteric artery (IMA) peripheral from the origin of the left colic artery, whereas a high tie is performed by ligating the IMA close to its origin from the aorta. The reported advantages of a high ligation included an improved surgical radicalization, an improved nodal harvesting, and reduced

anastomotic tension [161–164]. However, the high ligation of the IMA might result in a decreased anastomotic perfusion, which may result in a higher rate of anastomotic leakage [165–167]. Several systematic reviews, meta-analyses, and randomized controlled trials found no significant difference in anastomotic leakage, survival, lymph node harvesting rate, oncological outcomes, bleeding risk, postoperative complications, and operative time between low-tie and high-tie ligations [168–171]. The HIGHLOW trial, a prospective randomized controlled trial demonstrated that a low ligation in low anterior resection (LAR) resulted in a superior genitourinary function preservation as opposed to a high ligation [171]. The ASCRS does not recommend the routine use of a high-tie ligation due to insufficient evidence supporting its oncological superiority, a potential increased risk of anastomotic leakage, and a decreased preservation of genitourinary function as opposed to a low-tie ligation [172]. The ASCRS only recommends to use a high-tie technique in selected patients when clinically suspicious lymph nodes are present at the level of the IMA and/or when a high tie is necessary to provide mobilization and achieve an adequate length for a tension-free anastomosis [172]. The ESMO, NCCN, and the Society of American Gastrointestinal and Endoscopic Surgeons (SAGES) guidelines do not provide recommendations on the choice of the tie technique.

In CRC surgery, it is necessary to resect not only the colon or rectum but also the mesentery which includes the lymph nodes and the lymphatic flow, to prevent any recurrence. However, such an extensive resection also increases the risk of complications. The balance of such factors is of paramount importance. Although the anatomical definitions and surgical techniques described above are based on efforts to reduce complications and recurrences, they remain controversial.

In addition, as this survey shows, there is still a significant gap between the recommendations of international guidelines and surgical societies and the procedures performed in the current medical practice. This gap is even more marked in centers where laparoscopic surgery is not used.

Image-guided surgery materializes the invisible during surgery. For example, visualization of vessels and assessment of intestinal perfusion can help to determine the line of bowel dissection, assess blood flow at the bowel anastomosis, and identify the lymph nodes that need to be removed, thereby simplifying surgery and potentially filling the gap.

4. Outline of this thesis

The scope of this thesis is to examine the adaptation and feasibility of novel approaches and techniques for the complete resection of CRC by means of image-guided surgery in order to promote better clinical outcomes and prevent recurrences and complications related to CRC.

Study 1 aimed to develop a new image-guided surgical technique to reduce the risk of CME, which is not yet widespread due to the risk of complications, and to perform CME more simply and accurately. We examined the feasibility of using an HSI system to capture anatomical tissues around the colon and analyze the image data using deep learning to automatically recognize the areas that should be resected and those that should be preserved.

Study 2 examined whether contrast-free MSI could be used in digestive surgery to assess intestinal blood flow that should be evaluated to prevent anastomotic leakage, a fatal complication that is common in colorectal surgery.

Study 3 investigated whether the use of an imaging system that has multiple NIR channels with fluorescent dyes (i.e., ICG and MB injected simultaneously) can detect mesenteric lymph nodes, a common cause of recurrence in CRC surgery. This study also assessed the use of two NIR dyes to mitigate individual disadvantages allowing for a thorough NIRF image-guided surgery.

EXPERIMENTAL WORK

Background and aims

STUDY 1: Computer-assisted differentiation Between Colon-Mesocolon and Retroperitoneum Using Hyperspectral Imaging (HSI) Technology

A sound understanding of colorectal anatomy is crucial to the correct performance of CME and prevention of surgical complications. Culligan *et al.* [173] precisely described the fusion fascia, which is located between the mesentery, the retroperitoneum, and a surgical exfoliation layer that is formed within the fusion fascia. The authors demonstrated that the surgical exfoliation layer can be deliberately dissected when mobilizing the colon and its mesentery. This extensive dissection between the mesentery and the retroperitoneum in CME is generally performed by visually assessing differences in the microvasculature, which is subjective and requires a high level of expertise. In addition, in some cases, it is challenging to recognize these subtle patterns with the naked eye or with white light laparoscopy. These technical details represent major obstacles to the identification of adequate cleavage and dissection planes during CME. The intraoperative identification of anatomical layers can protect organs from iatrogenic damage during colorectal surgery.

Machine learning and deep learning (DL), combined with optical imaging, are gaining popularity in the medical field to support surgical decision-making using large training datasets. Artificial intelligence (AI) and computer vision have improved computer-assisted diagnosis by recognizing dysplastic/neoplastic polyps in image-guided surgery by detecting critical steps during minimally invasive procedures such as endoscopic sleeve gastrectomy (ESG) [174]. At present, AI algorithms are frequently developed using standard color images with three optical channels of RGB, which have significant limitations, such as the lack of quantitative parameters. AI automatic recognition of colorectal tumors is still in its infancy and quantitative optical imaging modalities such HSI

could help further advance AI algorithms for higher accuracy and precision. The combination of HSI and AI has recently reported promising results. Using a four-layer neural network, Boris Jansen-Winkeln *et al.* achieved an 86% sensitivity and a 95% specificity in identifying CRC [175]. Barberio and Collins *et al.* show that HSI combined with convolutional neural networks (CNNs) could be used to automatically recognize key anatomical structures such as blood vessels and nerves [135]. Collins and Maktabi *et al.* [136] showed that colorectal and esophagogastric cancer could also be detected with various machine learning models, and a convolutional neural network (CNN) often produced the best results.

The aim of this study was to assess the accuracy of HSI technology in combination with CNNs to automatically distinguish colonic and mesenteric tissue (which are to be resected in CME) from retroperitoneal tissue (which is to be spared).

STUDY 2: Quantification of bowel ischaemia using real-time multispectral Single Snapshot Imaging of Optical Properties (SSOP)

Single snapshot of imaging optical properties (SSOP) has recently been developed and it is a contrast-free, real-time, non-invasive optical imaging technique, which allows to evaluate physiological tissue properties [176]. SSOP is based on the well-known diffuse optimal imaging method named spatial frequency domain imaging (SFDI), which uses light propagation models to quantify optical properties discriminating physiological contrast from tissue constituents [177]. As a result, multispectral SSOP can determine tissue oxygenation (StO2) by computing the fraction of oxygenated over total haemoglobin in real time. It has proven to be an efficient method since it allows to reduce the number of image acquisitions to a single frame, which is very convenient in the surgical setting, hence allowing for real time video-rate imaging of StO2 and preventing from workflow disruption [178]. The performance of multispectral SFDI and SSOP have previously been evaluated both ex vivo and in vivo and they have proven to achieve a high accuracy (i.e. less than a 10% error) [179–181].

The aim of this experimental study was to preclinically evaluate the accuracy of multispectral SSOP in quantifying bowel perfusion using normalised capillary lactate as a validated perfusion biomarker.

Study 3: Simultaneous, multi-channel, near-infrared fluorescence visualization of mesenteric lymph nodes using indocyanine green and methylene blue: a demonstration in a porcine model

NIRF imaging with ICG has also been used for sentinel node identification [119, 182, 183], and intraoperative real-time lymph flow visualization [10, 120, 184] since it is known that ICG has a tendency to migrate to lymphatic tissues. However, one of the drawbacks of ICG is its high affinity for albumin and progressive diffusion in tissues, which reduces its capacity to accurately locate affected areas [185].

NIRF imaging with MB has mostly been used in CRC surgery for intraoperative visualization of the urinary tract, and in particular, the ureter, due to its renal clearance [102, 107, 186]. There have been several studies using MB to detect sentinel lymph nodes in CRC [187] and for postoperative lymph node harvesting [188, 189].

MB has an excitation peak at 688 nm, which restricts its use to few optical imaging devices since most NIRF imaging systems are designed for imaging with ICG. An example of a dual imaging system in the QUEST SPECTRUM® 3 (Quest Medical Imaging, Middenmeer, The Netherlands), camera which has two dedicated NIR channels for simultaneous intraoperative fluorescence guidance, which thus enables imaging of both MB and ICG. As previously stated, the differences in peak excitation and pharmacodynamics between MB and ICG reflect their different principal applications in the clinical setting. In colorectal surgery, Polom *et al.* were able to identify the location of the ureter using MB while assessing intestinal perfusion to determine the optimal anastomotic site with ICG using a single camera system. Their results highlight the feasibility of multi-wave imaging to aid in preventing two of the most common complications in colorectal surgery, namely anastomotic leak and ureteral injury. The relevance of simultaneous, multi-

channel, near-infrared fluorescence imaging may represent a pathway towards increased surgical safety [190].

This study's primary aim was to validate whether intravenously administered MB and ICG act simultaneously as fluorescence dyes for lymph node detection. As a secondary aim, we compared the fluorescence performance of MB and ICG in lymph node detection.

Materials and methods

Ethics and animal models

STUDY 1: Computer-assisted differentiation Between Colon-Mesocolon and Retroperitoneum Using Hyperspectral Imaging (HSI)Technology

All experiments were performed at IRCAD (Strasbourg, France). A total of 20 adult pig models (Sus scrofa domesticus, ssp. large white, mean weight: 40 kg) were included. The study was part of the ELIOS protocol (Endoscopic Luminescent Imaging for Oncology Surgery), fully approved by the local Ethical Committee on Animal Experimentation (ICOMETH No. 38.2016.01.085) and by the French Ministry of Superior Education and Research (MESR) (APAFIS#8721-2017013010316298-v2). All animals used in the experimental laboratory were managed according to French laws for animal use and care and according to the directives of the European Community Council (2010/63/EU) and ARRIVE guidelines [191]. The animals were housed and acclimatized for 48 h in an enriched environment, respecting circadian cycles of light/darkness, and with constant humidity and temperature conditions. They were fasted 24 h before surgery, with ad libitum access to water, and finally sedated (zolazepam + tiletamine 10 mg/kg IM) 30 min before the procedure in order to decrease stress. Anesthesia induction was administered with propofol (3 mg/kg) injected intravenously (18 G IV catheter in an ear vein). The animals were maintained with rocuronium (0.8 mg/kg) along with inhaled isoflurane 2%. At the end of the protocol, animals were euthanized with a lethal dose of pentobarbital (40 mg/kg).

STUDY 2: Quantification of bowel ischaemia using real-time multispectral Single Snapshot Imaging of Optical Properties (SSOP)

All experiments were performed at IRCAD (Strasbourg, France). A total of 6 adult pig models (Sus scrofa domesticus, ssp. Large white, mean weight: 40 kg) were involved in this non-survival study. The present experimental study is part of the QuantSURG (Quantitative Surgical Guidance for Colorectal Surgery) project, which received full approval from the local Ethical Committee on Animal Experimentation (ICOMETH No. 038.2019.01.121) and from the French Ministry of Superior Education and Research (MESR) under the following reference: APAFIS #20,819– 2,019,052,411,591,088 v3. All animals used in the experimental laboratory were managed according to French laws for animal use and care and according to the directives of the European Community Council (2010/63/EU) and ARRIVE guidelines [191]. The animals were fasted for 24 h with free access to water before surgery. Animals were premedicated, 10 min before surgery with an intramuscular injection of ketamine (20 mg/kg) and azaperone (2 mg/kg) (Stresnil; Janssen-Cilag, Belgium). Intravenous propofol (3 mg/kg) combined with rocuronium (0.8 mg/kg) were used for induction. Anaesthesia was maintained with 2% isoflurane. At the end of the procedures, pigs were sacrificed with an intravenous injection of a lethal dose of potassium chloride.

Study 3: Simultaneous, multi-channel, near-infrared fluorescence visualization of mesenteric lymph nodes using indocyanine green and methylene blue: a demonstration in a porcine model

This study was performed at the animal laboratory of the Maastricht University Medical Center (MUMC+, Maastricht, The Netherlands). The experiments were performed in three female Dutch landrace pigs (mean weight: 40 kg). Animals were used in compliance with Dutch regulations and legislation concerning animal research, and the study was performed according to a protocol approved by the local animal ethics committee. All surgical procedures were performed under general anesthesia. Intramuscular injection of azaperone 3 mg/kg, ketamine 10 mg/kg, atropine 0.05 mg/kg, thiopental 10-15 mg/kg, isoflurane (dose depending on the effect), and oxygen 20-40 mL/kg/min was used as standard medication to ensure appropriate sedation and analgesia. All variations in vital parameters were continuously monitored. At the end of the protocol, animals were euthanized with a lethal dose of pentobarbital (40 mg/Kg).

Methods

STUDY 1: Computer-assisted differentiation Between Colon-Mesocolon and Retroperitoneum Using Hyperspectral Imaging (HSI)Technology

Hyperspectral Camera

The HSI camera (TIVITA®, Diaspective Vision GmbH, Germany) was a push-broom scanning device with a complementary metal oxide semiconductor (CMOS) image sensor with a spatial resolution of 640 × 476 pixels and a spectral range from 500 to 1000 nm (5 nm spectral resolution increments, totaling 100 bins). In the first increment, 501 wavelength bands were used from 500 to 1000 nm. In a second increment, 5x binning in wavelength direction was performed. The final cube included 100 bins, that is, the wavelength from 500 to 995 nm, but because of the binning the wavelength from 996 to 999 was included. The camera system is attached to a side arm of a medical cart carrying the PC (Figure 10).

Figure 10. The TIVITA® Tissue System is composed of the HSI camera attached to a side arm and integrated on a cart together with the PC; image © Diaspective Vision GmbH, Germany 2022

The HSI camera was positioned 50 cm above the ROI and, immediately before and during image capture, environmental lights and ventilation were paused. Capture time took approximately 6 s, and the placement of the camera during the procedure is represented in Figure 11.
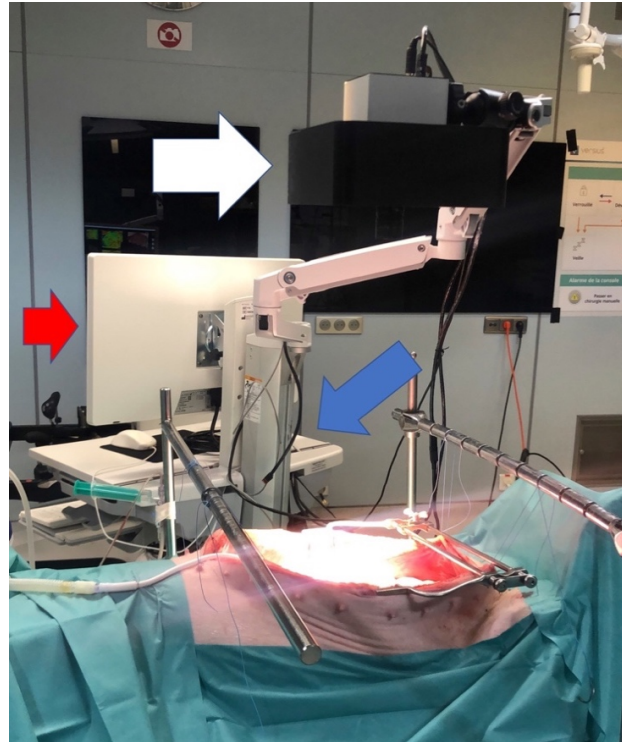
Figure 11. Set-up during experiments: The abdominal cavity was accessed via a midline laparotomy to expose the regions of interest (i.e., sigmoid colon, sigmoid mesocolon, and retroperitoneum). The distal lens of the hyperspectral camera was positioned 50 cm above the regions of interest. External light interference was avoided during the acquisition of images. The TIVITA™ tissue camera is composed of a lightning unit (white arrow), a medical cart (red arrow), and a Box PC (blue arrow).

Deep learning model

Based on a previous animal study from Barberio and Collins *et al.* comparing the two most successful deep learning models, support vector machines (SVMs) [192–194] and CNNs for HSI image segmentation, the CNN model achieved an overall higher sensitivity for all tissue classes (89.4%) except for the nerve class, which had a sensitivity of 76.3% [135]. Therefore, HSI

combined with deep learning allows to automatically discriminate six different tissue classes (artery, vein, adipose, muscle, skin, and nerve) supporting our decision to adopt the CNN model in this study.

Anatomical relevance and surgical procedure

Anatomical structures and their embryological phylogeny should be understood during surgery. The mesentery and the retroperitoneum are derived from the same embryological structure referred to as mesoderm and they are connected to the abdominal cavity. The mesentery is a double layer of peritoneum, which includes retroperitoneum, connective tissue, blood vessels, nerves, lymph nodes, and adipose tissue [195]. The mesentery and retroperitoneum spectral profiles differ based on several parameters, including but not limited to water content (peaking at about 980 nm) and adipose content (peaking at about 740 nm) [140]. In addition, the spectral profile of hemoglobin (Hb) significantly differs between the oxygenated and deoxygenated states and strongly contributes to the overall tissue spectral profile [196]. Changes in hemoglobin concentration and oxygen saturation due to vascular content can be measured using HSI. To expose intraperitoneal and retroperitoneal structures, the abdominal cavity was accessed via a midline laparotomy and a self-retaining retractor was placed to expose the region of interest (ROI). HSI images were obtained from the right or left side of the sigmoid colon mesentery at the level of the inferior mesenteric artery, including the sigmoid colon and the retroperitoneum.

Annotation

Immediately after each image acquisition, the operating surgeons used an image manipulation software (GIMP, GNU Image Manipulation Program, open source) to manually annotate the RGB images associated with each HSI (Figure 12A). Figure 12B shows example annotated images

visualized in grayscale with overlaid annotations represented as colored regions. Annotations in green represent tissue to be removed (colon and mesocolon), and purple annotations were used for the tissue to be preserved (retroperitoneum). The total number of annotated colon-mesocolon pixels was 357,811, with an average of 17890 ± 12438 (SD) per image. The total number of annotated peritoneum pixels was 81,655, with an average of 4083 ± 3749 (SD) per image. Consequently, the data had a moderate class imbalance of 4.32:1.

A CNN was then trained to distinguish colon and mesocolon tissue from retroperitoneal tissue using deep learning.
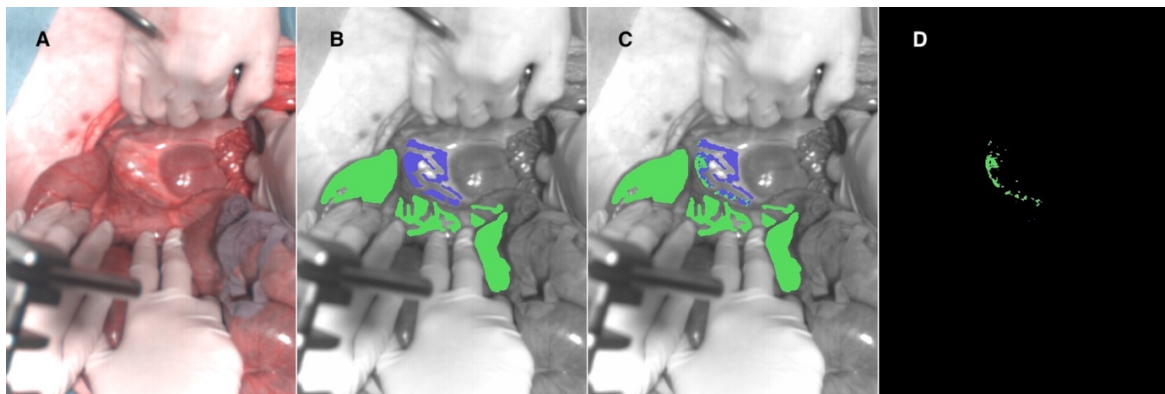
Figure 12. Example visualization of automatic tissue recognition results provided by CNN model automatic recognition. A. The RGB image was extracted from HSI data. B. The image was annotated by expert surgeons. C. The predicted classifications from the CNN model. D. The error map. Green annotations represent tissues to be resected (colon and mesocolon) and purple annotations are for the tissues to be preserved (retroperitoneum) during CME.

CNN model training and evaluation

Image processing pipeline with a trained CNN

For each pixel of interest in an HSI, one HSI sub-volume was extracted and centered on the corresponding spatial coordinates of the pixel. This sub-volume was then integrated into a trained CNN, which generated a predictive score for the two tissue classes, and the tissue class with the

highest score was associated with the pixel. This process was then repeated for each pixel, generating a spatial tissue prediction map (also known as image segmentation).

CNN architecture

CNNs have been the dominant machine learning model for pattern recognition in optical image data, including HSI [197, 198]. A CNN learns relevant spatio-spectral features through a series of trainable convolutional filters (hidden layers). The extracted features are fed to the following layer in order to generate a hierarchy of spatio-spectral features. The filter weights are trainable parameters, which are automatically adjusted during training. Deeper hidden layers are used to extract higher level features. Based on the extracted features, the last layer determines the classification prediction.

The CNN architecture that we selected [199] has been shown to work well on related tissue recognition problems [135, 136], and its architecture is provided in Table 1 in the supplementary material. The architecture of the CNN is provided in Figure 13. The CNN used a spatial window of 5 by 5 pixels, and had 31,532 trainable parameters with 7 hidden layers, including 6 convolutional layers with ReLU activations. It had one fully connected final layer with 2 output neurons corresponding to two classes; the first class was colon or mesocolon tissue (colon-mesocolon), and the second class was retroperitoneal tissue. Class imbalance was handled in the training loss function by down-weighting the majority class using Inverse Frequency Median Weighting [200].
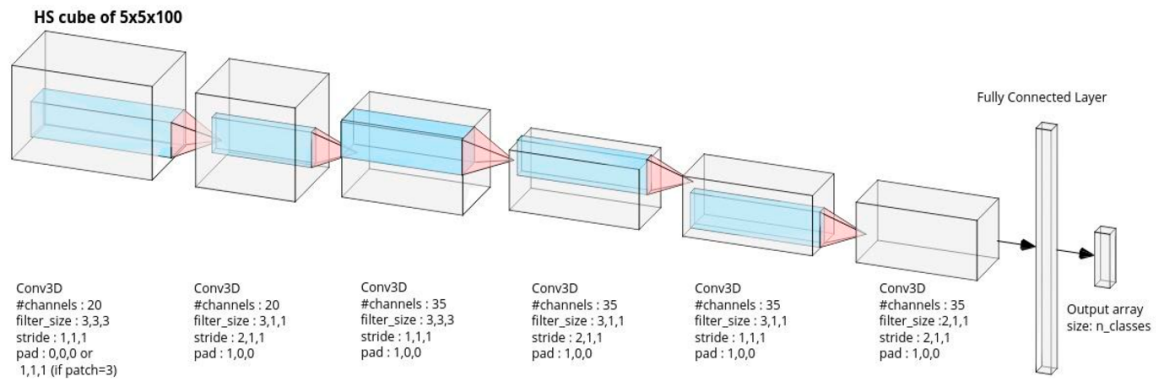
Figure 13. Convolutional neural network architecture: The input is an HSI sub-volume cube centered on a given pixel, with 5 × 5 spatial dimensions and 100 wavelength dimensions. The input is transformed into a final 1D feature space vector using down-sampling convolutional operations a. This is followed by a final, fully-connected layer to produce the tissue prediction scores. (From: Barberio, Collins, *et al.* Deep Learning Analysis of In Vivo Hyperspectral Images for Automated Intraoperative Nerve Detection. Diagnostics (Basel). 2021 Aug 21;11(8):1508.)

Table 2: Details of the CNN architecture

Layer	Filter shape	Number of output channels	Stride	Number of trainable parameters
Conv1	(3.3.3)	20	(1.1.1)	560
ReLU	/	/	/	/
Pool1	(3.1.1)	20	(2.1.1)	1220
Conv2	(3.3.3)	35	(1.1.1)	18935
ReLU	/	/	/	/
Pool2	(3.1.1)	35	(2.1.1)	3710
Conv3	(3.1.1)	35	(1.1.1)	3710
ReLU	/	/	/	/
Pool3	(2.1.1)	35	(2.1.1)	2485
ReLU	/	/	/	/
FC	(455.2.1)	2	/	912

Total trainable parameters: 31532

Table 2. Details of the CNN architecture. The CNN comprises three convolutional layers (Conv1, Conv2, and Conv3) and three pooling layers (Pool1, Pool2, and Pool3). All 3 pooling layers were implemented as 1D convolutional filters (filtering in the spectral dimension), and they included a stride of 2in the spectral dimension, and a stride of 1in the two spatial dimensions. The stride had the effect of reducing the spectral dimension by one half at each pooling layer.

CNN training

HSI sub-volumes were centered on every annotated hyperspectral image pixel, forming spatial patches of 5 by 5 pixels, corresponding to 5 by 5 by 100 sub-volumes. The third sub-volume dimension corresponded to the spectral dimension, which represented 100 spectral wavelengths produced by the camera. In total, there were 439,466 training samples. To train and test the CNN, annotated sub-volume samples were split into training and test sets using 5-fold cross-validation (CV). Importantly, this was conducted so that the CNN was never trained and tested on data from the same animal. The 20 hyperspectral images (1 per animal) were randomly partitioned into 5 sets (S1, ...S5), with each set having 4 HSIs. Five CNN models were then trained. The first CNN was trained using the annotated HSI sub-volumes in sets S1, S2, S3, and S4, (16 images) then its performance was tested on the annotated sub-volumes in set S5 (4 images). Four other CNN models were trained similarly, each using a different test set that was excluded from its training set. The CNNs were trained using batch gradient descent with binary cross entropy loss function and inverse median frequency class balancing. Training was run for 250 epochs using a batch size of 8192, a learning rate of 0.01 and a weight decay of 0.0005. The CNNs were implemented using PyTroch v1.4.

Performance metrics and statistical methods

Performance was evaluated with standard metrics used in machine learning, implemented by means of Python scikit-learn (https://scikit-learn.org). Sensitivity, specificity, and two other well-established performance metrics were used, i.e., the F1 score, and the Receiver operator curve area-under-curve (ROC AUC). Unlike sensitivity and specificity, F1 gives a single performance score (the harmonic mean of recall and precision). The ROC-AUC is a complementary

performance statistic, which shows the model's ability to rank samples (it gives a higher score for a true class compared to a false class). Unlike sensitivity, specificity and F1, ROC AUC is popular since it indicates the model's predictive performance without requiring any decision threshold.

STUDY 2: Quantification of bowel ischaemia using real-time multispectral Single Snapshot Imaging of Optical Properties (SSOP)

SSOP imaging

SSOP is based on the projection of spatially modulated patterns of light on the sample and on the acquisition with a camera of the diffused back reflected light. SSOP was developed as a real-time implementation of more time-consuming spatial frequency domain imaging (SFDI) methods, which require several frames for the extraction of the optical properties of tissues. Indeed, in a standard SFDI workflow, two different spatial frequency (f_x) profiles (e.g. $f_x = 0$ mm^{-1}, $f_x = 0.2$ mm^{-1}) with three-phase shifts for each of them are projected on the sample surface, allowing for the demodulation of the signal into its DC and AC components [201]. Differently, SSOP requires only a single high-frequency pattern to be projected on the tissue, thanks to a Fourier's domain filtering approach for the demodulation step [176, 179, 181], thereby reducing from 6 to 1 the number of frames required for the acquisition and allowing for a real-time capability of the imaging system. Further to the demodulation, both SFDI and SSOP share the same workflow starting from a calibration step involving the measurement of a calibration phantom with known optical properties. The measurements of this tissue-mimicking phantom allow to compute the diffuse reflectance maps for the sample, i.e. R_{DC} ($f_x = 0$ mm^{-1}) and R_{AC} ($f_x = 0.2$ mm^{-1}). Finally, a Monte Carlo-based lookup table (MCLUT) algorithm allows to retrieve the optical properties of the

sample (i.e. absorption and reduced scattering coefficients) for each pixel of the image [202]. The natural consequences of the single frame approach are a degradation in image quality and the presence of edge artefacts. Nevertheless, significant improvements have been achieved in recent years by first optimising the filtering technique [203] and by adopting deep neural network approaches for the demodulation [179, 181]. Additionally, the latest developments on SSOP also account for a tridimensional profile correction of the sample in order to reduce the quantification error of SSOP associated with a variation of light intensity across non-flat sample surfaces [179]. Further information regarding SFDI is available as follows: http://opensfdi.org.

Deep learning method for SSOP

For this study, the latest SSOP deep learning-based approach has replaced the standard Fourier's domain filtering technique to improve the overall image quality, as described by Aguénounon *et al.* [179]. In brief, two dedicated CNNs based on a U-Net architecture were used for the extraction of the modulation amplitude of the signal for each spatial frequency, and for the profilometry analysis of the surface profile of the sample. Both networks were trained using high-quality images obtained with SFDI acquisition sequences (with 7-phase shifts instead of 3 in order to enhance quantification accuracy and image quality) and optimised for efficient and low-cost computation performances, allowing for a real-time capability and achieving high visual quality optical property quantification for up to 1-megapixel images. The training dataset consisted of a total of 200 high-quality images divided into n = 40 images of tissue-mimicking silicone phantoms with different optical properties ranging from $\mu_a = 0.005$ to 0.05 mm^{-1} for absorption and from $\mu_s' = 0.5$ to 3 mm^{-1} for reduced scattering; n = 52 images of hands from different Caucasian men and women in various configurations; n = 108 images from ex vivo and in vivo swine organs in several

orientations (stomach, small bowel, colon, kidney, pancreas, liver, and spleen). Additional information regarding SSOP and its deep learning implementation (code and sample data) are available as follows: https://healthphotonics.org/ressources/ sfdi-resources/.

Trident imaging system

The Trident imaging system is based on a digital micro-mirror device (DMD, Vialux GmbH, Chemnitz, Sachsen, Germany) to project structured light in the form of sinusoidal patterns at a 45 ± 5 cm working distance. The projection system is fibre-coupled to a dedicated, custom-made class 3R high-power laser source composed of laser diodes (LDX Optronics, Maryville, TN, United States), which is used to project patterns at 2 wavelengths (i.e. 665 nm and 860 nm) for oxygen saturation multispectral measurements [204]. A white high-power LED lamp (FTIII24017-12, Fiberoptics Technology Inc., Pomfret Center, CT, United States) is also used to illuminate the surgical field to provide anatomical visualisation specifically filtered to prevent impeding oxygen saturation measurements. The imaging head is built with three CMOS cameras (JAI GO-5000 M-USB, JAI Ltd., Kanagawa, Japan, PCO.edge 4.2, Excelitas PCO GmbH, Kelheim, Germany, JAI GO-5000C-USB, JAI Ltd., Kanagawa, Japan) sharing the same field of view of 15 by 15 cm^2 for the collection of the NIR1 (665 nm), NIR2 (860 nm), and the RGB channels with a resolution of 1024 by 1280 pixels. In addition, low-pass and high-pass filters are used in the optical path to isolate the different wavelengths (Chroma Technology Corp., Bellows Falls, VT, United States). A pair of linear polarisers (PPL05C, Moxtek, Orem, UT, United States) in a crossed configuration are also used at the projection and imaging sides to reject the contribution from specular reflections at the surface of the sample.

A silicone-based optical phantom (21 by 21 by 2 cm) with known optical properties (μ_a = 0.01 mm^{-1} and μ_s' = 1.1 mm^{-1} at 665 nm, and μ_a = 0.02mm^{-1} and μ_s' = 0.8mm^{-1} at 860 nm) is used for the calibration of the Trident imaging system. The imaging workflow consists of the simultaneous projection of a high-frequency sinusoidal pattern (here f_x = 0.3mm^{-1}) at the two wavelengths (665 nm and 860 nm) followed by the three-channel acquisition of the images for the extraction of the oxygen saturation level of the tissue.

Surgical set-up of pure ischaemia model

A central venous line was placed by means of an internal jugular vein dissection. A midline laparotomy was performed using electrocautery. A self-retaining retractor was then placed and a 10 cm small bowel loop was exposed in order to create bowel ischaemia by dividing arcade branches. Five regions of interest (ROIs) were marked with an interrupted suture in the antimesenteric border (ROI 1: central ischaemic; ROI 2: left marginal; ROI 3: left vascularised (2.5 cm from ROI 2); ROI 4: right marginal; ROI 5: right vascularised (2.5 cm from ROI 4)). The small bowel was imaged with the multispectral camera through SSOP before and after ischaemia at different time points (T0, T15, T30, T45, T60 min). The SSOP image acquisitions were performed in the dark (i.e. with the light turned off in the operating room), in order to reduce the risk of bias. Nevertheless, the system can also be operated in standard ambient light conditions via an adapted calibration routine.

Surgical set-up of ischaemia/reperfusion model

To assess the accuracy of the Trident system in detecting oxygenation changes, we created a short ischaemia/reperfusion model. Same surgical principles were respected for laparotomy. Six 10 cm

small bowel loops were exposed in order to create short bowel ischaemia by dividing the peritoneal layer of the mesentery with sufficient length to apply a bulldog clamp. Similarly, to the pure ischaemic model, five regions of interest (ROIs) were marked with an interrupted suture in the antimesenteric border (ROI 1: central ischae- mic; ROI 2: left marginal; ROI 3: left vascularised (2.5 cm from ROI 2); ROI 4: right marginal; ROI 5: right vascularised (2.5 cm from ROI 4) in each loop. Small bowel loops were imaged with the Trident system through SSOP before, during clamping, and after declamping at the reperfusion phase (T0, and T10, and T15 min, respectively).

Figure 14: (A) The ischaemic bowel loop is placed in a standard position in order to facilitate image acquisition using the Trident imaging system. The white arrow points to the camera head, which is mounted onto an articulated arm. A standardised picture orientation and distance is used, in order to prevent any bias. It should be noted that light interference is avoided during image acquisition.

(B) Preclinical patient cart of the Trident imaging system for fluorescence, SFDI, and SSOP imaging. Imaging head enclose three separate channels for RGB, NIR1, and NIR2 imaging. A DMD-based projection system is also mounted onto the head for the generation of structured illumination over the field of view. The light source is delivered to the projector via a fiber-based coupling system. An illumination ring is used to homogeneously deliver white light illumination of the surgical field and fluorescence excitation wavelength. The main body of the cart contains the laser sources, the white light lamp, and the PC workstation.

(C) Schematics of the optical path in the trident imaging system for the co-registration of the 3 imaging channels, together with the configuration of the DMD-based projector. A pair of filtering cubes are used to isolate the NIR1 and NIR2 channels, polarisers (P) are used to reduce the influence of specular reflections, and a set of mirrors are used to align the field of view of the 3 cameras.

Analysis of capillary and systemic lactates

At each time point, capillary lactates (mmol/L) were measured by means of a portable analyser (EDGE ®lactate analyser, ApexBio, Taipei, Taiwan, People's Republic of China) by puncturing the bowel's serosal side at each ROI. Lactate is the product of glycolysis and its accumulation reflects a lowered mitochondrial activity in the presence of reduced O_2 concentration. This method has been described earlier in studies on the metabolic effect of bowel resection [205, 206]. Systemic lactates were also measured in venous blood retrieved from the central line and using the EPOC® Blood Analysis System (Siemens Healthineers, Erlangen, Ger- many), a portable blood analyser.

Pathological examination

For the pure ischaemic model, full-thickness biopsies were retrieved at the end of the procedure, and specimens were fixed in a 4% formalin solution for at least 24 h. Four-μm- thick sections were cut from paraffin-embedded tissues and stained with haematoxylin and eosin. Biopsies were taken from each ROI after 60 min of ischaemia and one from a distal part before the creation of the ischaemic loop, which served as a control. A microscopic assessment was made (Leica 2000 LED, Leica Biosystems GmbH, Wetzlar, Germany) using Park/Chiu's scoring system of intestinal ischaemic damage [207, 208].

Statistical analysis

All statistical analyses were performed using the GraphPad Prism software for macOS (GraphPad Software, Inc., San Diego, CA, United States), version 9.1.1. Data are shown as mean and standard deviations (SD) unless otherwise indicated. Capillary lactates were normalised according to systemic lactates to reduce variability. In order to assess a possible correlation between normalised lactates and SSOP-StO2, a Pearson's rank correlation coefficient was calculated. A Student's t-test was used to compare continuous variables after confirmation of a parametric distribution using the Kolmogorov-Smirnov normality test. A p value < 0.05 was considered statistically significant.

Study 3: Simultaneous, multi-channel, near-infrared fluorescence visualization of mesenteric lymph nodes using indocyanine green and methylene blue: a demonstration in a porcine model

Fluorescence imaging system

The QUEST SPECTRUM® 3 system was developed for NIRF image-guided surgery in an open surgical setting. This fluorescence imaging system has two dedicated NIR channels in the electromagnetic spectrum (700 and 800 nm), which allows for simultaneously visualization of ICG and MB. The channels were changed directly on the monitor touchscreen by simply clicking on the preferred channel. Screen settings included the RGB image, NIRF response in grayscale image, overlay of fluorescent image in green with the color image, and overlay of the fluorescent response image in Color (Blue to Red) on the Color image in grayscale.

Preparation of the dyes

ICG (Verdye, Diagnostic Green GmbH, Aschheim, Germany) was diluted in a sterile H_2O solution to a concentration of 2.5 mg/mL and was injected intravenously at a concentration of 0.2 mg/kg body weight via a peripheral venous line. The dose is based on the findings of our previous publication in which this was the most frequently used dose in clinical settings [100].

MB (Provepharm Life Solutions, Marseille, France) was diluted in a sterile phosphate-buffered saline solution to a concentration of 1 mg/mL and was injected intravenously at a concentration of 0.25 mg/kg body immediately following the injection of ICG. This dosage was determined based on previous literature [101, 107].

Surgical procedure

To expose the ROI mesenteric lymph nodes and small bowel, the abdominal cavity was accessed via a midline laparotomy, and a self-retaining abdominal wall retractor was placed. The camera tip was positioned at 15 cm above the ROI. During NIRF imaging, environmental lights were turned off preventing ambient light interference, and the average capture time was 20 seconds per image. The experimental surgical setting is represented in Figure 15.

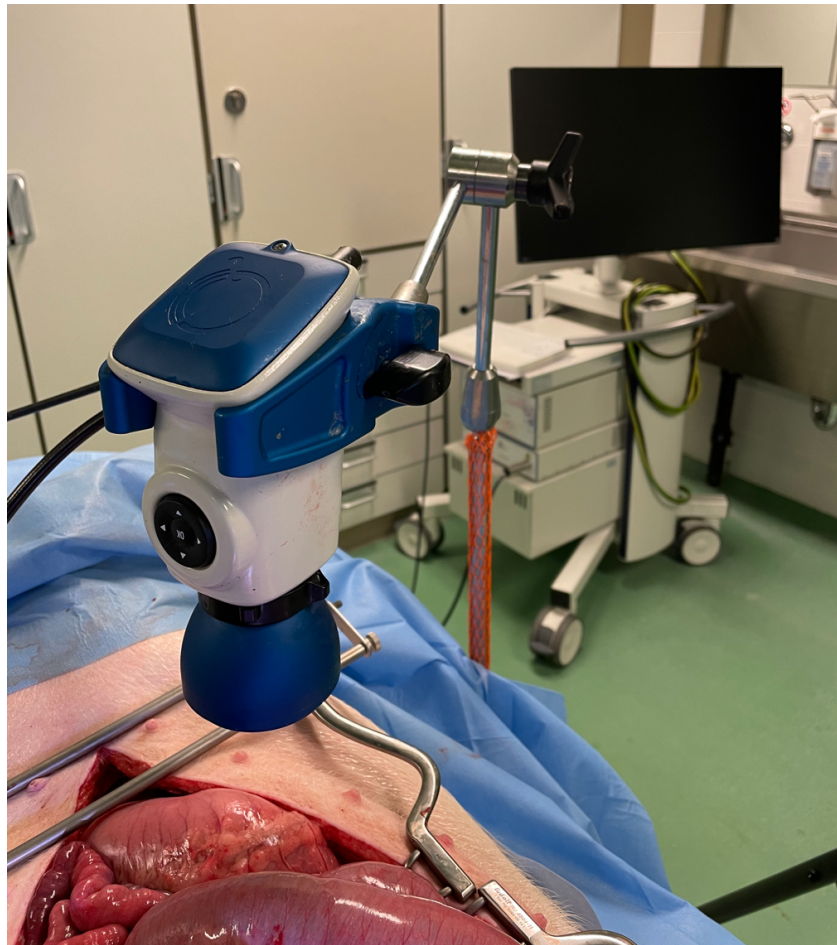**Figure 15.** Set-up during experiments: The abdominal cavity was accessed via a midline laparotomy to expose the regions of interest (i.e., small bowel and mesenteric lymph nodes). The distal lens of the QUEST camera® 3 (Quest Medical Imaging, Middenmeer, The Netherlands) was positioned 15 cm above the regions of interest. External light interference was avoided during the acquisition of images.

Image acquisition and statistical analysis

NIRF images were acquired from video recording after 1, 10, 20, 30, 40, 50, and 60 minutes of dye administration, respectively, using the QUEST SPECTRUM® 3.

First, the target (mesenteric lymph nodes and small bowel) and the background (vessels-free field of the mesentery) were highlighted as ROI, and corresponding fluorescence intensities (FI) which were expressed in arbitrary units (a.u.) from these ROIs were measured. Fluorescence intensity measurement was performed using the Quest Artemis (Quest Medical Imaging, Middenmeer, The Netherlands) software (TBR tool v1.0.). The target-to-background ratio (TBR) was then computed as the mean FI of the target divided by the mean FI of the background.

To identify any potential superiority in terms of dye performance, ratios were used dividing lymph node TBR/small bowel TBR per dye. A ratio comparison of MB and ICG was made using a Mann-Whitney U test for continuous variables. A two-tailed analysis with a p value <0.05 was considered statistically significant. These analyses were performed using commercially available database software (Excel version 2021, Microsoft Corporation, Redmond, WA, USA).

Results

STUDY 1: Computer-assisted differentiation Between Colon-Mesocolon and Retroperitoneum Using Hyperspectral Imaging (HSI)Technology

Performance visualization

Visually, the CNNs performed differentiation well between colon-mesocolon and retroperitoneum with minimal errors. Representative results are shown in Figure 12. Figure 12C is the predicted tissue annotations computed by the model. Figure 12D represents the error map. It can be seen that the majority of colon-mesocolon tissue has been correctly recognized (green regions), in accordance with the relatively high colon-mesocolon sensitivity score of 0.86 (Table 3). Most of the retroperitoneum tissue has been correctly recognized (blue regions), however there is some mis-classification with colon-mesocolon. This is in line with the lower retroperitoneum sensitivity score of 0.79 (Table 3).

Table 3: Performance Metrics

Mean ± SD	Recall (Sensitivity)	Specificity	F1 score	MCC	ROC AUC
Tissue to be resected (Colon-Masocolon) n = 20	0.86 +/- 0.16	0.79 +/- 0.21	0.90 +/- 0.11	0.60 +/- 0.23	0.92 +/- 0.12
Tissue to be left (Retroperitneum) n = 20	0.79 +/- 0.21	0.86 +/- 0.16	0.65 +/- 0.25	0.60 +/- 0.23	0.92 +/- 0.12

MCC: Matthews correlation coefficient; ROC AUC: Receiver Operator Curve Area-Under-Curve

Table 3. Model performance metrics: sensitivity, specificity, F1 score, MCC, and ROC AUC.

Performance metrics

The quantitative results are summarized in Table 2. The CNNs achieved relatively high sensitivity for colon-mesocolon (86.0 ± 16.0 %) and retroperitoneum (79.0 ± 21.0 %). The mean F1 score was 0.90 ± 0.11 for colon-mesocolon and 0.65 ± 0.25 for retroperitoneum. The mean ROC-AUC was 0.92 ± 0.12 for colon-mesocolon and 0.92 ± 0.12 for retroperitoneum, both of which are considered outstanding performances [209] (Figure 16).
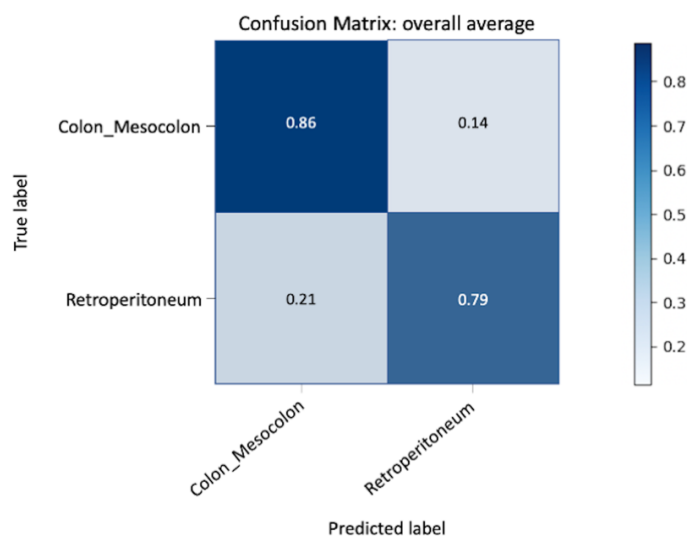

Figure 16. Predictive performance visualized as a confusion matrix: the X-axis represents predic-tive labels, and the Y-axis represents true labels. The navy-blue boxes represent true positives.

STUDY 2: Quantification of bowel ischaemia using real-time multispectral Single Snapshot Imaging of Optical Properties (SSOP)

In the pure ischaemia model, the oxygenation parameter for each ROI was assessed using SSOP-StO2 (Figure 17). The mean value of SSOP-StO2 in ROI 1 was 30.08% ± 6.963 and significantly lower when compared to marginal ROIs (ROI 2 + ROI 4: 45.67% ± 10.02, p = < 0.0001), and to vascular- ised ROIs (ROI 3 + ROI 5: 48.08% ± 7.083, p = < 0.0001). Although the SSOP-StO2 was higher in vascularised ROIs, this difference was not statistically significant (p = 0.1298) (Figure 18A and B).

The mean value of normalised lactates in ROI 1 was 4.804 mmol/L ± 2.591 and significantly higher when compared to marginal ROIs (ROI 2 + ROI 4: 1.026 mmol/L ± 0.472 p < 0.0001), and to vascularised ROIs (ROI 3 + ROI 5: 0.749 ± 0.246 mmol/L, p < 0.0001). The difference between marginal and vascularised ROIs also showed a statistically significant difference (p < 0.0001) (Figure 18C and D). The cumulative Pearson's correlation analysis between normalised lactates and SSOP-StO2 was -0.5892, p < 0.0001 (Figure 18E).
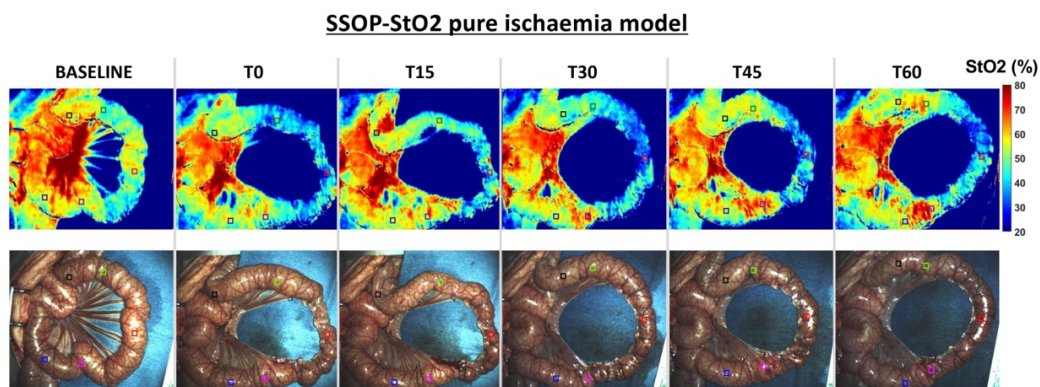

Figure 17. SSOP images showing StO2% during the full ischaemic period in the small bowel loop from baseline to T60, and corresponding true colour (RGB) images.
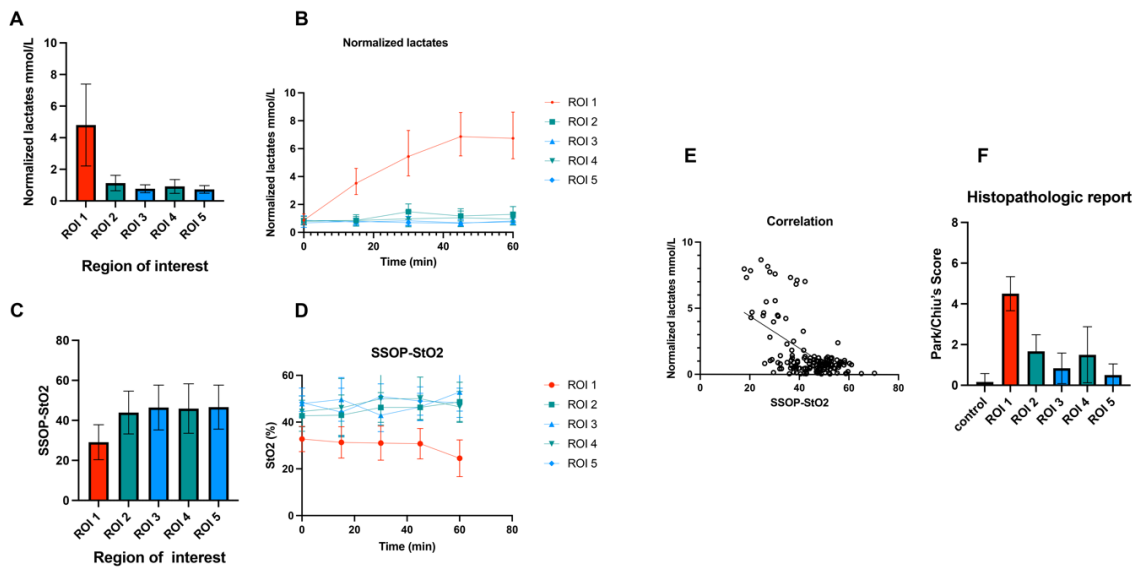
Figure 18. (A) SSOP-StO2 values during 1 h of ischaemia: the mean value of SSOP-StO2 in ROI 1 was 30.08± 6.963 and significantly lower when compared to marginal ROIs (ROI 2+ROI 4: 45.67 ± 10.02 p = < 0.0001), and to vascularised ROIs (ROI 3 + ROI 5: 48.08 ± 7.083, p = < 0.0001). Although SSOP-StO2 was higher in vascularised ROIs, it did not show any statistically significant difference (p=0.1298). (B) Kinetics of StO2 cartography in each ROI. (C) Normalised lactates (mmol/L) during 1 h of ischaemia: the mean value of normalised lactates in ROI 1 was 4.804 ± 2.591 and significantly higher when compared to marginal ROIs (ROI 2+ROI 4: 1.026± 0.472, p<0,0001), and to vascularised ROIs (ROI 3+ROI 5: 0.749± 0.246, p<0.0001). The difference between marginal and vascularised ROIs also showed a statistically significant difference p<0.0001. (D) Kinetics of normalised lactates (mmol/L). (E) Pearson's correlation analysis between normalised lactates and SSOP- StO2 in correspondence to all ROIs. (F) Histopathological report: the mean Park/Chiu's score at ROI 1 was 4.500± 0.8367 and significantly higher than marginal zones (ROI 2 and ROI 4: 1.583± 1.097, p<0,0001) and vascularised (ROI 3 and ROI 5: 0.667± 0.650, p < 0.0001)

As for the histopathological confirmation, the mean Park/Chiu's score at ROI 1 was 4.500 ± 0.8367

and was significantly higher than marginal zones (ROI 2+ROI 4: 1.583 ± 1.097) p < 0.0001 and

vascularised ROIs (ROI 3 + ROI 5: 0.667 ± 0.650), p < 0.0001 (Figure. 18F).

At T65, the Park/Chiu's score correlation between SSOP- StO2 was r =− 0.6251, p = 0.0002 and

between normalised lactates was r = 0.7102, p < 0.0001.

In the short ischaemia/reperfusion model, we found that ROI 1 has a mean 57.54 ± 5.35, 37.6 ± 4.12, and 62.40 ± 7.28 SSOP-StO2 at T0, T10, and T15, respectively. The difference in terms of SSOP-StO2 value from occlusion to reperfusion was statistically significant ($p = 0.00017$) (Figuress. 19 and 20). Marginal ROIs (ROI 2 + ROI 4) had a mean of 57.22 ± 5.61, 56.89 ± 5.49, and 60.93 ± 6.91 SSOP-StO2 at T0, T10, and T15, respectively, while vascularised ROIs (ROI 3 + ROI 5) had a mean of 62.53 ± 5.43, 59.71 ± 6.37, and 64.40 ± 6.80 SSOP-StO2 at T0, T10, and T15, respectively. In marginal ROIs (ROI 2 + ROI 4), the differences in terms of SSOP-StO2 from occlusion to reperfusion were not statistically significantly different ($p = 0.1511$), similarly to vascularised ones ($p = 0.1167$).
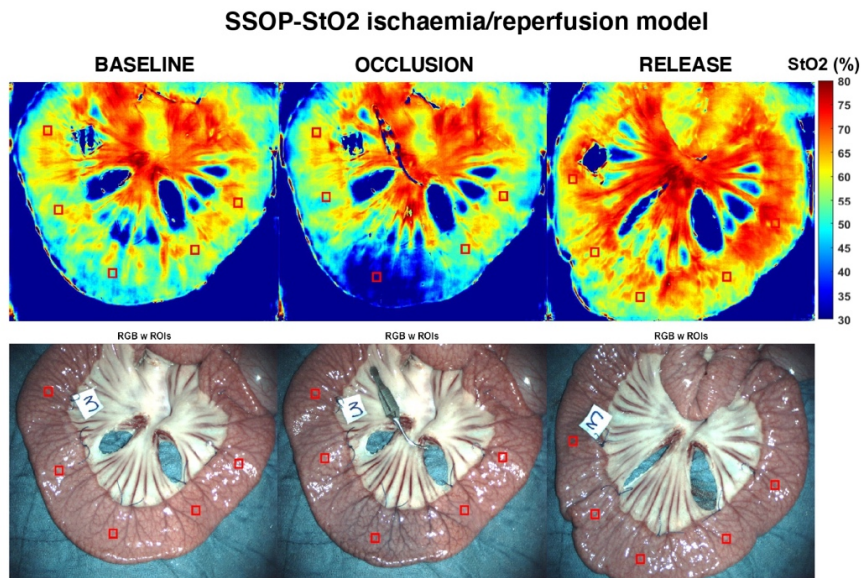
Figure 19. Ischaemia/reperfusion model. Characteristic SSOP GPU-accelerated DL (upper row) and RGB small bowel images (lower row) at baseline, during occlusion and after clamp release corresponding to reperfusion phase. ROIs are also represented by red squares.
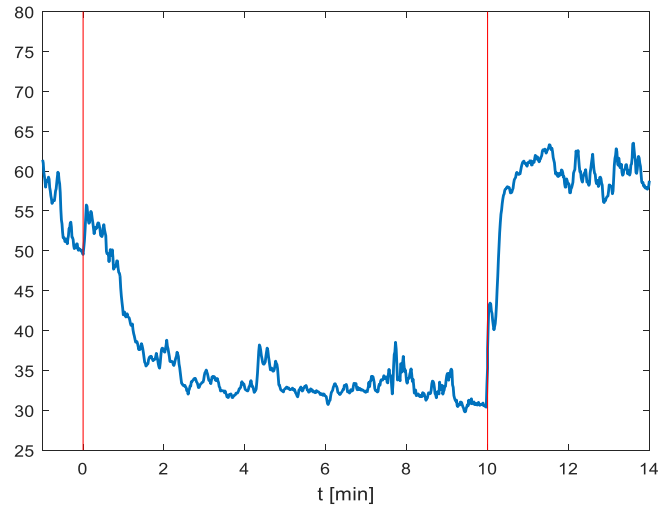
Figure 20. Over-time evolution of small bowel SSOP-StO2 in the ischaemia/reperfusion model. The graph shows the overtime evolution of StO2 parameter at the central ROI which reflects a decrease SSOP-StO2 during the ischaemic period (red lines) and saturation improvement after clamp releases (10 minutes).

Study 3: Simultaneous, multi-channel, near-infrared fluorescence visualization of mesenteric lymph nodes using indocyanine green and methylene blue: a demonstration in a porcine model

In all three animals included, it was possible to clearly visualize the lymph nodes under NIRF imaging using either of the dyes administered during the overall surgical procedure (Figure 21).

Figure 21. Picture of mesenteric lymph nodes and bowel after 20 minutes of intravenous MB and ICG administrations. (A) The RGB image. (B) Overlay fluorescence picture at 700 nm (fluorescence for MB). (C) Overlay fluorescence picture at 800 nm (fluorescence for ICG).

Subjective evaluation of lymph node visualization with two dyes by two experienced surgeons was performed on a 4-point scale (Excellent / Good / Average / Poor), with Good or Excellent at all intraoperative time points. The TBR for each time point is represented in Figure 22. The TBRs of MB and ICG were greater than 2.0 at all measured time points. The mean TBR of ICG in lymph nodes and small bowel was 4.57 ± 1.00 and 4.37 ± 1.70, respectively, for the overall experimental time. Regarding MB, the mean TBR in lymph nodes and small bowel was 4.60 ± 0.92 and 3.27 ± 0.62, respectively. The Mann-Whitney U test of lymph node TBR/small bowel TBR comparing ICG to MB showed that the value for MB was statistically significantly higher ($p = 0.012$). No complications related to dye administrations occurred.
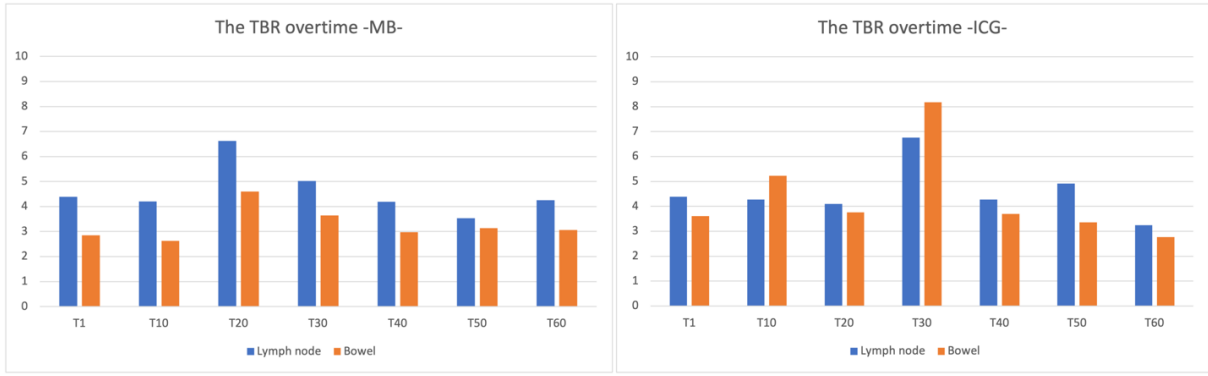
Figure 22. The TBR over time, (A) MB (B) ICG

Discussion

STUDY 1: Computer-assisted differentiation Between Colon-Mesocolon and Retroperitoneum Using Hyperspectral Imaging (HSI)Technology

The highlight of this study is the demonstrated ability of the combination HSI and CNNs trained with deep learning to discriminate between tissues to be resected (colon and mesocolon) from tissues to be preserved (retroperitoneum) during colorectal resection.

The mainstay of image-guided surgery in recent decades has been NIRF. NIRF-guided surgery has had excellent results in improving the visualization of tissue with blood and lymphatic flow [10, 95–99, 119, 120]. However, the recognition of the dissection planes necessary for accurate colorectal surgery is difficult to distinguish using NIRF. As previously stated, this requires the injection of a dye into the blood stream to map vascular structures. However, the relevant anatomical dissection plane during CME is the so-called "avascular plane" in which only microscopic blood vessels pass [210]. Therefore, NIRF has limitations in discriminating relevant anatomical layers in colorectal surgery [136, 175]. Although NIRF may support surgeons in better defining vascular structures within the mesentery and therefore guiding CME dissection there are drawbacks such as ICG allergy related issues. ICG is a non-toxic dye with a very low allergy probability (1:42,000 - 1:60,000) and is considered a contrast agent that does not interfere with blood composition or the coagulation system [91–93]. However, there have been several reports of fatal anaphylaxis in the past 40 years, and preoperative allergy testing is considered necessary [93]. Additionally, in case of diffuse bleeding, ICG diffusion in the surgical field can lead to inaccurate differentiation [185].

HSI has become a powerful tool to objectively assess the unseen, based on the interaction of emitted, absorbed, reflected, and scattered light with biochemical tissue components. This technique, which is contrast-free and non-invasive, has the potential to become future

intraoperative guidance and a valuable navigation tool [64, 134]. However, HSI data is very difficult for the surgeon to directly interpret. Surgeons must have access to advanced machine learning algorithms to process such data to automatically recognize tissue patterns based on their spatio-spectral signatures; this provides surgeons with precise and relevant tissue information which is not visible with the naked eye or a standard RGB camera.

In the current in vivo non-survival porcine model, using HSI in combination with a CNN, we were able to automatically recognize the anatomy of the mesothelial layer that needs to be dissected during CME and constitutes a critical key step during colonic resection.

The potential clinical relevance of HSI lies in the better replicability of CME assuring removal of all lymph nodes while decreasing the recurrence rate. An HSI-guided dissection could help achieve more accurate and extensive dissection adhering to embryological planes while preventing damage to other retroperitoneal organs, and also preventing neoplastic tissue from being unresected.

Very promising results were obtained in this study. However, there are some limitations. The HSI camera system had a limited electromagnetic spectral range (500–1000 nm), a relatively low spectral resolution (5 nm), and low spatial resolution (640 by 476 pixels). Consequently, the use of low-resolution images could well decrease accuracy in the annotation process, even when performed by experienced hands, which may introduce errors in the dataset. To minimize such errors, two experienced surgeons made annotations in the operating room while controlling dissection planes intraoperatively. The main reason for using this type of camera was that the spectral profile could be understood at the molecular level in this spectral range (500–1000 nm) [196]. It also did not disrupt the surgical workflow (approximately 6 s in acquisition time), and it was clinically approved, making it easier to translate our study results into clinical trials and future research applications in colorectal surgery.

A second limitation lies in the fact that this is a small number of samples using porcine models in which the mesentery is significantly thinner as compared to human models that have more adipose tissue. As a result, it is uncertain whether similar results could be obtained in clinical human studies. In humans, there is a well-described fusion fascia between the retroperitoneum and the mesocolon dissected during CME. Because pig models do not have a fusion fascia, this study used HSI to recognize the mesentery and retroperitoneum in the sigmoid colon only before any dissection took place and the potential effects of energy sources on spectral images were not evaluated. Previously, our group identified that electrocautery resulted in low-level oxygen perfusion while using HSI data in a liver resection model [134]. The peritoneum is a thin mesothelial layer. Consequently, the use of electrocautery could cause inaccurate recognition during surgical dissection. The next sensible step including the clinical translation of using HSI in combination with a CNN as a navigation tool for colorectal surgery is to study whether the system can achieve high sensitivity and specificity in humans. The objective would be to recognize the boundary of the mesothelial layer that needs to be dissected and determine whether surgical techniques that are essential in performing the dissections required in CME affect the accuracy of the recognition system.

Finally, due to the camera set-up, a laparotomy was required for the acquisition of images. At present, minimally invasive laparoscopic surgery is the standard of care in oncological colorectal resections. Zuzak *et al.* developed a NIR laparoscopic HSI system prototype to guide laparoscopic liver resection and differentiate the portal vein from the extrahepatic biliary duct and the hepatic artery [95]. Recently, HSI-equipped laparoscopic cameras are now commercially available. As a result, further studies are necessary to establish the accuracy of HSI systems during minimally invasive surgery.

STUDY 2: Quantification of bowel ischaemia using real-time multispectral Single Snapshot Imaging of Optical Properties (SSOP)

In the present experimental pure bowel ischaemia model, the Trident imaging system could provide accurate quantification of tissue StO2, which is a useful biomarker of tissue viability and is also correlated with a validated marker of tissue perfusion [206]. Capillary lactates have been substantially studied by our research group as a ground truth assessing NIR optical imaging technologies [124, 211].

Local bowel capillary lactates were normalised via systemic lactates to reduce the variability between animals. The high number of paired normalised capillary lactates and StO2 datasets (175) at different time points allowed to compute a negative correlation between those two parameters. Previously, our group reported a correlation between StO2 and lactates using HSI within similar ranges ($r = -0.7$) [134].

Additionally, StO2 images from the Trident imaging system were also correlated with the Park/Chiu's score which is based on histopathological assessment of all intestinal layers. Although it is well-known that the intestinal mucosa and submucosa are the first ones affected by impaired perfusion since they receive most of the mesenteric blood flow (70%), the muscularis and serosal layers can also be damaged during ischaemic periods [211]. Since the evaluation of the StO2 images was performed on the serosal side, histopathological repercussions in external layers were elements of interest. Nevertheless, this was a short-term ischaemia model (1 h), and transmural necrosis is mostly developed after longer ischaemic periods (6 h) [211]. In fact, the higher Park/Chiu's score of 6 was found in one case only.

To verify the accuracy of the Trident system, we created the short ischaemia/reperfusion model in which the Trident system could detect the variation of StO2 as soon as the vascular clamp was applied and released.

Intraoperative perfusion assessment constitutes a critical issue during digestive surgery. In NIR-FA, ICG has so far been the most commonly used fluorophore to evaluate local microperfusion [212]. ICG-FA has been rapidly expanded by the increasing availability of optical imaging systems [213–215]. However, most ICG-FA optical systems are based on relative fluorescence intensity (FI) without considering diffusion, which can potentially lead to overestimation on non-perfused areas. Secondly, FI is inversely correlated to the source-to-target distance. This fact makes those structures closer to the source brighter than areas far away. To prevent any distance bias, distance standardization between the NIR endoscope and the surgical field and/or the use of a reference calibration tool must be performed during image acquisition [216].

In order to overcome ICG-FA drawbacks, quantification methods which are irrespective of distance have been developed to obtain a perfusion cartogram based on the dynamic uptake of the fluorophore over time such as FLER [211] or Q-ICG [217, 218]. Although the use of quantitative methods offers a reproducible and robust solution, they have not been extensively adopted at present and there is still no standardised approach regarding its use as reported in the IHU- IRCAD-EAES EURO-FIGS registry [100].

As compared to FA, endogenous imaging methods including SSOP can provide a greater amount of quantitatively significant data by characterising several tissue components including StO2, which reflects intracellular metabolic changes induced by ischaemia. HSI is an eminent well-known example of endogenous imaging. Its accuracy in assessing perfusion during oesophagectomy has been studied in 22 patients by discriminating between gastric conduits with

and without laparoscopic ischaemic preconditioning (StO2 66 vs. 78%, p = 0.03) [131]. In colorectal surgery, HSI has been compared between to FA, showing comparable results in detecting the optimal demarcation line [219].

Although HSI is an efficient technology, it does not allow for a video-rate acquisition and the large datasets require postprocessing algorithms to discriminate features according to spectral curves. To overcome this limitation, our group created the concept of HYPerspectral Enhanced Reality (HYPER) which had promising results in the preclinical setting [124]. However, HYPER requires image superimposition using augmented reality onto real-time videos to achieve real-time intraoperative guidance, making its use currently limited [64].

At present, SSOP is a more adapted surgical navigation system method since it allows for a video rate (> 25 frames per second), and a wide-field (> 100 cm^2), non-invasive, quantitative multispectral characterisation of metabolic properties through a single frame acquisition [201, 220, 221].

A strong point is that SSOP is based on SFDI that in one of the first in-human pilot trials has proven to be accurate in assessing the oxygenation of microsurgical deep inferior epigastric perforator flaps during reconstructive breast surgery [222]. However, standard SFDI is time-consuming since it requires the acquisition of several images (in this case, 6 images), being inconvenient for the surgical workflow.

To address such constraints, SSOP was developed as an enhanced fast optical intraoperative navigation tool. However, with the conventional process using image reduction, SSOP initially suffered from degraded visual quality as compared to the 7-phase SFDI. Artificial intelligence has been used to overcome such issues. A Graphics Processing Units (GPU)-accelerated DL as a processing technology has been previously described. SSOP GPU-accelerated DL evaluation of *in*

vivo human hands and *ex vivo* animal organs showed superiority in terms of image resolution and degradation as compared to a classical SSOP-filtering approach. The DL processing methodology has shown errors as low as $7.5 \pm 2.7\%$ [179].

In this study, the Trident imaging system uses SSOP GPU-accelerated DL using CCNs and allows for a non-contrast physiological real-time multispectral assessment in an in vivo one-hour ischaemic model (Figure 17). Additionally, the use of artificial intelligence helped to maintain high image quality comparable to the 7-phase SFDI. The promising results presented in this article of SSOP-StO2 can be potentially expanded into other fields for surgical guidance.

This study relies on a robust methodology. The limited number of animals represents a constraint since only 6 pigs were studied, in which SSOP-StO2 and capillary lactates standard deviations between marginal and vascularised ROIs were high. Although SSOP-StO2 was high in vascularised compared to marginal ROIs, it was not statistically significant. Less variability could be encountered if sample size is increased during future experiments. Another downside of the present study lies in the postprocessing time GPU-accelerated DL and in its non-survival design, which does not make it possible to evaluate the impact of multispectral SSOP on anastomotic healing. As a result, the next logical step would be to evaluate multispectral SSOP performance in a survival anastomotic model.

Since the current SSOP-based optical imaging system is designed for open settings, a potential improvement making way for clinical translation relies on hardware refinement. Presently, our group is strongly considering this parameter to enhance such an optical imaging technology.

Study 3: Simultaneous, multi-channel, near-infrared fluorescence visualization of mesenteric lymph nodes using indocyanine green and methylene blue: a demonstration in a porcine model

In CRC, lymph node metastasis modifies staging, and the stage determines whether postoperative adjuvant chemotherapy is indicated. Results of a secondary analysis of the Intergroup trial INT-0089 showed that an increased number of lymph nodes retrieved correlates with a prolonged survival rate in both negative and positive cases of lymph node metastasis [223]. Swanson et al. showed that the number of lymph nodes examined, even in T3N0 colon cancer without preoperative lymph node metastasis, linearly correlated with 5-year survival [224]. International guidelines recommend the evaluation of 12 or more lymph nodes [225–227]. However, scientific evidence is still lacking and it is still unclear if there is an absolute number that is considered as a gold standard for routine analysis [228]. Goldstein stated that a minimum of 30 lymph nodes in a hypothetical specimen was required to reach a probability of 80% to identify a single metastasis [229]. In other words, intraoperative lymph node detection and resection represent an essential component in predicting the long-term prognosis of CRC and in determining postoperative treatment strategies.

In this study, we validated that the two dyes (MB and ICG) can be used in parallel in an animal model for the identification of lymph nodes. After simultaneous intravenous administration in both modes, the NIRF imaging of lymph nodes and bowel was possible with the TBR of MB in mesenteric lymph nodes, and was not inferior to that of ICG. The potential explanation for these results is correlated with the lower MB FI in the small bowel than the ICG FI and the higher overall ICG FI in perfused areas as compared to MB. ICG possesses a higher FI background even in the vessels-free field of the mesentery. Additionally, since MB has a shorter washout time from the

bowel than ICG, it may offer an enhanced capacity for mesenteric lymph node detection as the FI background decreases more rapidly than when using ICG.

A systematic review and meta-analysis by Emile *et al.* showed that studies on fluorescent lymph node imaging differ with respect to ICG concentration, dose, injection site (submucosal, subserosal, combined submucosal and subserosal, intravenous), and timing of injection (preoperative, intraoperative, both preoperative and intraoperative) [230].

For fluorescence lymph node detection and lymphatic mapping using ICG, the dye is often injected in the subserosal or the submucosal layers where the main lymphatic network is located around the cancerous tissue [230–232]. However, this technique requires high technical precision during injection to prevent dye spillage, since abdominal cavity leakage alters the surgical field with false-positive fluorescence regions [123]. Regarding technical details during laparoscopic subserosal ICG injection, the lack of tactile feedback could cause the needle tip to reach the muscle layer, hence injecting the wrong layer resulting in inadequate dye absorption into the lymphatics [230]. Nishigori *et al.* studied 21 patients who underwent laparoscopic CRC surgery to evaluate both lymphatic and blood flow with ICG fluorescence imaging. To evaluate lymph flow, authors injected ICG into the submucosa around the tumor under colonoscopic guidance, with a timing of injection comprised either between 1 and 3 days before surgery or intraoperatively. To evaluate blood flow, ICG was injected intravenously during the procedure. Inadequate lymphatic flow delineation resulted in non-detection in three cases. In the two cases involving intraoperative IV injection, ICG leakage was a problem in both [10].

On the other hand, Liberale *et al.* reported that intraoperative IV administration of ICG for lymph node detection was feasible. Authors showed that intraoperative and postoperative fluorescence imaging might be a new tool to detect metastatic lymph nodes in patients with CRC, allowing for

a more accurate staging [233]. In the previously quoted systematic review, the IV administration of ICG showed the second highest sensitivity, specificity, and accuracy for lymph node detection behind the combined subserosal and submucosal injection [230]. However, pooled results were based on only two lymph node mapping studies using IV ICG. At present, the preferred method of administration and dosage of ICG for fluorescence lymph node mapping is still under debate, and further clinical trials are highly necessary to establish the best reliable technique. ICG also diffuses into ascites and edema because of its albumin binding. In this experiment, some animals developed a degree of ascites or mesenteric edema after laparotomy. In those that did, ICG fluorescence images showed comparable FI in edema ROIs to that of the lymph nodes (Figure 23).
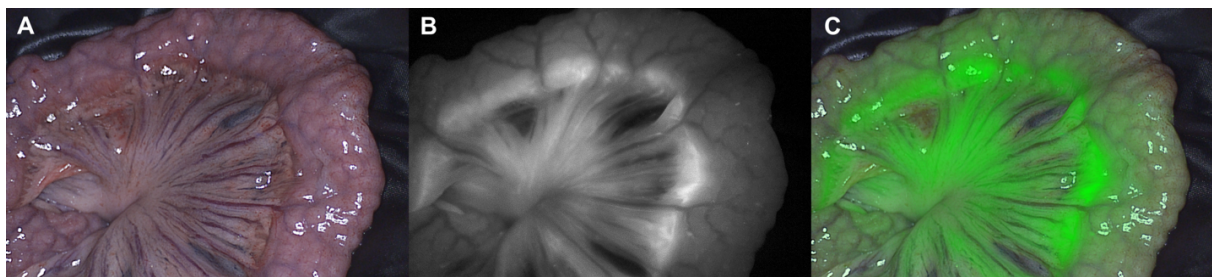
Figure 23. Picture of mesenteric edema after 40 minutes of IV ICG administration. (A) The RGB image. (B) Fluorescence picture at 800 nm (C) Overlay fluorescence picture at 800 nm

As a result, the ICG fluorescence present in either ascites or edema may reduce the sensitivity of mesenteric lymph node detection during NIRF-guided surgery.

MB is hydrophobic and does not bind to albumin as opposed to ICG. Jun Li *et al*. reported NIRF imaging using MB for the identification of lymphatic vessels, sentinel lymph node location, and breast lymphatic flow patterns in breast cancer. They reported that MB causes less background fluorescence contamination than ICG, and MB could be suitable for observation due to its higher absorption and to the fact that it can be clearly detected across the skin and adipose tissue [234].

The fluorescence of MB injected simultaneously with ICG could be used to confirm whether the fluorescent ROIs are either mesenteric lymph nodes or mesenteric edema. The intravenous injection of two dyes may increase the sensitivity of mesenteric lymph node detection, thereby avoiding complex procedures such as subserosal and submucosal injections. In addition, this may prevent any excessive mesenteric injury or inadequate lymph node resection that could occur when ICG is administered alone.

Additionally, MB in the lymphatic network and lymph nodes stains a blue color in the specimen. The number of detectable lymph nodes depends on age, gender, type of malignancy, and tumor location [235]. Besides, preoperative adjuvant chemoradiation has become the standard of care for advanced rectal cancer in recent years. Neoadjuvant chemoradiotherapy reduces lymph node size, which causes a decrease in lymph node harvesting [236–238]. Märkl *et al.* reported a study in which MB was injected into the superior rectal artery *ex vivo*, originally performed to evaluate the accuracy of TME [239]. Other authors found that injecting MB postoperatively directly into the vessels of rectal resection specimens improved the lymph node detection rate [188]. Although it must be mentioned that this is an arterial injection and the concentration administered is high, they have shown that MB transferred from the blood vessels into the lymphatic flow stains the lymph nodes. Several studies have shown that higher doses of MB improved postoperative lymph node harvesting from rectal cancer specimens [188, 189].

Another potential application of the presented imaging set-up, apart from the tested lymph node and bowel detection, is to assess blood flow and ureteral recognition as these are two other properties of the ICG and MB dyes. Ureteral injury is a serious complication during intrapelvic surgery, and the majority of iatrogenic ureteral injuries may lead to severe morbidity and even mortality [67, 68]. Visualization of the ureter is extremely important, especially after reoperation

or radiation therapy. Intraoperative ureteral identification also contributes to the education of young surgeons in the field of anatomy. As referred to earlier, ICG is cleared via the bile juice. The fluorescent urinary tract visualization with ICG requires the insertion of one or several ureteral catheter(s) via cystoscopy requiring an additional invasive procedure which may increase the risk of perioperative complications [240]. Several studies have been published on ureteral fluorescence using preclinical fluorophores with emission peaks similar to ICG. Since these novel fluorophores (including IRDye® 800CW, IRDye® 800BK, IRDye® 800NOS [241], and IS-001 [242]) contribute to urinary clearance, they have shown promising results in detecting the ureter. However, further clinical translation is necessary since these dyes are currently not available in the marketplace.

As a result, since MB is excreted through the urine, it may represent the best way to intraoperatively identify ureters during colorectal surgery. Several studies have been published in which MB is injected intravenously and the ureter is visualized with fluorescence [102, 107, 243]. The first study of NIRF visualization of the ureter using MB was proposed by Verbeek *et al.* in 12 patients. In this study, the authors showed correct visualization of both ureters after intravenous injection of MB [243]. Later on, Polom *et al.* published a study on simultaneous fluorescent visualization of ureter and bowel perfusion via the administration of MB and ICG respectively using the laparoscopic camera system that was used in our study. The fluorescent visualization of the ureter was successful in 11 out of 12 patients (96.1%), and in all patients, bowel perfusion by means of ICG was successfully confirmed [190]. As a result, simultaneous assessment using MB and ICG is feasible and represent a comprehensive NIR guidance, helping surgeons to detect lymph nodes, to reduce the risk of anastomotic leakage by assessing local tissue perfusion, and to reduce the risk of complications by detecting ureters.

However, there are some drawbacks regarding the administration of MB that should be discussed. MB is contraindicated in patients with glucose-6-phosphate dehydrogenase (G6PD) deficiency and Heinz body anemia. MB is a safe agent when used at therapeutic doses of 2mg/kg or less [244]. In high doses or in patients with renal failure, MB may induce severe adverse effects, such as coronary vasoconstriction, arrhythmias, and hemolytic anemia [104]. While it is prudent to use the lowest dose of MB necessary for a given case to minimize the potential for toxic manifestations [106], several studies of fluorescence ureteral visualization with the administration of MB showed that higher doses of MB resulted in better ureteral visualization [107, 243]. MB administration may cause false elevations in methemoglobin levels with CO-oximetry and pulse oximetry [245]. Finally, excess doses of MB may paradoxically increase oxidant stress and methemoglobinemia [246]. During this experiment, we did not observe any such changes in vital signs after MB administration.

Further experiments are necessary to determine the optimal method of administration, timing, and dosage of MB dye, particularly for lymph node mapping based on these previous studies.

The limitation of the present study lies in the fact that a small-number pilot study using porcine models was used. The mesentery of an adult human is not as thin as that of a pig. The mesenteric lymph nodes of humans, which are usually embedded in adipose tissue, are generally more difficult to detect, impairing our ability to predict whether this method can be generalized to humans. Additionally, the system was used in open surgery settings, and laparotomy was required for image acquisition. Currently, minimally invasive laparoscopic surgery has become the standard treatment in CRC surgery. At present, a laparoscopic camera equipped with a double-wavelength imaging system is available, enabling further research to establish the accuracy of this imaging system in minimally invasive surgery settings.

Conclusion

We have studied three methods of intraoperative image guidance for CRC surgery in this work.

The first method is the automatic recognition of the anatomical structures necessary for accurate colorectal surgery using the HSI camera and artificial intelligence (AI). HSI has been combined with CNNs and deep learning (DL) to accurately distinguish two tissue groups (i.e., the colon and its mesentery from the retroperitoneum). HSI recognition may have a potential role in intraoperative guidance for CME.

The second method is the quantification of bowel ischemia using real-time multispectral SSOP. It shows that multispectral SSOP allows for a contrast-free accurate assessment of small bowel perfusion identifying physiological tissue oxygenation as confirmed with perfusion biomarkers.

The third method is the use of fluorescence optical imaging technology, that allows for double-wavelength assessment. This feasibility study proves that lymph nodes can be discriminated using two different fluorophores (MB and ICG) with different wavelengths. The results suggest that MB performance may represent a more accurate way of detecting lymphatic tissue during image-guided surgery.

This feasibility study proves that mesenteric lymph nodes can be discriminated using two different fluorophores (MB and ICG) at different wavelengths. Based on a superior discrimination from the background, MB performance may represent a pathway to better detect lymphatic tissue during image-guided surgery.

These new surgical methods and imaging techniques were shown to be feasible in animal experiments and demonstrated equal or better results than conventional methods. They may replace conventional technologies in the future.

Further research will need to investigate whether such technologies may be applied to the human body with similar accuracy and determine whether they can be applied to the clinical practice.

References

1. Sung H, Ferlay J, Siegel RL, Laversanne M, Soerjomataram I, Jemal A, Bray F (2021) Global Cancer Statistics 2020: GLOBOCAN Estimates of Incidence and Mortality Worldwide for 36 Cancers in 185 Countries. CA: A Cancer Journal for Clinicians 71:209–249

2. Heald RJ, Husband EM, Ryall RD (1982) The mesorectum in rectal cancer surgery--the clue to pelvic recurrence? Br J Surg 69:613–616

3. Hohenberger W, Weber K, Matzel K, Papadopoulos T, Merkel S (2009) Standardized surgery for colonic cancer: complete mesocolic excision and central ligation - technical notes and outcome. Colorectal Disease 11:354–364

4. Dip F, Boni L, Bouvet M, et al (2022) Consensus Conference Statement on the General Use of Near-infrared Fluorescence Imaging and Indocyanine Green Guided Surgery: Results of a Modified Delphi Study. Ann Surg 275:685–691

5. Cancer. https://www.who.int/news-room/fact-sheets/detail/cancer. Accessed 3 Sep 2020

6. Institute NC, National Cancer Institute (2020) Surveillance, Epidemiology, and End Results Program. Definitions. https://doi.org/10.32388/5owtl5

7. Cancer.net https://www.cancer.net/cancer-types/colorectal-cancer/risk-factors-and-prevention.

8. Liu P-H, Wu K, Ng K, et al (2019) Association of Obesity With Risk of Early-Onset Colorectal Cancer Among Women. JAMA Oncol 5:37–44

9. Kerr J, Anderson C, Lippman SM (2017) Physical activity, sedentary behaviour, diet, and cancer: an update and emerging new evidence. Lancet Oncol 18:e457–e471

10. Nishigori N, Koyama F, Nakagawa T, et al (2016) Visualization of Lymph/Blood Flow in Laparoscopic Colorectal Cancer Surgery by ICG Fluorescence Imaging (Lap-IGFI). Annals of Surgical Oncology 23:266–274

11. Agnus V, Pesce A, Boni L, et al (2020) Fluorescence-based cholangiography: preliminary results from the IHU-IRCAD-EAES EURO-FIGS registry. Surg Endosc 34:3888–3896

12. Keller DS, Joshi HM, Rodriguez-Justo M, Walsh D, Coffey JC, Chand M (2017) Using fluorescence lymphangiography to define the ileocolic mesentery: proof of concept for the watershed area using real-time imaging. Techniques in Coloproctology 21:757–760

13. Okuno K (2007) Surgical treatment for digestive cancer. Current issues - colon cancer. Dig Surg 24:108–114

14. Enker WE, Laffer UT, Block GE (1979) Enhanced survival of patients with colon and rectal cancer is based upon wide anatomic resection. Ann Surg 190:350–360

15. West NP, Kobayashi H, Takahashi K, Perrakis A, Weber K, Hohenberger W, Sugihara K, Quirke P (2012) Understanding optimal colonic cancer surgery: comparison of Japanese D3 resection and European complete mesocolic excision with central vascular ligation. J Clin Oncol 30:1763–1769

16. Heald RJ, Ryall RD (1986) Recurrence and survival after total mesorectal excision for rectal cancer. Lancet 1:1479–1482

17. Scott N, Jackson P, al-Jaberi T, Dixon MF, Quirke P, Finan PJ (1995) Total mesorectal excision and local recurrence: a study of tumour spread in the mesorectum distal to rectal cancer. Br J Surg 82:1031–1033

18. Enker WE, Thaler HT, Cranor ML, Polyak T (1995) Total mesorectal excision in the operative treatment of carcinoma of the rectum. J Am Coll Surg 181:335–346

19. Quirke P, Dixon MF, Durdey P, Williams NS (1986) LOCAL RECURRENCE OF RECTAL ADENOCARCINOMA DUE TO INADEQUATE SURGICAL RESECTION. The Lancet 328:996–999

20. Adam IJ, Martin IG, Finan P, Johnston D, Mohamdee MO, Scott N, Dixon MF, Quirke P (1994) Role of circumferential margin involvement in the local recurrence of rectal cancer. The Lancet 344:707–711

21. Emile SH, de Lacy FB, Keller DS, Martin-Perez B, Alrawi S, Lacy AM, Chand M (2018) Evolution of transanal total mesorectal excision for rectal cancer: From top to bottom. World J Gastrointest Surg 10:28–39

22. Steele RJ (1999) Anterior resection with total mesorectal excision. J R Coll Surg Edinb 44:40–45

23. Crane J, Hamed M, Borucki JP, El-Hadi A, Shaikh I, Stearns AT (2021) Complete mesocolic excision versus conventional surgery for colon cancer: A systematic review and meta-analysis. Colorectal Dis 23:1670–1686

24. Wang C, Gao Z, Shen K, Shen Z, Jiang K, Liang B, Yin M, Yang X, Wang S, Ye Y (2017) Safety, quality and effect of complete mesocolic excision *vs* non-complete mesocolic excision in patients with colon cancer: a systemic review and meta-analysis. Colorectal Disease 19:962–972

25. Bokey EL, Chapuis PH, Dent OF, Mander BJ, Bissett IP, Newland RC (2003) Surgical Technique and Survival in Patients Having a Curative Resection for Colon Cancer. Diseases of the Colon & Rectum 46:860–866

26. Kotake K, Mizuguchi T, Moritani K, Wada O, Ozawa H, Oki I, Sugihara K (2014) Impact of D3 lymph node dissection on survival for patients with T3 and T4 colon cancer. International Journal of Colorectal Disease 29:847–852

27. Storli KE, Søndenaa K, Furnes B, Nesvik I, Gudlaugsson E, Bukholm I, Eide GE (2014) Short term results of complete (D3) vs. standard (D2) mesenteric excision in colon cancer shows improved outcome of complete mesenteric excision in patients with TNM stages I-II. Techniques in Coloproctology 18:557–564

28. Bertelsen CA, Neuenschwander AU, Jansen JE, et al (2015) Disease-free survival after complete mesocolic excision compared with conventional colon cancer surgery: a retrospective, population-based study. The Lancet Oncology 16:161–168

29. Bertelsen CA, Neuenschwander AU, Jansen JE, et al (2019) 5-year outcome after complete mesocolic excision for right-sided colon cancer: a population-based cohort study. The Lancet Oncology 20:1556–1565

30. Voyer TEL, Le Voyer TE, Sigurdson ER, Hanlon AL, Mayer RJ, Macdonald JS, Catalano PJ, Haller DG (2003) Colon Cancer Survival Is Associated With Increasing Number of Lymph Nodes Analyzed: A Secondary Survey of Intergroup Trial INT-0089. Journal of Clinical Oncology 21:2912–2919

31. Sjo OH, Merok MA, Svindland A, Nesbakken A (2012) Prognostic Impact of Lymph Node Harvest and Lymph Node Ratio in Patients With Colon Cancer. Diseases of the Colon & Rectum 55:307–315

32. De Simoni O, Barina A, Sommariva A, Tonello M, Gruppo, Mario, Mattara G, Toniato A, Pilati P, Franzato B (2020) Complete mesocolic excision versus conventional hemicolectomy in patients with right colon cancer: a systematic review and meta-analysis. Int J Colorectal Dis 36:881–892

33. Díaz-Vico T, Fernández-Hevia M, Suárez-Sánchez A, García-Gutiérrez C, Mihic-Góngora L, Fernández-Martínez D, Álvarez-Pérez JA, Otero-Díez JL, Granero-Trancón JE, García-Flórez LJ (2021) Complete Mesocolic Excision and D3 Lymphadenectomy versus Conventional Colectomy for Colon Cancer: A Systematic Review and Meta-Analysis. Annals of Surgical Oncology 28:8823–8837

34. Alhassan N, Yang M, Wong-Chong N, Liberman AS, Charlebois P, Stein B, Fried GM, Lee L (2019) Comparison between conventional colectomy and complete mesocolic excision for colon cancer: a systematic review and pooled analysis : A review of CME versus conventional colectomies. Surg Endosc 33:8–18

35. Selçuk İ, Ersak B, Tatar İ, Güngör T, Huri E (2018) Basic clinical retroperitoneal anatomy for pelvic surgeons. Turk J Obstet Gynecol 15:259–269

36. Semm K (1983) Endoscopic Appendectomy. Endoscopy 15:59–64

37. Litynski GS (1998) Erich Mühe and the rejection of laparoscopic cholecystectomy (1985): a surgeon ahead of his time. JSLS 2:341–346

38. Litynski GS (1999) Profiles in laparoscopy: Mouret, Dubois, and Perissat: the laparoscopic breakthrough in Europe (1987-1988). JSLS 3:163–167

39. Jacobs M, Verdeja JC, Goldstein HS (1991) Minimally invasive colon resection (laparoscopic colectomy). Surg Laparosc Endosc 1:144–150

40. Lacy AM, García-Valdecasas JC, Delgado S, Castells A, Taurá P, Piqué JM, Visa J (2002) Laparoscopy-assisted colectomy versus open colectomy for treatment of non-metastatic colon cancer: a randomised trial. Lancet 359:2224–2229

41. Fleshman J, Sargent DJ, Green E, et al (2007) Laparoscopic colectomy for cancer is not inferior to open surgery based on 5-year data from the COST Study Group trial. Ann Surg 246:655–62; discussion 662–4

42. Jayne DG, Guillou PJ, Thorpe H, Quirke P, Copeland J, Smith AMH, Heath RM, Brown JM (2007) Randomized Trial of Laparoscopic-Assisted Resection of Colorectal Carcinoma: 3-Year Results of the UK MRC CLASICC Trial Group. Journal of Clinical Oncology 25:3061–3068

43. Bonjer HJ, Jaap Bonjer H, Deijen CL, et al (2015) A Randomized Trial of Laparoscopic versus Open Surgery for Rectal Cancer. New England Journal of Medicine 372:1324–1332

44. Stevenson ARL, Solomon MJ, Lumley JW, Hewett P, Clouston AD, Gebski VJ, Davies L, Wilson K, Hague W, Simes J (2015) Effect of Laparoscopic-Assisted Resection vs Open Resection on Pathological Outcomes in Rectal Cancer. JAMA 314:1356

45. Fleshman J, Branda M, Sargent DJ, et al (2015) Effect of Laparoscopic-Assisted Resection vs Open Resection of Stage II or III Rectal Cancer on Pathologic Outcomes: The ACOSOG Z6051 Randomized Clinical Trial. JAMA 314:1346–1355

46. Al-Taher M, Okamoto N, Mutter D, Stassen LPS, Marescaux J, Diana M, Dallemagne B (2022) International survey among surgeons on laparoscopic right hemicolectomy: the gap between guidelines and reality. Surg Endosc 36:5840–5853

47. Al-Difaie Z, Okamoto N, Scheepers MHMC, Mutter D, Stassen LPS, Bouvy ND, Marescaux J, Dallemagne B, Diana M, Al-Taher M (2022) International survey among surgeons on the perioperative management of rectal cancer. Surg Endosc. https://doi.org/10.1007/s00464-022-09702-z

48. Mascagni P, Longo F, Barberio M, Seeliger B, Agnus V, Saccomandi P, Hostettler A, Marescaux J, Diana M (2018) New intraoperative imaging technologies: Innovating the surgeon's eye toward surgical precision. J Surg Oncol 118:265–282

49. Hukkeri VS, Mishra S, Qaleem M, Jindal S, Aggarwal R, Choudhary V, Govil D (2015) Minimizing locoregional recurrences in colorectal cancer surgery. Apollo Medicine 12:185–188

50. Guraya SY (2019) Pattern, Stage, and Time of Recurrent Colorectal Cancer After Curative Surgery. Clin Colorectal Cancer 18:e223–e228

51. Xu W, He Y, Wang Y, Li X, Young J, Ioannidis JPA, Dunlop MG, Theodoratou E (2020) Risk factors and risk prediction models for colorectal cancer metastasis and recurrence: an umbrella review of systematic reviews and meta-analyses of observational studies. BMC Med 18:172

52. Augestad KM, Bakaki PM, Rose J, Crawshaw BP, Lindsetmo RO, Dørum LM, Koroukian SM, Delaney CP (2015) Metastatic spread pattern after curative colorectal cancer surgery. A retrospective, longitudinal analysis. Cancer Epidemiol 39:734–744

53. Haria PD, Baheti AD, Palsetia D, Ankathi SK, Choudhari A, Guha A, Saklani A, Sinha R (2021) Follow-up of colorectal cancer and patterns of recurrence. Clinical Radiology 76:908–915

54. Kim S-E (2015) Sex- and gender-specific disparities in colorectal cancer risk. World Journal of Gastroenterology 21:5167

55. Song IH, Hong S-M, Yu E, Yoon YS, Park IJ, Lim S-B, Kim JC, Yu CS, Kim J (2019) Signet ring cell component predicts aggressive behaviour in colorectal mucinous adenocarcinoma. Pathology 51:384–391

56. Hartman DJ, Nikiforova MN, Chang DT, Chu E, Bahary N, Brand RE, Zureikat AH, Zeh HJ, Choudry H, Pai RK (2013) Signet ring cell colorectal carcinoma: a distinct subset of mucin-poor microsatellite-stable signet ring cell carcinoma associated with dismal prognosis. Am J Surg Pathol 37:969–977

57. Horn A, Dahl O, Morild I (1991) Venous and neural invasion as predictors of recurrence in rectal adenocarcinoma. Dis Colon Rectum 34:798–804

58. Pugh SA, Shinkins B, Fuller A, Mellor J, Mant D, Primrose JN (2016) Site and Stage of Colorectal Cancer Influence the Likelihood and Distribution of Disease Recurrence and Postrecurrence Survival: Data From the FACS Randomized Controlled Trial. Ann Surg 263:1143–1147

59. Zare-Bandamiri M, Fararouei M, Zohourinia S, Daneshi N, Dianatinasab M (2017) Risk Factors Predicting Colorectal Cancer Recurrence Following Initial Treatment: A 5-year Cohort Study. Asian Pac J Cancer Prev 18:2465–2470

60. Zafar SN, Hu C-Y, Snyder RA, Cuddy A, You YN, Lowenstein LM, Volk RJ, Chang GJ (2020) Predicting Risk of Recurrence After Colorectal Cancer Surgery in the United States: An Analysis of a Special Commission on Cancer National Study. Ann Surg Oncol 27:2740–2749

61. Lee JH, Kim DY, Kim SH, et al (2015) Carcinoembryonic antigen has prognostic value for tumor downstaging and recurrence in rectal cancer after preoperative chemoradiotherapy and curative surgery: A multi-institutional and case-matched control study of KROG 14-12. Radiother Oncol 116:202–208

62. Dindo D, Demartines N, Clavien P-A (2004) Classification of Surgical Complications. Annals of Surgery 240:205–213

63. Frasson M, Flor-Lorente B, Rodríguez JLR, Granero-Castro P, Hervás D, Rico MAA, Brao MJG, González JMS, Garcia-Granero E (2015) Risk Factors for Anastomotic Leak After Colon Resection for Cancer. Annals of Surgery 262:321–330

64. Barberio M, Longo F, Fiorillo C, et al (2020) HYPerspectral Enhanced Reality (HYPER): a physiology-based surgical guidance tool. Surgical Endoscopy 34:1736–1744

65. McDermott FD, Heeney A, Kelly ME, Steele RJ, Carlson GL, Winter DC (2015) Systematic review of preoperative, intraoperative and postoperative risk factors for colorectal anastomotic leaks. British Journal of Surgery 102:462–479

66. Pampiglione T, Chand M (2022) Enhancing colorectal anastomotic safety with indocyanine green fluorescence angiography: An update. Surgical Oncology 43:101545

67. Mueller MG, Kenton K (2019) Re: Complications of Recognized and Unrecognized Iatrogenic Ureteral Injury at Time of Hysterectomy: A Population Based Analysis. Journal of Urology 202:1054–1055

68. Marcelissen TAT, Den Hollander PP, Tuytten TRA, Sosef MN (2016) Incidence of Iatrogenic Ureteral Injury During Open and Laparoscopic Colorectal Surgery: A Single Center Experience and Review of the Literature. Surgical Laparoscopy, Endoscopy & Percutaneous Techniques 26:513–515

69. da Silva G, Boutros M, Wexner SD (2012) Role of prophylactic ureteric stents in colorectal surgery. Asian J Endosc Surg 5:105–110

70. Halabi WJ, Jafari MD, Nguyen VQ, Carmichael JC, Mills S, Pigazzi A, Stamos MJ (2014) Ureteral Injuries in Colorectal Surgery. Diseases of the Colon & Rectum 57:179–186

71. Rao D, Yu H, Zhu H, Duan P (2012) The diagnosis and treatment of iatrogenic ureteral and bladder injury caused by traditional gynaecology and obstetrics operation. Archives of Gynecology and Obstetrics 285:763–765

72. Palaniappa NC (2012) Incidence of Iatrogenic Ureteral Injury After Laparoscopic Colectomy. Archives of Surgery 147:267

73. Al-Awadi K, Kehinde EO, Al-Hunayan A, Al-Khayat A (2005) Iatrogenic Ureteric Injuries: Incidence, Aetiological Factors and the Effect of Early Management on Subsequent Outcome. International Urology and Nephrology 37:235–241

74. Nam Y-S, Wexner SD (2002) Clinical value of prophylactic ureteral stent indwelling during laparoscopic colorectal surgery. J Korean Med Sci 17:633–635

75. Speicher PJ, Goldsmith ZG, Nussbaum DP, Turley RS, Peterson AC, Mantyh CR (2014) Ureteral stenting in laparoscopic colorectal surgery. J Surg Res 190:98–103

76. Andersen P, Andersen LM, Iversen LH (2015) Iatrogenic ureteral injury in colorectal cancer surgery: a nationwide study comparing laparoscopic and open approaches. Surgical Endoscopy 29:1406–1412

77. Yellinek S, Krizzuk D, Nogueras JJ, Wexner SD (2018) Ureteral Injury During Colorectal Surgery: Two Case Reports and a Literature Review. Journal of the Anus, Rectum and Colon 2:71–76

78. (1970) On a new kind of rays. By W.C. Rontgen. Translated by Arthur Stanton from the Sitzungsberichte der Würzburger Physic-medic. Gesellschaft, 1895. Nature, January 23, 1896. Radiography 36:185–188

79. Filler A, Filler A (2009) The History, Development and Impact of Computed Imaging in Neurological Diagnosis and Neurosurgery: CT, MRI, and DTI. Nature Precedings. https://doi.org/10.1038/npre.2009.3267

80. Lauterbur PC (1973) Image Formation by Induced Local Interactions: Examples Employing Nuclear Magnetic Resonance. Nature 242:190–191

81. Hideki Hayashi (2009) Near-infrared bioimaging with the Use of a Fluorescent Dye.The journal of the Institute of Image Electronics Engineers of Japan : visual computing, devices & communications 38 (3), 309-313, 2009 (Japanese)

82. Morimoto T, Kobayashi T, Hirata H, Otani K, Sugimoto M, Tsukamoto M, Yoshihara T, Ueno M, Mawatari M (2022) XR (Extended Reality: Virtual Reality, Augmented Reality, Mixed Reality) Technology in Spine Medicine: Status Quo and Quo Vadis. Journal of Clinical Medicine 11:470

83. Sakai D, Joyce K, Sugimoto M, Horikita N, Hiyama A, Sato M, Devitt A, Watanabe M (2020) Augmented, virtual and mixed reality in spinal surgery: A real-world experience. J Orthop Surg 28:2309499020952698

84. Mishra R, Narayanan MDK, Umana GE, Montemurro N, Chaurasia B, Deora H (2022) Virtual Reality in Neurosurgery: Beyond Neurosurgical Planning. Int J Environ Res Public Health. https://doi.org/10.3390/ijerph19031719

85. Yoshida S, Sugimoto M, Fukuda S, Taniguchi N, Saito K, Fujii Y (2019) Mixed reality computed tomography-based surgical planning for partial nephrectomy using a head-mounted holographic computer. Int J Urol 26:681–682

86. D'Agostino J, Diana M, Vix M, Nicolau S, Soler L, Bourhala K, Hassler S, Wu H-S, Marescaux J (2013) Three-dimensional metabolic and radiologic gathered evaluation using VR-RENDER fusion: a novel tool to enhance accuracy in the localization of parathyroid adenomas. World J Surg 37:1618–1625

87. Gioux S, Choi HS, Frangioni JV (2010) Image-guided surgery using invisible near-infrared light: fundamentals of clinical translation. Mol Imaging 9:237–255

88. Nguyen QT, Tsien RY (2013) Fluorescence-guided surgery with live molecular navigation--a new cutting edge. Nat Rev Cancer 13:653–662

89. Novotny HR, Alvis D (1960) A method of photographing fluorescence in circulating blood of the human eye. Tech Doc Rep SAMTDR USAF Sch Aerosp Med 60-82:1–4

90. Dzurinko VL, Gurwood AS, Price JR (2004) Intravenous and indocyanine green angiography. Optometry 75:743–755

91. Holm C, Mayr M, Höfter E, Dornseifer U, Ninkovic M (2009) Assessment of the patency of microvascular anastomoses using microscope-integrated near-infrared angiography: A preliminary study. Microsurgery 29:509–514

92. Holm C, Dornseifer U, Sturtz G, Ninkovic M (2010) Sensitivity and specificity of ICG angiography in free flap reexploration. J Reconstr Microsurg 26:311–316

93. Perry D, Bharara M, Armstrong DG, Mills J (2012) Intraoperative fluorescence vascular angiography: during tibial bypass. J Diabetes Sci Technol 6:204–208

94. Benya R, Quintana J, Brundage B (1989) Adverse reactions to indocyanine green: A case report and a review of the literature. Catheterization and Cardiovascular Diagnosis 17:231–233

95. Nagata J, Fukunaga Y, Akiyoshi T, Konishi T, Fujimoto Y, Nagayama S, Yamamoto N, Ueno M (2016) Colonic Marking With Near-Infrared, Light-Emitting, Diode-Activated Indocyanine Green for Laparoscopic Colorectal Surgery. Diseases of the Colon & Rectum 59:e14–e18

96. Jafari MD, Lee KH, Halabi WJ, Mills SD, Carmichael JC, Stamos MJ, Pigazzi A (2013) The use of indocyanine green fluorescence to assess anastomotic perfusion during robotic assisted laparoscopic rectal surgery. Surg Endosc 27:3003–3008

97. Jafari MD, Wexner SD, Martz JE, McLemore EC, Margolin DA, Sherwinter DA, Lee SW, Senagore AJ, Phelan MJ, Stamos MJ (2015) Perfusion assessment in laparoscopic left-sided/anterior resection (PILLAR II): a multi-institutional study. J Am Coll Surg 220:82–92.e1

98. Kudszus S, Roesel C, Schachtrupp A, Höer JJ (2010) Intraoperative laser fluorescence angiography in colorectal surgery: a noninvasive analysis to reduce the rate of anastomotic leakage. Langenbeck's Archives of Surgery 395:1025–1030

99. Sherwinter DA, Gallagher J, Donkar T (2013) Intra-operative transanal near infrared imaging of colorectal anastomotic perfusion: a feasibility study. Colorectal Disease 15:91–96

100. Spota A, Al-Taher M, Felli E, et al (2021) Fluorescence-based bowel anastomosis perfusion evaluation: results from the IHU-IRCAD-EAES EURO-FIGS registry. Surgical Endoscopy 35:7142–7153

101. van Manen L, Handgraaf HJM, Diana M, Dijkstra J, Ishizawa T, Vahrmeijer AL, Mieog JSD (2018) A practical guide for the use of indocyanine green and methylene blue in fluorescence-guided abdominal surgery. J Surg Oncol 118:283–300

102. Barnes TG, Hompes R, Birks J, Mortensen NJ, Jones O, Lindsey I, Guy R, George B, Cunningham C, Yeung TM (2018) Methylene blue fluorescence of the ureter during colorectal surgery. Surgical Endoscopy 32:4036–4043

103. Cwalinski T, Polom W, Marano L, Roviello G, D'Angelo A, Cwalina N, Matuszewski M, Roviello F, Jaskiewicz J, Polom K (2020) Methylene Blue—Current Knowledge, Fluorescent Properties, and Its Future Use. Journal of Clinical Medicine 9:3538

104. Ginimuge PR, Jyothi SD (2010) Methylene blue: revisited. J Anaesthesiol Clin Pharmacol 26:517–520

105. Budner O, Cwalinski T, Skokowski J, Marano L, Resca L, Cwalina N, Kalinowski L, Hoveling R, Roviello F, Polom K (2022) Methylene Blue Near-Infrared Fluorescence Imaging in Breast Cancer Sentinel Node Biopsy. Cancers . https://doi.org/10.3390/cancers14071817

106. Matsui A, Tanaka E, Choi HS, Kianzad V, Gioux S, Lomnes SJ, Frangioni JV (2010) Real-time, near-infrared, fluorescence-guided identification of the ureters using methylene blue. Surgery 148:78–86

107. Al-Taher M, van den Bos J, Schols RM, Bouvy ND, Stassen LPS (2016) Fluorescence Ureteral Visualization in Human Laparoscopic Colorectal Surgery Using Methylene Blue. J Laparoendosc Adv Surg Tech A 26:870–875

108. Shin D, Vigneswaran N, Gillenwater A, Richards-Kortum R (2010) Advances in fluorescence imaging techniques to detect oral cancer and its precursors. Future Oncol 6:1143–1154

109. Stummer W, Pichlmeier U, Meinel T, Wiestler OD, Zanella F, Reulen H-J, ALA-Glioma Study Group (2006) Fluorescence-guided surgery with 5-aminolevulinic acid for resection of malignant glioma: a randomised controlled multicentre phase III trial. Lancet Oncol 7:392–401

110. D'Hallewin M-A, Bezdetnaya L, Guillemin F (2002) Fluorescence detection of bladder cancer: a review. Eur Urol 42:417–425

111. Tsuruki ES, Saito Y, Abe S, Takamaru H, Yamada M, Sakamoto T, Nakajima T, Matsuda T, Sekine S, Taniguchi H (2016) Evaluating the efficacy and safety of a novel endoscopic fluorescence imaging modality using oral 5-aminolevulinic acid for colorectal tumors. Endosc Int Open 4:E30–5

112. McElroy M, Kaushal S, Luiken GA, Talamini MA, Moossa AR, Hoffman RM, Bouvet M (2008) Imaging of primary and metastatic pancreatic cancer using a fluorophore-conjugated anti-CA19-9 antibody for surgical navigation. World J Surg 32:1057–1066

113. Cao HST, Tran Cao HS, Kaushal S, et al (2011) Tumor-Specific Fluorescence Antibody Imaging Enables Accurate Staging Laparoscopy in an Orthotopic Model of Pancreatic Cancer. Hepatogastroenterology. https://doi.org/10.5754/hge11836

114. Hall MA, Pinkston KL, Wilganowski N, Robinson H, Ghosh P, Azhdarinia A, Vazquez-Arreguin K, Kolonin AM, Harvey BR, Sevick-Muraca EM (2012) Comparison of mAbs targeting epithelial cell adhesion molecule for the detection of prostate cancer lymph node metastases with multimodal contrast agents: quantitative small-animal PET/CT and NIRF. J Nucl Med 53:1427–1437

115. Nakajima T, Mitsunaga M, Bander NH, Heston WD, Choyke PL, Kobayashi H (2011) Targeted, activatable, in vivo fluorescence imaging of prostate-specific membrane antigen (PSMA) positive tumors using the quenched humanized J591 antibody-indocyanine green (ICG) conjugate. Bioconjug Chem 22:1700–1705

116. Rosbach KJ, Williams MD, Gillenwater AM, Richards-Kortum RR (2012) Optical Molecular Imaging of Multiple Biomarkers of Epithelial Neoplasia: Epidermal Growth Factor Receptor Expression and Metabolic Activity in Oral Mucosa. Translational Oncology 5:160–171

117. Hellebust A, Richards-Kortum R (2012) Advances in molecular imaging: targeted optical contrast agents for cancer diagnostics. Nanomedicine 7:429–445

118. Yu Z, Eich C, Cruz LJ (2020) Recent Advances in Rare-Earth-Doped Nanoparticles for NIR-II Imaging and Cancer Theranostics. Front Chem. https://doi.org/10.3389/fchem.2020.00496

119. Cahill RA, Anderson M, Wang LM, Lindsey I, Cunningham C, Mortensen NJ (2012) Near-infrared (NIR) laparoscopy for intraoperative lymphatic road-mapping and sentinel node identification during definitive surgical resection of early-stage colorectal neoplasia. Surgical Endoscopy 26:197–204

120. Watanabe J, Ota M, Suwa Y, Ishibe A, Masui H, Nagahori K (2016) Real-Time Indocyanine Green Fluorescence Imaging–Guided Complete Mesocolic Excision in Laparoscopic Flexural Colon Cancer Surgery. Diseases of the Colon & Rectum 59:701–705

121. Sevick-Muraca EM, Houston JP, Gurfinkel M (2002) Fluorescence-enhanced, near infrared diagnostic imaging with contrast agents. Curr Opin Chem Biol 6:642–650

122. Petz W, Bertani E, Borin S, Fiori G, Ribero D, Spinoglio G (2021) Fluorescence-guided D3 lymphadenectomy in robotic right colectomy with complete mesocolic excision. Int J Med Robot 17:e2217

123. Chand M, Keller DS, Joshi HM, Devoto L, Rodriguez-Justo M, Cohen R (2018) Feasibility of fluorescence lymph node imaging in colon cancer: FLICC. Techniques in Coloproctology 22:271–277

124. Barberio M, Felli E, Seyller E, et al (2020) Quantitative fluorescence angiography versus hyperspectral imaging to assess bowel ischemia: A comparative study in enhanced reality. Surgery 168:178–184

125. Clancy NT, Soares AS, Bano S, Lovat LB, Chand M, Stoyanov D (2021) Intraoperative colon perfusion assessment using multispectral imaging. Biomedical Optics Express 12:7556

126. Soares AS, Bano S, Clancy NT, Stoyanov D, Lovat LB, Chand M (2022) Multisensor perfusion assessment cohort study: Preliminary evidence toward a standardized assessment of indocyanine green fluorescence in colorectal surgery. Surgery 172:69–73

127. Lu G, Fei B (2014) Medical hyperspectral imaging: a review. J Biomed Opt 19:10901

128. Li Q (2012) Hyperspectral Imaging Technology Used in Tongue Diagnosis. Recent Advances in Theories and Practice of Chinese Medicine. https://doi.org/10.5772/27474

129. Zuzak KJ, Naik SC, Alexandrakis G, Hawkins D, Behbehani K, Livingston E (2008) Intraoperative bile duct visualization using near-infrared hyperspectral video imaging. The American Journal of Surgery 195:491–497

130. Akbari H, Uto K, Kosugi Y, Kojima K, Tanaka N (2011) Cancer detection using infrared hyperspectral imaging. Cancer Science 102:852–857

131. Martinez B, Leon R, Fabelo H, et al (2019) Most Relevant Spectral Bands Identification for Brain Cancer Detection Using Hyperspectral Imaging. Sensors 19:5481

132. Köhler H, Jansen-Winkeln B, Maktabi M, et al (2019) Evaluation of hyperspectral imaging (HSI) for the measurement of ischemic conditioning effects of the gastric conduit during esophagectomy. Surgical Endoscopy 33:3775–3782

133. Jansen-Winkeln B, Maktabi M, Takoh JP, Rabe SM, Barberio M, Köhler H, Neumuth T, Melzer A, Chalopin C, Gockel I (2018) Hyperspektral-Imaging bei gastrointestinalen Anastomosen. Der Chirurg 89:717–725

134. Urade T, Felli E, Barberio M, et al (2020) Hyperspectral enhanced reality (HYPER) for anatomical liver resection. Surg Endosc 35:1844–1850

135. Barberio M, Collins T, Bencteux V, Nkusi R, Felli E, Viola MG, Marescaux J, Hostettler A, Diana M (2021) Deep Learning Analysis of In Vivo Hyperspectral Images for Automated Intraoperative Nerve Detection. Diagnostics 11:1508

136. Collins T, Maktabi M, Barberio M, Bencteux V, Jansen-Winkeln B, Chalopin C, Marescaux J, Hostettler A, Diana M, Gockel I (2021) Automatic Recognition of Colon and Esophagogastric Cancer with Machine Learning and Hyperspectral Imaging. Diagnostics (Basel). https://doi.org/10.3390/diagnostics11101810

137. Hagen NA, Kudenov MW (2013) Review of snapshot spectral imaging technologies. Organ Ethic 52:090901

138. Multispectral Image Processing | The Nature of Geographic Information". www.e-education.psu.edu. Retrieved 2019-11-14.

139. Baronti S, Casini A, Lotti F, Porcinai S (1998) Multispectral Imaging System for the Mapping of Pigments in Works of Art by use of Principal-Component Analysis. Appl Opt 37:1299–1309

140. Clancy NT, Jones G, Maier-Hein L, Elson DS, Stoyanov D (2020) Surgical spectral imaging. Med Image Anal 63:101699

141. Olweny EO, Faddegon S, Best SL, Jackson N, Wehner EF, Tan YK, Zuzak KJ, Cadeddu JA (2013) Renal oxygenation during robot-assisted laparoscopic partial nephrectomy: characterization using laparoscopic digital light processing hyperspectral imaging. J Endourol 27:265–269

142. Akter S, Kawauchi S, Sato S, Aosasa S, Yamamoto J, Nishidate I (2017) imaging of hepatic hemodynamics and light scattering property during ischemia-reperfusion in rats based on spectrocolorimetry. Biomed Opt Express 8:974–992

143. Mori M, Chiba T, Nakamizo A, et al (2014) Intraoperative visualization of cerebral oxygenation using hyperspectral image data: a two-dimensional mapping method. Int J Comput Assist Radiol Surg 9:1059–1072

144. Khouj Y, Dawson J, Coad J, Vona-Davis L (2018) Hyperspectral Imaging and K-Means Classification for Histologic Evaluation of Ductal Carcinoma. Front Oncol 8:17

145. Wisotzky EL, Uecker FC, Arens P, Dommerich S, Hilsmann A, Eisert P (2018) Intraoperative hyperspectral determination of human tissue properties. J Biomed Opt 23:1–8

146. Lin J, Clancy NT, Qi J, Hu Y, Tatla T, Stoyanov D, Maier-Hein L, Elson DS (2018) Dual-modality endoscopic probe for tissue surface shape reconstruction and hyperspectral imaging enabled by deep neural networks. Med Image Anal 48:162–176

147. Rawla P, Sunkara T, Barsouk A (2019) Epidemiology of colorectal cancer: incidence, mortality, survival, and risk factors. Prz Gastroenterol 14:89–103

148. You YN, Hardiman KM, Bafford A, Poylin V, Francone TD, Davis K, Paquette IM, Steele SR, Feingold DL, On Behalf of the Clinical Practice Guidelines Committee of the American Society of Colon and Rectal Surgeons (2020) The American Society of Colon and Rectal Surgeons Clinical Practice Guidelines for the Management of Rectal Cancer. Dis Colon Rectum 63:1191–1222

149. Benson AB, Venook AP, Al-Hawary MM, et al (2020) NCCN Guidelines Insights: Rectal Cancer, Version 6.2020. J Natl Compr Canc Netw 18:806–815

150. Glynne-Jones R, Wyrwicz L, Tiret E, Brown G, Rödel C, Cervantes A, Arnold D, ESMO Guidelines Committee (2018) Rectal cancer: ESMO Clinical Practice Guidelines for diagnosis, treatment and follow-up. Ann Oncol 29:iv263

151. D'Souza N, de Neree Tot Babberich MPM, d'Hoore A, et al (2019) Definition of the Rectum: An International, Expert-based Delphi Consensus. Ann Surg 270:955–959

152. Li F, Wang B, Lu S, Wang Y, Sun T, Wang H, Zhou X, Fu W (2020) Comparison of the sigmoid take-off with other definitions of the rectosigmoid junction: A retrospective comparative cohort analysis. Int J Surg 80:168–174

153. Bogveradze N, Lambregts DMJ, El Khababi N, Dresen RC, Maas M, Kusters M, Tanis PJ, Beets-Tan RGH, MRI rectal study group (2022) The sigmoid take-off as a landmark to distinguish rectal from sigmoid tumours on MRI: Reproducibility, pitfalls and potential impact on treatment stratification. Eur J Surg Oncol 48:237–244

154. D'Souza N, Lord A, Shaw A, et al (2020) The sigmoid take-off: An anatomical imaging definition of the rectum validated on specimen analysis. Eur J Surg Oncol 46:1668–1672

155. Wu Q, Jin C, Hu T, Wei M, Wang Z (2017) Intracorporeal Versus Extracorporeal Anastomosis in Laparoscopic Right Colectomy: A Systematic Review and Meta-Analysis. J Laparoendosc Adv Surg Tech A 27:348–357

156. Mari GM, Crippa J, Costanzi ATM, Pellegrino R, Siracusa C, Berardi V, Maggioni D (2018) Intracorporeal Anastomosis Reduces Surgical Stress Response in Laparoscopic Right Hemicolectomy: A Prospective Randomized Trial. Surg Laparosc Endosc Percutan Tech 28:77–81

157. Ricci C, Casadei R, Alagna V, Zani E, Taffurelli G, Pacilio CA, Minni F (2017) A critical and comprehensive systematic review and meta-analysis of studies comparing intracorporeal and extracorporeal anastomosis in laparoscopic right hemicolectomy. Langenbecks Arch Surg 402:417–427

158. Milone M, Elmore U, Vignali A, Gennarelli N, Manigrasso M, Burati M, Milone F, De Palma GD, Delrio P, Rosati R (2018) Recovery after intracorporeal anastomosis in laparoscopic right hemicolectomy: a systematic review and meta-analysis. Langenbecks Arch Surg 403:1–10

159. van Oostendorp S, Elfrink A, Borstlap W, Schoonmade L, Sietses C, Meijerink J, Tuynman J (2017) Intracorporeal versus extracorporeal anastomosis in right hemicolectomy: a systematic review and meta-analysis. Surg Endosc 31:64–77

160. Emile SH, Elfeki H, Shalaby M, Sakr A, Bassuni M, Christensen P, Wexner SD (2019) Intracorporeal versus extracorporeal anastomosis in minimally invasive right colectomy: an updated systematic review and meta-analysis. Tech Coloproctol 23:1023–1035

161. Charan I, Kapoor A, Singhal MK, Jagawat N, Bhavsar D, Jain V, Kumar V, Kumar HS (2015) High Ligation of Inferior Mesenteric Artery in Left Colonic and Rectal Cancers: Lymph Node Yield and Survival Benefit. Indian J Surg 77:1103–1108

162. Kessler H, Hohenberger W (2013) Extended lymphadenectomy in colon cancer is crucial. World J Surg 37:1789–1798

163. Chin C-C, Yeh C-Y, Tang R, Changchien C-R, Huang W-S, Wang J-Y (2008) The oncologic benefit of high ligation of the inferior mesenteric artery in the surgical treatment of rectal or sigmoid colon cancer. International Journal of Colorectal Disease 23:783–788

164. Alici A, Kement M, Gezen C, Akin T, Vural S, Okkabaz N, Basturk E, Yegenoglu A, Oncel M (2010) Apical lymph nodes at the root of the inferior mesenteric artery in distal colorectal cancer: an analysis of the risk of tumor involvement and the impact of high ligation on anastomotic integrity. Tech Coloproctol 14:1–8

165. Zeng J, Su G (2018) High ligation of the inferior mesenteric artery during sigmoid colon and rectal cancer surgery increases the risk of anastomotic leakage: a meta-analysis. World Journal of Surgical Oncology. https://doi.org/10.1186/s12957-018-1458-7

166. Komen N, Slieker J, de Kort P, et al (2011) High tie versus low tie in rectal surgery: comparison of anastomotic perfusion. Int J Colorectal Dis 26:1075–1078

167. Fan D, Zhang C, Li X, Yao C, Yao T (2018) Evaluation of the clinical efficacy of preserving the left colic artery in laparoscopic resection for rectal cancer: A meta-analysis. Mol Clin Oncol 9:553–560

168. Hajibandeh S, Hajibandeh S, Maw A (2020) Meta-analysis and Trial Sequential Analysis of Randomized Controlled Trials Comparing High and Low Ligation of the Inferior Mesenteric Artery in Rectal Cancer Surgery. Dis Colon Rectum 63:988–999

169. Zhang C, Chen L, Cui M, et al (2020) Short- and long-term outcomes of rectal cancer patients with high or improved low ligation of the inferior mesenteric artery. Sci Rep 10:15339

170. Yang Y, Wang G, He J, Zhang J, Xi J, Wang F (2018) High tie versus low tie of the inferior mesenteric artery in colorectal cancer: A meta-analysis. Int J Surg 52:20–24

171. Mari GM, Crippa J, Cocozza E, et al (2019) Low Ligation of Inferior Mesenteric Artery in Laparoscopic Anterior Resection for Rectal Cancer Reduces Genitourinary Dysfunction: Results From a Randomized Controlled Trial (HIGHLOW Trial). Ann Surg 269:1018–1024

172. The American Cancer Society (2018) The American Cancer Society's Oncology in Practice: Clinical Management. John Wiley & Sons

173. Culligan K, Walsh S, Dunne C, Walsh M, Ryan S, Quondamatteo F, Dockery P, Coffey C J (2014) The mesocolon – A histological and electron microscopic characterisation of

the mesenteric attachment of the colon prior to and after surgical mobilisation. Annals of Medicine and Surgery 3:47

174. Hashimoto DA, Rosman G, Rus D, Meireles OR (2018) Artificial Intelligence in Surgery: Promises and Perils. Ann Surg 268:70–76

175. Jansen-Winkeln B, Barberio M, Chalopin C, Schierle K, Diana M, Köhler H, Gockel I, Maktabi M (2021) Feedforward Artificial Neural Network-Based Colorectal Cancer Detection Using Hyperspectral Imaging: A Step towards Automatic Optical Biopsy. Cancers . https://doi.org/10.3390/cancers13050967

176. Giessen M van de, van de Giessen M, Angelo JP, Gioux S (2015) Real-time, profile-corrected single snapshot imaging of optical properties. Biomedical Optics Express 6:4051

177. Gioux S, Mazhar A, Cuccia DJ (2019) Spatial frequency domain imaging in 2019: principles, applications, and perspectives. Journal of Biomedical Optics 24:1

178. Schmidt M, Aguénounon E, Nahas A, Torregrossa M, Tromberg BJ, Uhring W, Gioux S (2019) Real-time, wide-field, and quantitative oxygenation imaging using spatiotemporal modulation of light. Journal of Biomedical Optics 24:1

179. Aguénounon E, Smith JT, Al-Taher M, Diana M, Intes X, Gioux S (2020) Real-time, wide-field and high-quality single snapshot imaging of optical properties with profile correction using deep learning. Biomedical Optics Express 11:5701

180. Gioux S, Stockdale A, Oketokoun R, et al (2011) First-in-human pilot study of a spatial frequency domain oxygenation imaging system. Journal of Biomedical Optics 16:1

181. Panigrahi S, Gioux S (2018) Machine learning approach for rapid and accurate estimation of optical properties using spatial frequency domain imaging. Journal of Biomedical Optics 24:1

182. Kusano M, Tajima Y, Yamazaki K, Kato M, Watanabe M, Miwa M (2008) Sentinel Node Mapping Guided by Indocyanine Green Fluorescence Imaging: A New Method for Sentinel Node Navigation Surgery in Gastrointestinal Cancer. Digestive Surgery 25:103–108

183. Verbeek FPR, Tummers QRJ, Rietbergen DDD, Peters AAW, Schaafsma BE, van de Velde CJH, Frangioni JV, van Leeuwen FWB, Gaarenstroom KN, Vahrmeijer AL (2015) Sentinel Lymph Node Biopsy in Vulvar Cancer Using Combined Radioactive and Fluorescence Guidance. International Journal of Gynecologic Cancer 25:1086–1093

184. Watanabe J, Ota M, Suwa Y, Ishibe A, Masui H, Nagahori K (2017) Evaluation of lymph flow patterns in splenic flexural colon cancers using laparoscopic real-time indocyanine green fluorescence imaging. Int J Colorectal Dis 32:201–207

185. Raabe A, Nakaji P, Beck J, Kim LJ, Hsu FPK, Kamerman JD, Seifert V, Spetzler RF (2005) Prospective evaluation of surgical microscope—integrated intraoperative near-infrared indocyanine green videoangiography during aneurysm surgery. Journal of Neurosurgery 103:982–989

186. Dasgupta Y, Golovine K, Nieborowska-Skorska M, Luo L, Matlawska-Wasowska K, Mullighan CG, Skorski T (2018) Drugging DNA repair to target T-ALL cells. Leuk Lymphoma 59:1746–1749

187. Staniloaie D, Budin C, Vasile D, et al (2021) Role of methylene blue in detecting the sentinel lymph node in colorectal cancer: *In vivo* vs. *ex vivo* technique. Experimental and Therapeutic Medicine. https://doi.org/10.3892/etm.2021.10995

188. Märkl B, Kerwel TG, Wagner T, Anthuber M, Arnholdt HM (2007) Methylene blue injection into the rectal artery as a simple method to improve lymph node harvest in rectal cancer. Mod Pathol 20:797–801

189. Liu J, Huang P, Zheng Z, Chen T, Wei H (2017) Modified methylene blue injection improves lymph node harvest in rectal cancer. ANZ J Surg 87:247–251

190. Polom W, Migaczewski M, Skokowski J, Swierblewski M, Cwalinski T, Kalinowski L, Pedziwiatr M, Matuszewski M, Polom K (2022) Multispectral Imaging Using Fluorescent Properties of Indocyanine Green and Methylene Blue in Colorectal Surgery-Initial Experience. J Clin Med Res. https://doi.org/10.3390/jcm11020368

191. Kilkenny C, Browne WJ, Cuthill IC, Emerson M, Altman DG (2010) Improving Bioscience Research Reporting: The ARRIVE Guidelines for Reporting Animal Research. PLoS Biology 8:e1000412

192. Ji Y, Sun L, Li Y, Li J, Liu S, Xie X, Xu Y (2019) Non-destructive classification of defective potatoes based on hyperspectral imaging and support vector machine. Infrared Physics & Technology 99:71–79

193. Lukin V, Abramov S, Krivenko S, Kurekin A, Pogrebnyak O (2013) Analysis of classification accuracy for pre-filtered multichannel remote sensing data. Expert Systems with Applications 40:6400–6411

194. Qiao T, Ren J, Wang Z, Zabalza J, Sun M, Zhao H, Li S, Benediktsson JA, Dai Q, Marshall S (2017) Effective Denoising and Classification of Hyperspectral Images Using Curvelet Transform and Singular Spectrum Analysis. IEEE Transactions on Geoscience and Remote Sensing 55:119–133

195. Ba-Ssalamah A, Fakhrai N, Baroud S, Shirkhoda A (2013) Mesentery, Omentum, Peritoneum: Embryology, Normal Anatomy and Anatomic Variants. Abdominal Imaging 1563–1576

196. Chen P-C, Lin W-C (2011) Spectral-profile-based algorithm for hemoglobin oxygen saturation determination from diffuse reflectance spectra. Biomedical Optics Express 2:1082

197. Paoletti ME, Haut JM, Plaza J, Plaza A (2019) Deep learning classifiers for hyperspectral imaging: A review. ISPRS Journal of Photogrammetry and Remote Sensing 158:279–317

198. Hu W, Huang Y, Wei L, Zhang F, Li H (2015) Deep Convolutional Neural Networks for Hyperspectral Image Classification. Journal of Sensors 2015:1–12

199. Hamida AB, Ben Hamida A, Benoit A, Lambert P, Ben Amar C (2018) 3-D Deep Learning Approach for Remote Sensing Image Classification. IEEE Transactions on Geoscience and Remote Sensing 56:4420–4434

200. Eigen D, Fergus R (2015) Predicting Depth, Surface Normals and Semantic Labels with a Common Multi-scale Convolutional Architecture. 2015 IEEE International Conference on Computer Vision (ICCV). https://doi.org/10.1109/iccv.2015.304

201. Cuccia DJ, Bevilacqua F, Durkin AJ, Ayers FR, Tromberg BJ (2009) Quantitation and mapping of tissue optical properties using modulated imaging. Journal of Biomedical Optics 14:024012

202. Angelo J, Vargas CR, Lee BT, Bigio IJ, Gioux S (2016) Ultrafast optical property map generation using lookup tables. Journal of Biomedical Optics 21:110501

203. Aguénounon E, Dadouche F, Uhring W, Gioux S (2019) Single snapshot of optical properties image quality improvement using anisotropic two-dimensional windows filtering. Journal of Biomedical Optics 24:1

204. Mazhar A, Dell S, Cuccia DJ, Gioux S, Durkin AJ, Frangioni JV, Tromberg BJ (2010) Wavelength optimization for rapid chromophore mapping using spatial frequency domain imaging. Journal of Biomedical Optics 15:1

205. Quero G, Lapergola A, Barberio M, et al (2018) Discrimination between arterial and venous bowel ischemia by computer-assisted analysis of the fluorescent signal. Surg Endosc 33:1988–1997

206. Diana M, Noll E, Diemunsch P, Moussallieh F-M, Namer I-J, Charles A-L, Lindner V, Agnus V, Geny B, Marescaux J (2015) Metabolism-Guided Bowel Resection. Surgical Innovation 22:453–461

207. Quaedackers JSLT, Quaedackers JSL, Beuk RJ, Bennet L, Charlton A, oude Egbrink MG, Gunn AJ, Heineman E (2000) An evaluation of methods for grading histologic injury following ischemia/reperfusion of the small bowel. Transplantation Proceedings 32:1307–1310

208. Chiu C-J (1970) Intestinal Mucosal Lesion in Low-Flow States. Archives of Surgery 101:478

209. Hosmer DW, Lemeshow S (2000) Applied Logistic Regression. https://doi.org/10.1002/0471722146

210. Hüscher CGS, Lirici MM, Marks JH, Dapri G, Ancona E (2021) Laparoscopic left colectomy: modern technique based on key anatomical landmarks reported by giants of the past. Minimally Invasive Therapy & Allied Technologies 30:1–11

211. Seeliger B, Agnus V, Mascagni P, et al (2019) Simultaneous computer-assisted assessment of mucosal and serosal perfusion in a model of segmental colonic ischemia. Surg Endosc 34:4818–4827

212. Diana M, Agnus V, Halvax P, Liu Y-Y, Dallemagne B, Schlagowski A-I, Geny B, Diemunsch P, Lindner V, Marescaux J (2015) Intraoperative fluorescence-based enhanced reality laparoscopic real-time imaging to assess bowel perfusion at the anastomotic site in an experimental model. British Journal of Surgery 102:e169–e176

213. Hirche C, Engel H, Kolios L, Cognie J, Hünerbein M, Lehnhardt M, Kremer T (2013) An Experimental Study to Evaluate the Fluobeam 800 Imaging System for Fluorescence-Guided Lymphatic Imaging and Sentinel Node Biopsy. Surgical Innovation 20:516–523

214. Yamashita S-I, Tokuishi K, Anami K, et al (2011) Video-assisted thoracoscopic indocyanine green fluorescence imaging system shows sentinel lymph nodes in non–small-cell lung cancer. The Journal of Thoracic and Cardiovascular Surgery 141:141–144

215. Meershoek P, KleinJan GH, van Willigen DM, et al (2020) Multi-wavelength fluorescence imaging with a da Vinci Firefly—a technical look behind the scenes. J Robot Surg 15:751–760

216. D'Urso A, Agnus V, Barberio M, Seeliger B, Marchegiani F, Charles A-L, Geny B, Marescaux J, Mutter D, Diana M (2021) Computer-assisted quantification and visualization of bowel perfusion using fluorescence-based enhanced reality in left-sided colonic resections. Surgical Endoscopy 35:4321–4331

217. Nerup N, Andersen HS, Ambrus R, Strandby RB, Svendsen MBS, Madsen MH, Svendsen LB, Achiam MP (2017) Quantification of fluorescence angiography in a porcine model. Langenbeck's Archives of Surgery 402:655–662

218. Gosvig K, Jensen SS, Qvist N, Nerup N, Agnus V, Diana M, Ellebæk MB (2021) Quantification of ICG fluorescence for the evaluation of intestinal perfusion: comparison between two software-based algorithms for quantification. Surg Endosc 35:5043–5050

219. Jansen-Winkeln B, Germann I, Köhler H, et al (2021) Comparison of hyperspectral imaging and fluorescence angiography for the determination of the transection margin in colorectal resections—a comparative study. International Journal of Colorectal Disease 36:283–291

220. Vervandier J, Gioux S (2013) Single snapshot imaging of optical properties. Biomedical Optics Express 4:2938

221. Dögnitz N, Wagnières G (1998) Determination of tissue optical properties by steady-state spatial frequency-domain reflectometry. Lasers in Medical Science 13:55–65

222. Nguyen JT, Lin SJ, Tobias AM, et al (2013) A Novel Pilot Study Using Spatial Frequency Domain Imaging to Assess Oxygenation of Perforator Flaps During Reconstructive Breast Surgery. Annals of Plastic Surgery 71:308–315

223. Le Voyer TE, Sigurdson ER, Hanlon AL, Mayer RJ, Macdonald JS, Catalano PJ, HallerDG (2003) Colon cancer survival is associated with increasing number of lymph nodes analyzed: a secondary survey of intergroup trial INT-0089. J Clin Oncol 21:2912–2919

224. Swanson RS, Compton CC, Stewart AK, Bland KI (2003) The Prognosis of T3N0 Colon Cancer Is Dependent on the Number of Lymph Nodes Examined. Annals of Surgical Oncology 10:65–71

225. Institute NC, National Cancer Institute (2020) AJCC Cancer Staging Manual 8th Edition. Definitions. https://doi.org/10.32388/b30ldk

226. Compton CC (2006) Key issues in reporting common cancer specimens: problems in pathologic staging of colon cancer. Arch Pathol Lab Med 130:318–324

227. Benson AB, Venook AP, Al-Hawary MM, et al (2021) Colon Cancer, Version 2.2021, NCCN Clinical Practice Guidelines in Oncology. J Natl Compr Canc Netw 19:329–359

228. Wong SL, Ji H, Hollenbeck BK, Morris AM, Baser O, Birkmeyer JD (2007) Hospital lymph node examination rates and survival after resection for colon cancer. JAMA 298:2149–2154

229. Goldstein NS (2002) Lymph Node Recoveries From 2427 pT3 Colorectal Resection Specimens Spanning 45 Years. The American Journal of Surgical Pathology 26:179–189

230. Emile SH, Elfeki H, Shalaby M, Sakr A, Sileri P, Laurberg S, Wexner SD (2017) Sensitivity and specificity of indocyanine green near-infrared fluorescence imaging in detection of metastatic lymph nodes in colorectal cancer: Systematic review and meta-analysis. J Surg Oncol 116:730–740

231. Watanabe J, Ota M, Suwa Y, Ishibe A, Masui H, Nagahori K (2017) Evaluation of lymph flow patterns in splenic flexural colon cancers using laparoscopic real-time indocyanine green fluorescence imaging. Int J Colorectal Dis 32:201–207

232. Martijn H.G.M. van der Pas, Marjolein Ankersmit, Hein B.A.C. Stockmann, Rob Silvis, Nicole C.T. van Grieken, Herman Bril, and Wilhelmus J.H.J. Meijerink (2013) Laparoscopic Sentinel Lymph Node Identification in Patients with Colon Carcinoma Using a Near-Infrared Dye: Description of a New Technique and Feasibility StudyJournal of Laparoendoscopic & Advanced Surgical Techniques 2013 23:4, 367-371

233. Liberale G, Vankerckhove S, Galdon MG, Donckier V, Larsimont D, Bourgeois P (2015) Fluorescence imaging after intraoperative intravenous injection of indocyanine green for detection of lymph node metastases in colorectal cancer. Eur J Surg Oncol 41:1256–1260

234. Jiang L, Liu T, Wang X, Li J, Zhao H (2020) Real-time near-infrared fluorescence imaging mediated by blue dye in breast cancer patients. Journal of Surgical Oncology 121:964–966

235. Sarli L, Bader G, Iusco D, Salvemini C, Mauro DD, Mazzeo A, Regina G, Roncoroni L (2005) Number of lymph nodes examined and prognosis of TNM stage II colorectal cancer. Eur J Cancer 41:272–279

236. (1999) Efficacy of Adjuvant Fluorouracil and Folinic Acid in B2 Colon Cancer. Journal of Clinical Oncology 17:1356–1356

237. (2001) Adjuvant radiotherapy for rectal cancer: a systematic overview of 8507 patients from 22 randomised trials. The Lancet 358:1291–1304

238. Sauer R, Becker H, Hohenberger W, et al (2004) Preoperative versus Postoperative Chemoradiotherapy for Rectal Cancer. New England Journal of Medicine 351:1731–1740

239. Hermanek P, Hohenberger W, Klimpfinger M, Köckerling F, Papadopoulos T (2003) The pathological assessment of mesorectal excision: implications for further treatment and quality management. Int J Colorectal Dis 18:335–341

240. Chahin F, Dwivedi AJ, Paramesh A, Chau W, Agrawal S, Chahin C, Kumar A, Tootla A, Tootla F, Silva YJ (2002) The implications of lighted ureteral stenting in laparoscopic colectomy. JSLS 6:49–52

241. van den Bos J, Al-Taher M, Bouvy ND, Stassen LPS (2019) Near-infrared fluorescence laparoscopy of the ureter with three preclinical dyes in a pig model. Surg Endosc 33:986–991

242. Farnam RW, Arms RG, Klaassen AH, Sorger JM (2019) Intraoperative ureter visualization using a near-infrared imaging agent. J Biomed Opt 24:1–8

243. Verbeek FPR, van der Vorst JR, Schaafsma BE, Swijnenburg R-J, Gaarenstroom KN, Elzevier HW, van de Velde CJH, Frangioni JV, Vahrmeijer AL (2013) Intraoperative Near Infrared Fluorescence Guided Identification of the Ureters Using Low Dose Methylene Blue: A First in Human Experience. J Urol. https://doi.org/10.1016/j.juro.2013.02.3187

244. Ginimuge PR, Jyothi SD (2010) Methylene blue: revisited. J Anaesthesiol Clin Pharmacol 26:517–520

245. Sinex JE (1999) Pulse oximetry: principles and limitations. Am J Emerg Med 17:59–67

246.Mokhlesi B, Leikin JB, Murray P, Corbridge TC (2003) Adult toxicology in critical care: Part II: specific poisonings. Chest 123:897–922

Liste des publications

(relatifs au cancer colorectal ou à la chirurgie guidée par l'image)

- **Quantification of bowel ischaemia using real-time multispectral Single Snapshot Imaging of Optical Properties (SSOP).**
  Rodríguez-Luna MR, **Okamoto N**, Cinelli L, Baratelli L, Ségaud, S, Rodriguez-Gomez A, Keller DS, Marescaux J, Diana M, Gioux S.
  Surg Endosc. 2022 Nov 28. doi: 10.1007/s00464-022-09764-z. Epub ahead of print. PMID: 36443562.

- **Hyperspectral Imaging in Major Hepatectomies: Preliminary Results from the Ex-Machyna Trial.**
  Felli E, Cinelli L, Bannone E, Giannone F, Muttillo EM, Barberio M, Keller DS, Rodríguez-Luna MR, **Okamoto N**, Collins T, Hostettler A, Schuster C, Mutter D, Pessaux P, Marescaux J, Gioux S, Felli E, Diana M
  Cancers (Basel). 2022 Nov 14;14(22):5591. doi: 10.3390/cancers14225591. PMID: 36428685.

- **Trident: A dual oxygenation and fluorescence imaging platform for real-time and quantitative surgical guidance.**
  Ségaud S, Baratelli L, Felli E, Bannone E, Cinelli L, Rodríguez-Luna MR, **Okamoto N**, Keller DS, de Mathelin M, Lecler S, Diana M, Gioux S
  Front. Photonics 3 (2022) :1032776. doi: 10.3389/fphot.2022.1032776

- **International survey among surgeons on the perioperative management of rectal cancer.**
  Al-Difaie Z#, **Okamoto N#***, Scheepers MHMC, Mutter D, Stassen LPS, Bouvy ND, Marescaux J, Dallemagne B, Diana M, Al-Taher M (#: Co-first authors; *: Corresponding author)
  Surg Endosc 2022 Oct 18. doi: 10.1007/s00464-022-09702-z. Epub ahead of print. PMID: 36258001.

- **Computer-Assisted Differentiation between Colon-Mesocolon and Retroperitoneum Using Hyperspectral Imaging (HSI) Technology.**
  Okamoto N, Rodríguez-Luna MR, Bencteux V, Al-Taher M, Cinelli L, Felli E, Urade T, Nkusi R, Mutter D, Marescaux J, Hostettler A, Collins T, Diana M.
  Diagnostics. 2022; 12(9):2225. https://doi.org/10.3390/diagnostics12092225

- **In Vivo Imaging Evaluation of Fluorescence Intensity at Tail Emission of Near-Infrared-I (NIR-I) Fluorophores in a Porcine Model.**
  Rodríguez-Luna MR, **Okamoto N**, Al-Taher M, Keller DS, Cinelli L, Hoskere Ashoka A, Klymchenko AS, Marescaux J, Diana M.
  Life. 2022; 12(8):1123. https://doi.org/10.3390/life12081123

- **International survey among surgeons on laparoscopic right hemicolectomy: the gap between guidelines and reality.**
  Al-Taher M#, **Okamoto N#***, Mutter D, Stassen LPS, Marescaux J, Diana M, Dallemagne B
  (#: Co-first authors; *: Corresponding author)
  Surg Endosc. 2022 Jan 21:1–14.

- **Robotic endoscopic cooperative surgery for colorectal tumors: a feasibility study (with video).**
  Okamoto N, Al-Taher M, Mascagni P, Vazquez AG, Takeuchi M, Marescaux J, Diana M, Dallemagne B
  Surg Endosc. 2022 Jan 36 (1): 826-832.

- **Single Snapshot Imaging of Optical Properties (SSOP) for Perfusion Assessment during Gastric Conduit Creation for Esophagectomy: An Experimental Study on Pigs.**
  Cinelli L, Felli E, Baratelli L, Ségaud S, Baiocchini A, **Okamoto N**, Rodríguez-Luna MR, Elmore U, Rosati R, Partelli S, Marescaux J, Gioux S, Diana M
  Cancers (Basel). 2021 Dec 2;13(23):6079.

- **Influence of intraoperative vasopressor use on indocyanine green fluorescence angiography: first evaluation in an experimental model.**
  Al-Taher M, Pruimboom T, Schols R M., **Okamoto N**, Bouvy ND., Stassen LPS, van der Hulst R R. W. J., Kugler M, Hostettler A, Noll E, Marescaux J, Diemunsch S, Diana M
  Scientific Reports 2021; May 6; 11(1):9650

- **Noninvasive Near-Infrared Fluorescence Imaging of the Ureter During Robotic Surgery: A Demonstration in a Porcine Model.**
  Al-Taher M, **Okamoto N**, Felli E, Agnus V, Barberio M, Gioux S, Bouvy ND, Stassen LPS, Marescaux J, Diana M
  Journal of Laparoendoscopic & Advanced Surgical Techniques 2020; 30(9): 962-966

Liste des publications

(non relatifs au cancer colorectal ou à la chirurgie guidée par l'image)

- **Needlescopic appendectomy versus conventional laparoscopic appendectomy in young patients.**
  Okamoto N, Sujishi K, Tsugawa S, Jin L, Suzuki T, Waseda M
  Asian J Endosc Surg. 2022 Nov 24. doi: 10.1111/ases.13146. Epub ahead of print. PMID: 36426403.

- **Uterine perforation of pyometra with a sigmoid colon cancer: A case report.**
  Fukunaga N, Waseda M, Sujishi K, Maeda T, Sato R, **Okamoto N**, Suzuki T
  Journal of Japanese College of Surgeons 2022; 47(1):61-65

Liste des articles soumis pour publication

- **Simultaneous, multi-channel, near-infrared fluorescence visualization of mesenteric lymph nodes using indocyanine green and methylene blue: a demonstration in a porcine model.**
  Okamoto N, Al-Difaie Z, Scheepers MHMC, Heuvelings D, Rodríguez-Luna MR, Marescaux J, Diana M, Stassen LPS, Bouvy ND, Al-Taher M
  Diagnostics

- **Simultaneous fluorescence imaging of bowel perfusion and ureter delineation using methylene blue: a demonstration in a porcine model**
  Heuvelings D, Al-Difaie Z, Scheepers MHMC, **Okamoto N**, Diana M, Stassen LPS, Bouvy ND, Al-Taher M
  Surgical Endoscopy

Liste des articles en cours de rédaction

- **Multispectral deep learning differentiation of gastric third space.**

- **Multiple preclinical trials on targeted fluorescent agents in rectal cancer. Précision de la reconnaissance du cancer COLOrecTAl avec un fluoRophore ciblé pour améliorer la surveillance et réduire une chirurGie inutile (COLOTARG).**

- **Acronym of the "VIDI-VICI" Project. Title VIsualisation and quantification of the effects of surgical humiDIfication on intestinal perfusion and VIability in an acute porCIne model.**

- **Outlying differences in colorectal cancer treatment strategy. EAST vs. WEST results of an international survey.**

Liste des présentations orales

- **Robotic endoscopic cooperative surgery for colorectal tumors: a feasibility study.**
  29th International Congress of the European Association for Endoscopic Surgery, Spain, Nov 24, 2021

- **International survey among surgeons on laparoscopic right hemicolectomy: the gap between guidelines and reality. -Invited presentation-**
  83rd Annual Congress of Japan Surgical Association, Japan, Nov 19, 2021

謝辞/Remerciements/Acknowledgments

"No soy coreano ni soy japones. Yo soy desarraigado." (K. Kaneshiro, 2020, p87)
- I am not Korean and I am not Japanese. I am rootless.

This is a line from the main character in the Japanese novel. It vividly describes how the main character, who is a young student of Zainichi Korean (Korean with the status of special permanent residents of Japan), struggles with his nationality and human relationships, but finds his identity and lives his life. I liked this novel very much when I was a student, perhaps because the main character's experiences overlap a little with my own circumstances.

He says in the novel at the end, "I have to see the wider world." From that time on, I began to yearn for the world beyond the sea.

In 2019, I came to France. I had never studied overseas, so the world beyond the sea was much tougher than I had imagined, but I got to know many people in this doctoral program, and they helped and supported me a lot. I would like to take this opportunity to thank them again.

Dear **Prof. Michele Diana**, thank you for allowing me to join your team in 2020. And thank you for accepting my request for a doctoral program and becoming my director. You always came up with solutions to the problems I had. Since I joined your team, I was amazed and impressed by your wealth of knowledge, your determination to learn, and your ambition. It was a privilege to spend my doctoral period under your guidance. I hope that this relationship will go on for a long time.

Dear **Dr. Paul Montgomery**, I would also like to thank you for taking on the role of director for my doctoral program. Even though I have never worked in an academic institution, and I had no common sense as a scientist, you carefully and gently taught me the fundamentals of being a scientist. You were always there to help me when I was in need. I really appreciate your kindness.

Dear **Prof. Jacques Marescaux**, the first time when I visited IRCAD in 2018, you welcomed me with a smile as I clutched the recommendation letter and spoke nervous and broken English. IRCAD, the institution that you created in Strasbourg, is a gateway to "the wider world" and I have met many people there and all of my experiences have been wonderful. I have been a fellow at IRCAD for three and a half years now and have been fascinated by the place. There is not a day that goes by that I did not feel happy to be a fellow at IRCAD.

Thank you for changing my life and for everything you gave me.

I would like to express my sincere gratitude to Professors **Giuseppe Spinoglio**, **Salvador Morales-Conde**, **Sylvain Lecler**, **Ronan Cahill**, **Alexander L Vahrmeijer**, **Sylvain Gioux**, and **Dr. Elisa Cassinotti** for their agreement to become members of this jury.

Dear **Rita**, I don't know anyone else who is as talented, friendly, and considerate as you are. My greatest thanks also go to your husband, **Victor**. I am happy that I was able to spend my IRCAD life at the same time as you guys. Thank you so much for always helping me when I needed it most.

Dear **Mahdi**, you are one of the people that I really want to express my gratitude to. You led me to many places including communication opportunities, research opportunities, clinical settings, etc. I looked at you sometimes like my senior surgeon, sometimes like my friend, and sometimes like an older brother. You are one of the people who taught me, once again, the importance of knowing the world at large.

Dear **Sophie**, in experimenting with you as an anesthesiologist, I realized once again that surgery requires the cooperation of many different colleagues. I am very happy to have a friend like you who is very kind and to have performed experiments with you who is smart and talented. I would also like to express my gratitude to your father **Prof. Pierre Diemunsch** who always treated me kindly.

Dear **Alain**, you are one of the people who have supported me the most as a friend. From the very beginning of my arrival in France, you tried to listen and understand my poor English. I feel that everyone trusts and relies on you in the professional field as well. I always appreciated your thoughtfulness and kindness. My thanks also go to your family **Mélissa**, **Sofía,** and **Mia**.

Dear **Pietro**, I believe that you as a researcher are one of the most talented people. I am proud to have been able to conduct research with you and perform several studies. In addition, you have the kindness that is so essential for a surgeon. I do respect you not only as a researcher but also as a surgeon.

Dear **Juan**, your ideas were always beyond my conventional wisdom, and you taught me the importance of having a wide perspective. On the other hand, I respect your behavior as a father. Your family, **Marla**, **Thiago**, and **Myla** is always warm-hearted, and I would like to thank them once again.

Dear **Farid**, I think that you are the first friend I have had in Strasbourg. I was very impressed by your willingness to devote yourself to anything that interests you. Thank you so much for being a good friend.

Dear **Dr. Takeshi Urade**, thank you for your kind guidance and help as I was unfamiliar with the French lifestyle and with medical research. The COVID-19 pandemic forced us to change our plans and life and made it less easy for us to attend international conferences. It was a great pleasure to see you again in Europe at the EAES Annual Conference in Kraków, Poland in 2022. I would also like to thank your family, **Tsukushi** and **Koshi**, who were very kind to me during my stay.

Dear **Dr. Bernard Dallemagne**, thank you very much for giving me the opportunity and chance to conduct research when I came to IRCAD. That research has brought me so many good friends and colleagues.

Dear **Dr. Sang Hoo Kim**, it was a real pleasure meeting you in Strasbourg. You have supported me a lot in my research and in my personal life. Thank you very much again.

I am very excited and very honored to work with you in the future.

Dear **Zaid**, **Max**, **Danique**, **Prof. Stassen** and **Prof. Bouvy** at **Maastricht UMC+**, it was a pleasure to participate in your experiment in Maastricht and you made my time there very meaningful. Thank you so much. I am looking forward to meeting you again at international conferences.

Dear **Dr. Masahiro Waseda**, words cannot express my heartfelt gratitude to you. I am truly blessed to have studied surgery under your guidance. I would not be where I am today if I had not met you. I will keep on doing my best so that I can pass on what I have learned from you and what you have done for me to the next generation of doctors.

Dear **Dr. Tetsuya Kurosaki**, I would not be where I am today if you had not introduced me to IRCAD and recommended me. I would like to thank you again. I hope that I have left behind and passed the spirit as a Japanese surgeon on to future generations, the spirit that you had left behind at IRCAD 24 years ago.

Dear **Dr. Taro Yamanaka**, I am proud to have spent my resident program under your guidance at Yokohama Asahi Chuo General Hospital. Thank you for your willingness to agree to support me when I made the decision to stay in France. I will continue to practice medicine with "良心" in my heart.

I hope that I have included almost everything... if not, please accept my apologies.

Thanks for your kind understanding.

Finally, my regards to all my family,

Dear **Nene**, I am sorry that I was away from home for so long because of my selfishness. Thank you for staying with my parents. You are the kindest person that I know and I hope and believe that you will be a great doctor.

My dear **Mother**, as this acknowledgment shows, there are many people who have supported me a lot and for whom I would like to say thank you, beyond countries and languages. It is because you have taught me what kindness is since I was a child.

My dear **Father**, you have taught me how to be strong and tough as a man. I am very happy to be the son of a man that I respect more than anyone else as a man, a father, and a doctor.

Thank you so much for making me the person that I am today.

Nariaki OKAMOTO

L'application de l'imagerie optique peropératoire pour optimiser la chirurgie oncologique colorectale et prévenir les complications.

École doctorale

Mathématiques,

sciences de l'**information**

et de l'**ingénieur** | ED 269

Université de Strasbourg

Résumé

Le cancer colorectal est la troisième cause de cancer et la deuxième cause de mortalité liée au cancer dans le monde. Au cours des dernières décennies, l'approche chirurgicale du cancer colorectal a considérablement évolué, notamment grâce à l'introduction de techniques chirurgicales innovantes comme l'excision totale du mésorectum et l'excision complète du mésocôlon, grâce aux progrès des procédures mini-invasives et au recours à la chirurgie guidée par imagerie par fluorescence dans le proche infrarouge.

Les progrès significatifs et croissants de la chirurgie guidée par l'image peropératoire s'incarnent à travers son rôle déterminant dans le domaine chirurgical, comme en témoignent les nombreux symposiums régulièrement organisés lors de congrès de chirurgie dans le monde.

La présente recherche s'est polarisée sur la mise en œuvre de nouvelles approches en chirurgie colorectale utilisant l'imagerie optique peropératoire afin de promouvoir de meilleurs résultats cliniques et prévenir toutes récidives et complications.

Mots clés : Chirurgie du cancer colorectal, Imagerie optique, Imagerie hyperspectrale, Imagerie multispectrale, Chirurgie guidée par l'image de fluorescence, Intelligence artificielle, Apprentissage profond

Résumé en anglais

Colorectal cancer is the third leading cause of cancer and the second leading cause of cancer-related mortality worldwide. Over the last decades, the surgical approach to colorectal cancer has significantly changed, including the introduction of innovative surgical techniques such as total mesorectal excision (TME) and complete mesocolic excision (CME), advances in minimally invasive procedures, and near-infrared fluorescence (NIRF) image-guided surgery.
The overgrowing significant progress of intraoperative image-guided surgery accounts for its seminal place in the surgical field, along with new symposia and sessions being regularly organized during international surgical conferences.
The present research has focused on implementing novel approaches in colorectal surgery using intraoperative optical imaging to promote better clinical outcomes and prevent recurrences and complications.

Keywords : Colorectal cancer surgery, Optical imaging, Hyperspectral imaging, Multispectral imaging, Fluorescence image–guided surgery, Artificial intelligence, Deep learning